NUMERICAL SIMULATION OF THE DISSOCIATION OF I_2 BY $O_2(^1\Delta)$ IN A TWO DIMENSIONAL PARALLEL JET

THESIS

Jeffrey A. Miller
Captain, USAF

AFIT/GAE/AA/89M-3

DEPARTMENT OF THE AIR FORCE
AIR UNIVERSITY
AIR FORCE INSTITUTE OF TECHNOLOGY

Wright-Patterson Air Force Base, Ohio

AFIT/GAE/AA/89M-3

NUMERICAL SIMULATION OF THE DISSOCIATION OF I_2 BY $O_2(^1\Delta)$ IN A TWO DIMENSIONAL PARALLEL JET

THESIS

Jeffrey A. Miller
Captain, USAF

AFIT/GAE/AA/89M-3

AFIT/GAE/AA/89M-3

NUMERICAL SIMULATION OF THE DISSOCIATION OF I_2 BY $O_2(^1\Delta)$ IN A TWO DIMENSIONAL PARALLEL JET

THESIS

Presented to the Faculty of the School of Engineering

of the Air Force Institute of Technology

Air University

In Partial Fulfillment of the

Requirements for the Degree of

Master of Science in Aeronautical Engineering

Jeffrey A. Miller

Captain, USAF

March 1989

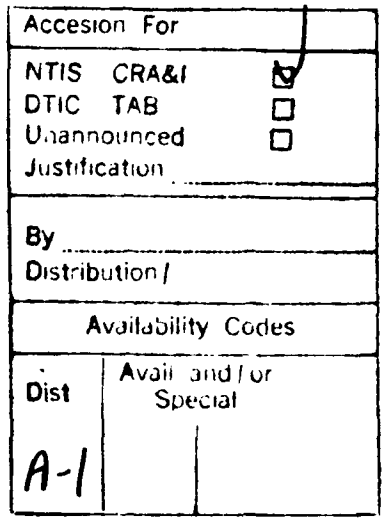

Approved for public release; distribution unlimited

Acknowledgements

This Master's Degree has been five years in the making. In that time there have been so many people, including instructors, co-workers, friends, and family, who have earned my gratitude and deserve my thanks for the support they have provided. I hope I have not forgotten to make my feelings known along the way. If not, thanks for keeping the faith.

There are several important people whom I must expressly thank here. Foremost, I am deeply indebted to my advisor, Lt Col Eric Jumper. Simply stated, I would not have finished without his support, guidance, and when needed, discipline. His enthusiasm and outstanding teaching drew me into the field of reacting flows while I was at AFIT. I am very fortunate to be working with him again three years later at the Air Force Weapons Laboratory.

Good teachers are rare; I was fortunate to have two while at AFIT, Lt Col Jumper and Dr James Hitchcock. I would like to thank Dr Hitchcock for his support and patience and for staying with me for five years.

Finally, I would like to acknowledge the support I have received from the Air Force Weapons Laboratory, especially the people I work with in the Advanced Chemical Lasers Branch. Without the time Lt Col Gerald Hasen and Maj Michael White provided me I could not have finished this job. Special thanks to Dr Gordon Hager for showing me the ropes.

Jeffrey A. Miller

Table of Contents

	Page
Acknowledgements	iii
List of Symbols	vi
List of Figures	ix
List of Tables	xi
Abstract	xii
I. Introduction	1
II. Background	6
Historical Development of COIL Kinetics	6
The Iodine Dissociation Mechanism	10
Modeling Difficulties	12
New Approach	17
Numerical Investigation	18
III. Governing Equations	21
Navier-Stokes Equations	21
Thin-Shear-Layer Equations	23
von Mises Transformation	25
Thermodynamic Properties	26
Transport Coefficients	27
Viscosity	28
Thermal Conductivity	29
Diffusivity	30
Chemical Reactions	31
Standard AFWL COIL Rate Package	31
Chemical Rate Equations	32
IV. Numerical Analysis	36
Integration Scheme	36
Finite-Difference Formulas	36
. .Interior Nodes	36
. .Boundary Nodes	38
Explicit Finite-Difference Equations	39
Numerical Stability	40
V. Results and Discussion	44
Introduction	44
Validation of COIL Chemistry Package	45
Mixing Studies	46
Geometry and Initial Conditions	48
Assumptions and Simplifications	49

General Results 55
Streamwise Comparisons 59
Transverse Comparisons 67
Effect of Water Quenching 80

VI. Conclusion 84

Appendix A: Concurrent Experiment: Configuration and Expected Operating Conditions 87

Appendix B: Coefficients for Generalized Finite-Difference Operators 91

Appendix C: COILFT Code Listing 92

Bibliography 105

Vita 108

List of Symbols

BHP	basic hydrogen peroxide, H_2O_2 + KOH
Cl_2	chlorine
c_p	specific heat of the mixture, (erg/g K)
c_{p_j}	specific heat of species j, (erg/g K)
D_j	diffusivity of species j into the mixture, (cm^2/sec)
D_{ij}	diffusivity of species i into j, (cm^2/sec)
$\dot{E}$	"chemical energy" flux, (kJ/sec)
E_i	heat of formation of species i, (erg/g)
F	hyperfine quantum number
g	gain, (cm^{-1})
He	helium
h	Planck constant, 6.63×10^{-27} (erg sec)
h	enthalpy, (erg/g)
h_j	enthalpy of species j, (cm^2/mole sec^2)
H_2O	water
I_2/O_2	ratio of iodine flow to oxygen flow
I_2	molecular iodine
$I_2^{\ddagger}$	vibrationally excited ground state iodine (v" $\geq$ 43) (also, I_2^*)
I	atomic iodine, $I(^2P_{3/2})$
I^*	lasing state, $I(^2P_{1/2})$
K_{eq}	equilibrium constant
k	Boltzmann's constant, 1.38×10^{-16} (erg/molecule K)
k	thermal conductivity, (erg/cm sec K)
k, k_f	forward rate constant, (cm^3/molecule sec)

k_i	thermal conductivity of species i, (erg/cm sec K)
k_r	reverse rate constant, (cm^3/molecule sec)
M	molecular weight of the mixture, (g/mole)
M_i	molecular weight of species i, (g/mole)
$\dot{m}$	mass flow rate, (g/sec)
N	empirical mixing and dissociation efficiency factor
N(x)	N calculated from the code
N_A	Avagadro's number, 6.023×10^{23} (molecules/mole)
$\dot{n}$	molar flow rate, (mole/sec)
$O_2(^3\Sigma)$	ground state oxygen
$O_2(^1\Delta)$	first electronic state of oxygen
$O_2(^1\Sigma)$	second electronic state of oxygen
P	pressure, (dyne/cm^2) or (torr)
P_{Aval}	power available in the O_2 flow, (kW)
$\bar{R}$	universal gas constant, 8.3143×10^7 (erg/mole K)
T	temperature, (K)
u	streamwise velocity component, (cm/sec)
u_i, u_j, u_k	tensor velocity component, (cm/sec)
v	normal velocity component, (cm/sec)
W_j	mass fraction of species j
$\dot{W}_j$	mass creation term, (g/cm^3sec)
x	streamwise position coordinate, (cm)
x_i, x_j, x_k	tensor position coordinate, (cm)
Y_Δ	$O_2(^1\Delta)$ fraction, $O_2(^1\Delta)/O_2$(total), yield
Y_0	threshold yield
y	normal position coordinate, (cm)

χ_i	mole fraction of species i
δ	shear-layer thickness
ϵ	excitation energy, (kJ/mole)
ϵ	maximum energy of attraction
ϕ	dissipation function
ψ	compressible stream function, (g/cm sec)
μ	viscosity, (g/cm sec)
μ_i	viscosity of species i, (g/cm sec)
ν_i	excitation energy of the i^{th} excited state, (cm^{-1})
ρ	density, (g/cm^3)
o	stimulated emission cross-section, (cm^2)
σ	characteristic diameter, (Å)
σ_{ij}	stress tensor
$\Omega_\mu = \Omega_k$	reduce collision integral
[ ]	concentration, ($\#/cm^3$)

List of Figures

Figure		Page
1.	O_2, I_2, and I Energy Level Diagram for the COIL System. (Ref 2)	9
2.	2-D Mixing Model Nozzle Geometry. (Ref 14)	13
3.	Comparison of 2-D Mixing Model Geometry to 3-D Injection Scheme. (Ref 14)	13
4.	Comparison of 1-D Remixed and 2-D Mixing Predictions for I_2 Dissociation. (Ref 14)	14
5.	Comparison of 1-D Premixed Model Prediction to Heidner's Experimental Results. (Refs 2 and 14)	16
6.	Comparison of the 2-D and 3-D I_2 Nozzle Geometries.	19
7.	Finite-Difference Grid Notation. a) Interior Node. b) Nozzle Centerline. c) Outer Streamline.	37
8.	Comparison of the O_2, I_2, and I^* Profiles Predicted by the Codes SENCHEM and COILFT.	46
9.	Schematic of the Computational Domain for the Parallel Jet Cases.	49
10.	Development of the Transverse Velocity Profiles as a Function of ψ.	56
11.	Development of the Transverse Temperature Profiles as a Function of ψ.	57
12.	Transverse Species Concentration Profiles for the 6/1 Jet Case 3 cm Downstream from the Nozzle Exit Plane.	58
13.	Streamwise Species Concentration Profiles for the 6/1 Jet Case on the Nozzle Centerline.	60
14.	Comparison of the Streamwise Variation in I_2 Dissociation for the 1-D, Premixed and Jet-Mixed Cases.	62
15.	Streamwise Development of the Species Concentration Profiles for the "6/1" Premixed Case.	63

16. Streamwise Development of the Species Concentration Profiles at the Jet Boundary for the 6/1 Jet Case. 64

17. Comparison of the Streamwise Variation of the I_2 Dissociation Efficiency for the 1-D, Premixed and Jet-Mixed Cases. 68

18. Transverse O_2 Mixing, I_2 Dissociation, Gain Profiles for the 6/1 Jet Case at x = 1 cm. 71

19. Transverse O_2 Mixing, I_2 Dissociation, and Gain Profiles for the 6/1 Jet Case at x = 3 cm. 73

20. Transverse O_2 Mixing, I_2 Dissociation, and Gain Profiles for the 6/1 Jet Case at x = 6 cm. 74

21. Comparison of the Transverse O_2 Mixing Profiles between the 1/1 Jet Case at x = 1cm, the 3/1 Jet Case at x = 3cm, and the 6/1 Jet Case at x = 6cm. 77

22. Comparison of the Transverse I_2 Dissociation Profiles between the 1/1 Jet Case at x = 1cm, the 3/1 Jet Case at x = 3cm, and the 6/1 Jet Case at x = 6cm. 78

23. Comparison of the Transverse Gain Profiles between the 1/1 Jet Case at x = 1cm, the 3/1 Jet Case at x = 3cm, and the 6/1 Jet Case at x = 6cm. 79

24. Effect of 2% (of the O_2 Flow) H_2O Vapor on the I_2 Dissociation for the 6/1 Premixed and Jet-Mixed Cases. . . . 81

25. Effect of 2% (of the O_2 Flow) H_2O Vapor on the I_2 Dissociation Efficiency for the 6/1 Premixed and Jet-Mixed Cases. 83

A1. COIL Diagnostic Flow Tube Assembly 88

A2. COIL Diagnostic Flow Tube I_2 Injection Nozzle 89

List of Tables

Table		Page
I.	Air Force Weapons Laboratory Reduced COIl Rate Package, 11 Reaction Set	32
II.	Available Temperature Dependent Rate Data for the COIL Kinetics	34
III.	Initial Conditions for COIL Chemistry Validation Case . .	47
IV.	Initial Conditions for the Jet-Mixing Cases	51
V.	Initial Conditions for the 1-D, Premixed Cases	52
B.	Coefficients for the Generalized Finite-Difference Operators	91

Abstract

The thin-shear-layer equations are solved for a two dimensional parallel jet of I_2 in an $O_2(^1\Delta)$ freestream, to investigate the effect of mixing and water vapor on I_2 dissociation in Chemical Oxygen-Iodine Lasers (COIL).

Predicting the dissociation of I_2 has been identified as the largest source of error in COIL performance modeling. Although some doubt still remains about the current COIL kinetics package, recent experimental and modeling experiences have indicated that much of the problem may be due to the coupled iodine mixing and dissociation process. The numerical code was used to study the combined mixing and dissociation problem on a simpler (i.e., simpler than laser nozzles) 2-D, parallel injection nozzle geometry. Comparison of a set of 1-D premixed cases and 2-D jet cases with varying jet velocity ratios (and therefore mixing rates) indicates that, counter to the accepted belief, imperfect mixing which results in initial regions of high I_2 concentration leads to faster dissociation rates. High laser gain, however, does require efficient mixing. The results of both premixed and jet-mixed cases with and without water vapor in the O_2 freestream demonstrate the strong dependence of the dissociation efficiency (i.e., the penalty paid to dissociate I_2) on both the device geometry and operating conditions which challenges the wisdom of using empirically determined efficiency factors to predict COIL performance.

I. Introduction

The chemical oxygen-iodine laser (COIL) was first demonstrated in 1977 at the Air Force Weapons Laboratory (AFWL) (1). The COIL laser is unique because it is a chemically pumped laser which operates on an electronic transition of the iodine atom instead of a vibrational or rotational transition as have all previous chemical lasers. Singlet delta oxygen ($O_2(^1\Delta)$),an energetic metastable molecule, is created by a liquid phase reaction of chlorine in a basic hydrogen peroxide solution. Transition of the $O_2(^1\Delta)$ molecule directly to the ground state is spin forbidden giving $O_2(^1\Delta)$ a relatively long radiative lifetime. When mixed with $O_2(^1\Delta)$, iodine molecules dissociate into iodine atoms which are then pumped rapidly into the ($^2P_{1/2}$) electronic state. Stimulated emission on the dominant hyperfine transition (F=3 $\longrightarrow$ F=4) of the $I(^2P_{1/2}) \longrightarrow I(^2P_{3/2})$ magnetic dipole transition produces photons at 1.315μm making COIL the shortest wavelength pure chemical laser in existence. In 1977, the first COIL laser produced 4 mW of output power. AFWL's most recent COIL program, Roto-COIL, has demonstrated power in excess of 25 kW. This demonstrated potential for scaling to high powers has generated considerable interest in COIL devices.

Although the data base for designing and operating COIL devices has grown significantly over the past decade, predicting the performance of new devices or even modeling the results of current devices is still somewhat of an art. Recent experience on the Roto-COIL program illustrates this point. The measured stable resonator power output exceeded the predicted performance by 40% even though the measured excited oxygen production was as expected. The power available in the

oxygen flow can be estimated using the simple empirical formula,

$$P_{Aval} = \dot{n}_{O_2} \left(Y_\Delta - Y_0 - N \frac{I_2}{O_2} \right) 91 \frac{kJ}{\text{mole } O_2} \qquad (1.1)$$

$\dot{n}_{O2}$ is the molar flow rate of oxygen (all species). Y_Δ is the fraction of oxygen in the excited state that is delivered to the mixing region. Y_0, the excited oxygen fraction required to reach lasing threshold, can be estimated from the spectroscopy of the iodine atom. Y_0 is approximately 0.15 at room temperature. I_2/O_2 is simply the ratio of the iodine injected to the total oxygen in the flow. N is an empirical value which is interpreted as the number of $O_2(^1\Delta)$ molecules required to dissociate one iodine molecule. N accounts for all of the energy lost during the mixing and dissociation process which is not available to pump the iodine atoms. The lower limit on N is set at 2 by the dissociation energy of iodine. Experimental results prior to the Roto-COIL program placed the value of N between 5 and 7, implying that the dissociation was less than perfectly efficient. With oxygen production near the expected value and the threshold yield fixed for Roto-COIL conditions, Eq (1.1) implies that most of the 40% increase in power must be due to more efficient iodine dissociation, i.e., N closer to 2. More sophisticated modeling has failed to shed light on this apparent discrepancy between the power available and and the measured extracted power. Even more troubling, optical measurements of the residual I_2 in the cavity indicate that the I_2 is better than 95% dissociated. The best estimates by computer models using the current AFWL approved rate package predict dissociation fractions closer to 50-70%.

The inability to accurately model the I_2 dissociation process in

COIL lasers is disturbing as we begin to consider larger devices at higher power. One might be tempted to be content with exceeding the predicted power of a laser by 40%. Unfortunately, laboratory devices like Roto-COIL tend to to be designed by brute force methods. Systems and subsystems (fluid supply, vacuum, etc) are designed with sufficient margin to allow for some optimization of the system performance. As the laser is scaled up, however, the cost of individual subsystems grows rapidly. Therefore, large systems are designed more for a single operating point and accurate prediction of device performance becomes an economic necessity. In addition, new designs can not depart with confidence from the current experimental data base. This is an important consideration as designers consider trade-offs in H_2O trapping efficiency against transport losses (H_2O vapor evolved in the oxygen generator rapidly quenches excited iodine) and longer extraction lengths for high power unstable resonators.

Because of these concerns, AFWL initiated a conference in August 1987 to review the current understanding of the kinetic processes involved in the COIL system and to recommend actions for improving modeling capability (2). While actions to improve confidence in several aspects of the overall COIL kinetics package were made, the summary of the COIL kinetics conference concluded that the largest uncertainty in modeling COIL lasers was due to uncertainties in the iodine dissociation mechanism. One major problem identified was the lack of a good data base to test the current dissociation model against. The kinetics data base was assembled from experiments at conditions quite different from laser operating conditions. In order to resolve rates of individual reactions, kinetics experiments are conducted in low pressure, low

velocity flow tubes and where the mixing considerations are intentionally designed out, although it is not at all clear that they actually were (c.f. below). The iodine dissociation kinetics are, by their nature, heavily influenced by the mixing process. In actual laser nozzle designs, the iodine is injected transverse to the primary flow to insure rapid entrainment of the oxygen stream into the iodine stream and vise versa. These flows are highly three dimensional, making it impossible to sort out modeling errors in the solution of the mixing problem and errors due to the chemical kinetics.

Acting on the recommendations from the conference, AFWL began an in-house experimental effort to acquire iodine dissociation data on a simple, well diagnosed mixing geometry against which the current kinetics package could be tested. The goals of this effort are to verify the existing model and identify its weaknesses and develop an experimental data base against which future changes can be validated.

This thesis outlines the development of a reactive flow numerical model which will eventually be used to aid in the design of these experiments and to model the experimental results although no comparisons to experimental data will be made here. This development is presented in the following order. Chapter II provides a brief history of the development of the COIL kinetics data base and identifies some of the sources of uncertainty in the iodine dissociation process. Results of some recent modeling efforts are presented as evidence that mixing plays a essential role in the dissociation process. A brief description of the planned experiment is given. Finally, the goals the code development and validation effort are reviewed. Chapter III presents the detailed development of the governing equations used to

model the two dimensional, reacting jet flow field. Chapter IV discusses the explicit integration scheme used to obtain a numerical solution to the flow equations. Chapter V presents the results of test cases used to verify the code and the results of several studies conducted to identify the roles of mixing and water vapor on the iodine dissociation. Chapter VI summarizes the results of the numerical effort and explores their implications to COIL system performance and further experimental and numerical investigations.

II. Background

Historical Development of COIL Kinetics

In 1966, Arnold, Finlayson, and Ogryzlo first noted the near resonant energy transfer between electronic states of molecular oxygen and atomic iodine (3).

$$O_2(^1\Delta) + I(2P_{3/2}) \longrightarrow O_2(^3\Sigma) + I^*(2P_{1/2}) \qquad (2.1)$$

Later, extensive investigation of this system by Derwent and Thrush suggested that this very rapid energy transfer ($k_f = 7.8\times10^{-11}$ (cm^3/molecule sec)) might provide an excellent pumping mechanism for a high energy laser based on the dominant hyperfine transition in the iodine atom, (F=3) $\rightarrow$ (F=4), at 1.315 μm (4) (5). Their work quantified the reaction in Eq (2.1) and showed that although the singlet delta state of oxygen is nearly resonant with an electronic state of atomic iodine, it is relatively immune to quenching. The primary loss mechanism for $O_2(^1\Delta)$ is homogeneous pooling.

$$O_2(^1\Delta) + O_2(^1\Delta) \longrightarrow O_2(^1\Sigma) + O_2(^3\Sigma) \qquad k = 2.7\times10^{-17} \qquad (2.2)$$

The singlet sigma state is rapidly quenched in the presence of water.

$$O_2(^1\Sigma) + H_2O \longrightarrow O_2(^3\Sigma) + H_2O \qquad k = 6.7\times10^{-12} \qquad (2.3)$$

Once the energy is transferred to the iodine atom, the primary energy loss mechanisms become energy pooling of $O_2(^1\Delta)$ and I^*,

$$O_2(^1\Delta) + I^* \longrightarrow O_2(^1\Sigma) + I \qquad k = 1.1\times10^{-13} \qquad (2.4)$$

and quenching of excited iodine by water.

$$I^* + H_2O \longrightarrow I + H_2O \qquad k = 2.0\times10^{-12} \tag{2.5}$$

The elimination of water vapor appears to be an important factor in the performance of a laser system.

Conveniently, the oxygen-iodine system also provides a mechanism for production of iodine atoms. Arnold et. al. (3) observed that molecular iodine dissociates rapidly in the presence of excited oxygen. Derwent and Thrush's (4) (5) early work identified $O_2(^1\Sigma)$ as the source of energy for this dissociation process. Figure 1. shows the relative differences between the excitation energies of the two molecules.

$$O_2(^1\Sigma) + I_2 \longrightarrow O_2(^3\Sigma) + I + I \qquad k = 4.0\times10^{-12} \tag{2.6}$$

$O_2(^1\Sigma)$ is created by the pooling process of Eq. (2.2) above.

The remaining requirement to demonstrate lasing was a source of $O_2(^1\Delta)$. As expected for a near resonant energy transfer, the reverse rate for the pumping reaction, Eq (2.1), is comparable to the forward rate ($k_r = 2.7\times10^{-11}$). This implies that large number densities of $O_2(^1\Delta)$ are required to produce a population inversion in the iodine atom. The ratio of $I(^2P_{1/2})$ to $I(^2P_{3/2})$ required to reach threshold (population inversion) is determined by the degeneracies of the states (6).

$$\frac{\left[I(^2P_{1/2})\right]}{\left[I(^2P_{3/2})\right]} = \frac{2}{4} = 0.5 \tag{2.7}$$

where [ ] denotes the concentration in (#/cm^3). The equilibrium condition for the reaction in Eq (2.1) is given by

$$k_f \left[O_2(^1\Delta)\right] \left[I(^2P_{1/2})\right] = k_r \left[O_2(^3\Sigma)\right] \left[I(^2P_{3/2})\right] \tag{2.8}$$

The fraction of oxygen in the excited state required to reach threshold is then

$$\frac{\left[O_2(^1\Delta)\right]}{\left[O_2(^3\Sigma)\right] + \left[O_2(^1\Delta)\right]} = \frac{0.5\ k_r/k_f}{1 + 0.5\ k_r/k_f} \tag{2.9}$$

The ratio of the forward rate to the reverse rate is given by the equilibrium constant which can be determined from statistical mechanics.

$$K_{eq} = \frac{k_f}{k_r} = 0.75\ e^{\left(\frac{401}{T}\right)} \tag{2.10}$$

At room temperature (298K) this ratio is 2.88. Using this value, in Eq (2.9), the fraction of $O_2(^1\Delta)$ in the total oxygen flow required to lase a COIL device must be at least 0.15. The standard method of producing $O_2(^1\Delta)$ for all of the early kinetics experiments was by microwave discharge. Unfortunately, the maximum excited oxygen production from a microwave discharge is only about 0.10. The chemical reaction of chlorine with a basic hydrogen peroxide (BHP) solution was found to produce large singlet delta oxygen fractions, (≅ 40 - 60%) (7).

$$H_2O_2 + 2KOH + Cl_2 \longrightarrow 2KCl + 2H_2O + O_2(^1\Delta) \tag{2.11}$$

Although other methods are being considered, this reaction is the only easily available source of large concentrations of $O_2(^1\Delta)$ identified to date.

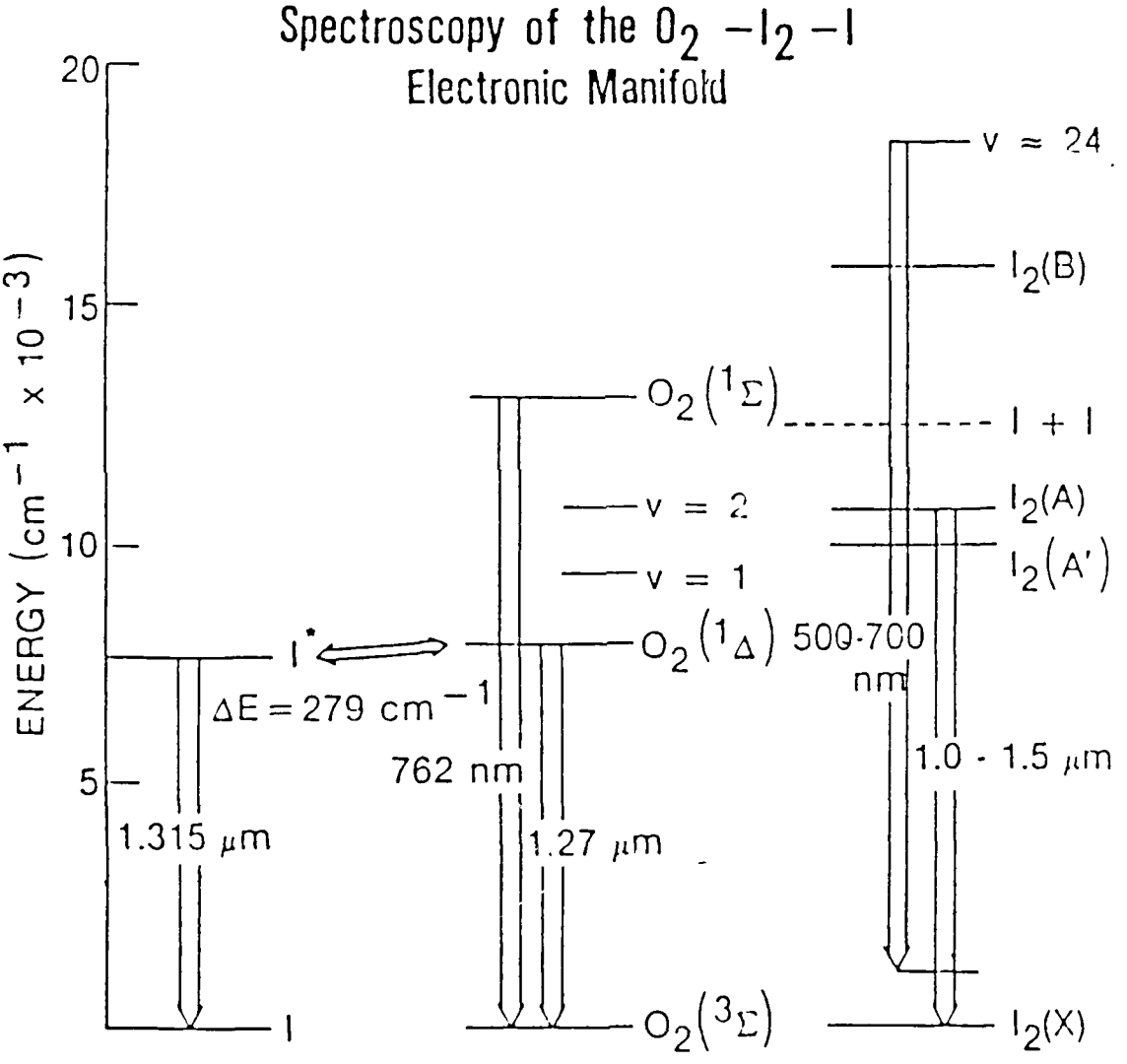

Figure 1. O_2, I_2, and I Energy Level Diagram for COIL System. (Ref 2)

Armed with this basic understanding of the transport and loss mechanisms of the COIL system, in 1977 McDermott, Pchelkin, Benard, and Bousek designed a simple longitudinal flow laser which produced 4 mW of power (1). Within a year, they had scaled the laser to 100 W in a transverse flow device (8).

The Iodine Dissociation Mechanism

These very first laser demonstrations provided the first indication that the iodine dissociation mechanism was not as simple or as well understood as originally thought. The experiments showed that high levels of I_2 dissociation were obtained even in the presence of high concentrations of water (8). Water is a strong quencher of $O_2(^1\Sigma)$ (see Eq (2.3) above). Heidner et. al. went on to show in carefully controlled flow tube experiments that the concentration of $O_2(^1\Sigma)$ could be drastically reduced while still obtaining significant iodine dissociation (9). Avilés et al. remeasured the rate of iodine dissociation by $O_2(^1\Sigma)$ (Eq (2.6)) and found it to be much smaller than originally thought (10). Too small, in fact, to account for the observed dissociation rates.

With $O_2(^1\Sigma)$ eliminated as the primary source of energy for I_2 dissociation, several teams of investigators began looking for an alternate dissociation mechanism to explain the experimental results. It is clear from the energy level diagram in Figure 1 that excluding $O_2(^1\Sigma)$, none of excited states present have sufficient energy to directly dissociate I_2 by a single collision. In 1982, Heidner et. al. proposed a two step process involving a highly vibrationally excited ($v' \geq 43$) intermediate of ground state iodine (denoted as $I_2^{\ddagger}$) (11). Such an excited state can be achieved by collisions with either $O_2(^1\Delta)$ or I^*.

$$O_2(^1\Delta) + I_2 \longrightarrow O_2(^3\Sigma) + I_2^{\ddagger} \qquad k = 7.0\times10^{-15} \qquad (2.12)$$

$$I^* + I_2 \longrightarrow I + I_2^{\ddagger} \qquad k = 3.8\times10^{-11} \qquad (2.13)$$

Once in the excited state, a further collision with an $O_2(^1\Delta)$ molecule quickly dissociates the intermediate producing iodine atoms.

$$I_2^{\ddagger} + O_2(^1\Delta) \longrightarrow I + I + O_2(^3\Sigma) \qquad k = 3.0\times10^{-10} \qquad (2.14)$$

Note, that $I_2^{\ddagger}$ is not a single state but represents a number of vibrational states. The distribution of energy in the vibrational levels above $v'' \geq 43$ has been investigated, but is still not quantified (12) (13).

The characteristics of this dissociation mechanism are quite different from the direct mechanism of Derwent and Thrush, Eq (2.6). Pumping to the intermediate $I_2^{\ddagger}$ state by I^* is much faster than by $O_2(^1\Delta)$. Initially however, no I^* atoms exist. The dissociation process is therefore initially controlled by the relatively slow process of direct dissociation by $O_2(^1\Sigma)$, Eq (2.6), or by multiple collisions with $O_2(^1\Delta)$, Eq (2.12) and Eq (2.14). Once an initial population of iodine atoms is created, however, they will be rapidly pumped to I^*, Eq (2.1), and pumping to $I_2^{\ddagger}$ by I^*, Eq (2.13), will quickly dominate the dissociation process.

This hand off of control from $O_2(^1\Sigma)$ and $O_2(^1\Delta)$ to I^* has a profound impact on laser design and greatly complicates the task of modeling system performance. $O_2(^1\Delta)$ has a relative long lifetime while the lifetime of I^* is very short. Typical laser design therefore involves the creation of $O_2(^1\Delta)$ in a liquid/gas reactor, transport through cold traps to remove evolved water vapor, and injection of

iodine molecules just before the gain region. If one considered only the $O_2(^1\Sigma)$ and $O_2(^1\Delta)$ process, the most efficient mixing scheme would be to rapidly mix the oxygen and iodine streams to achieve a uniform mixture. In reality, with the acceleration of the dissociation process due to I^*, somewhat slower mixing schemes resulting in regions of high I_2 concentrations appear to result in faster and more complete dissociation. This effect can be illustrated by recent modeling and experimental experiences.

Modeling Difficulties

R & D Associates (RDA), under the direction of AFWL, conducted several numerical experiments using the current AFWL approved COIL kinetics package (14). The first involved the comparison of dissociation results from a one dimensional (1-D) premixed numerical code with the results of a two dimensional (2-D) code. The 1-D code represented an ideal case of uniform mixing of the primary oxygen stream and the secondary iodine stream. The initial setup of the 2-D code is shown in Figure 2. The iodine streams are represented as discrete stream tubes with a specified velocity profile. Shear stress created by the velocity differential and molecular diffusion cause the the two streams to mix. The actual device involves a much more complex three dimensional (3-D) mixing of sonic transverse jets into the primary flow just upstream of a supersonic throat, see Figure 3. The 2-D calculation was an attempt to approximate the more complicated 3-D case. The results of the premixed and 2-D calculations are compared in Figure 4. The 2-D model predicts a higher level of dissociation, but both are well below the experimental value of nearly 100% dissociation by the nozzle exit plane.

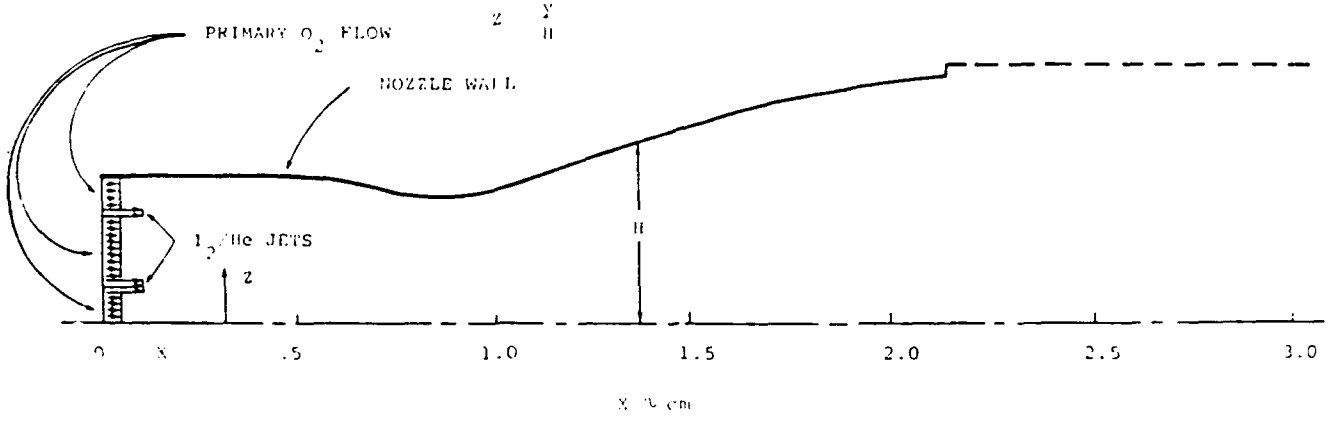

Figure 2. 2-D Mixing Model Nozzle Geometry. (Ref 14)

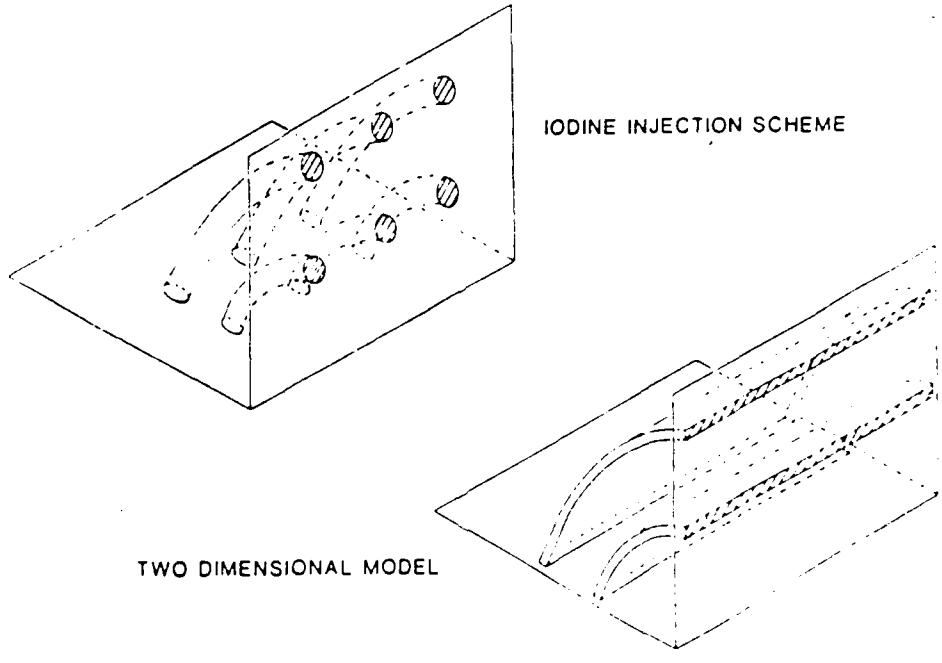

Figure 3. Comparison of 2-D Mixing Model Geometry to 3-D Injection Scheme. (Ref 14)

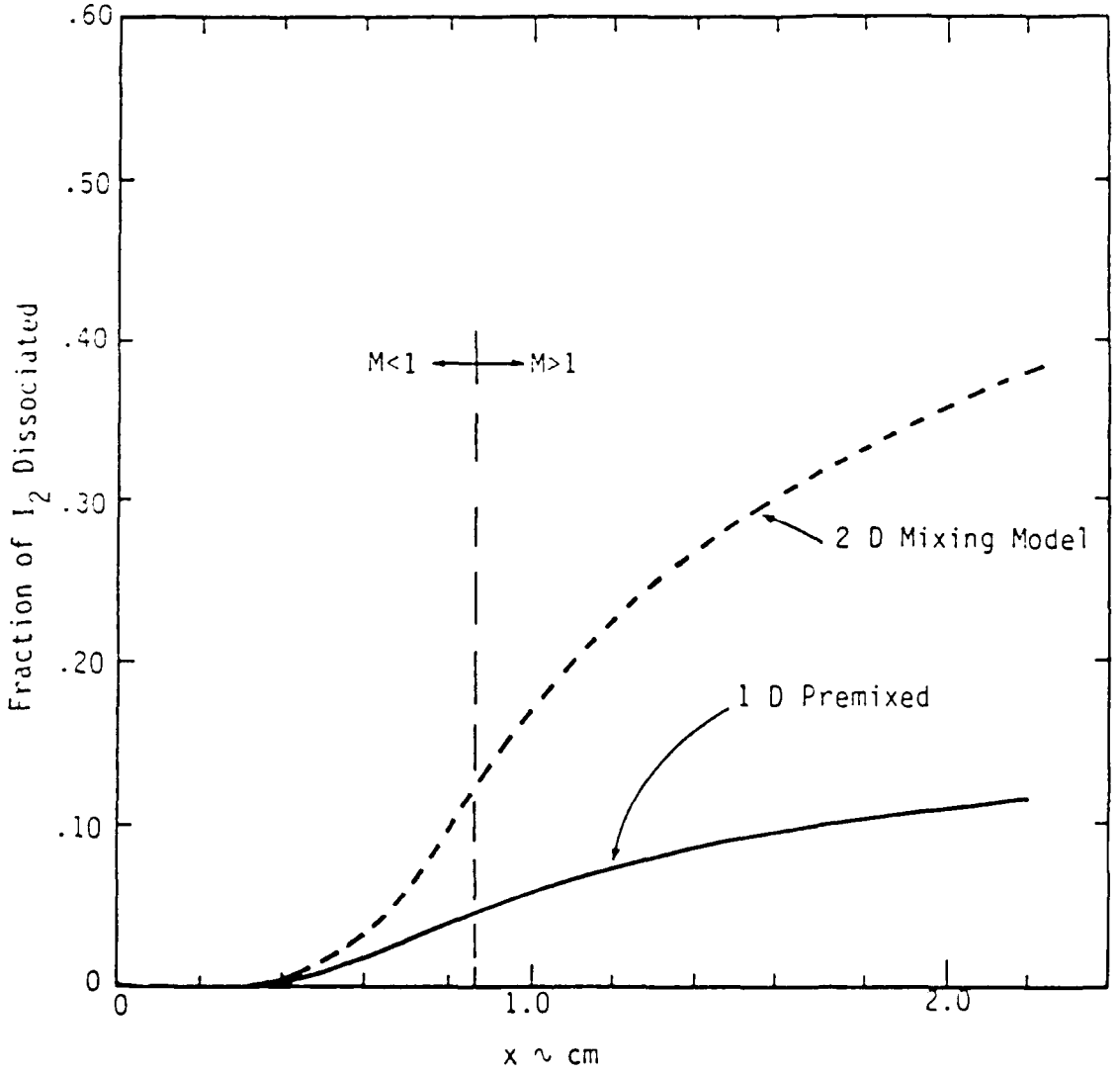

Figure 4. Comparison of 1-D Premixed and 2-D Mixing Predictions for I_2 Dissociation. (Ref 14)

The second numerical experiment was an effort to analytically predict the results of Heidner's iodine dissociation work (9) (11). Heidner conducted his experiments on a carefully controlled, low speed, low pressure flow tube. He used a microwave discharge to produce $O_2(^1\Delta)$ molecules. This method provided a very clean and easily controlled $O_2(^1\Delta)$ source, although the maximum singlet delta fractions obtainable were significantly lower than for BHP/Cl_2 reactors. Heidner believed that the iodine injectors were adjusted to remove fluid dynamic and mixing considerations from his experiment so that it could be treated as a 1-D premixed initial condition. RDA modeled the results of several of Heidner's cases using their 1-D premixed code and the AFWL COIL kinetics package (14). The I^* profiles are compared in Figure 5. The final levels match quite well. The calculated results, however, show a slower rise time. One possible explanation is that in the experiment the oxygen and iodine were not well mixed resulting in local regions of high I_2 concentrations and gradients. Unfortunately, Heidner's attempt to design a premixed experiment did not allow for detailed experimental investigation of the initial stages of the dissociation process or precise modeling of his experimental configuration.

These examples point out the need for increased care on the part of both experimentalist and modeler. Much of the early experimental work focused solely on improving the kinetics data base. Like Heidner's work, mixing and fluid dynamic considerations were supposedly removed. Experience demonstrates, however, that the kinetics and fluid mechanics are closely coupled making study of the kinetics without regard for the fluid mechanics both difficult and unwise. Moreover, most of the kinetics data base is derived from experiments on flow tubes very

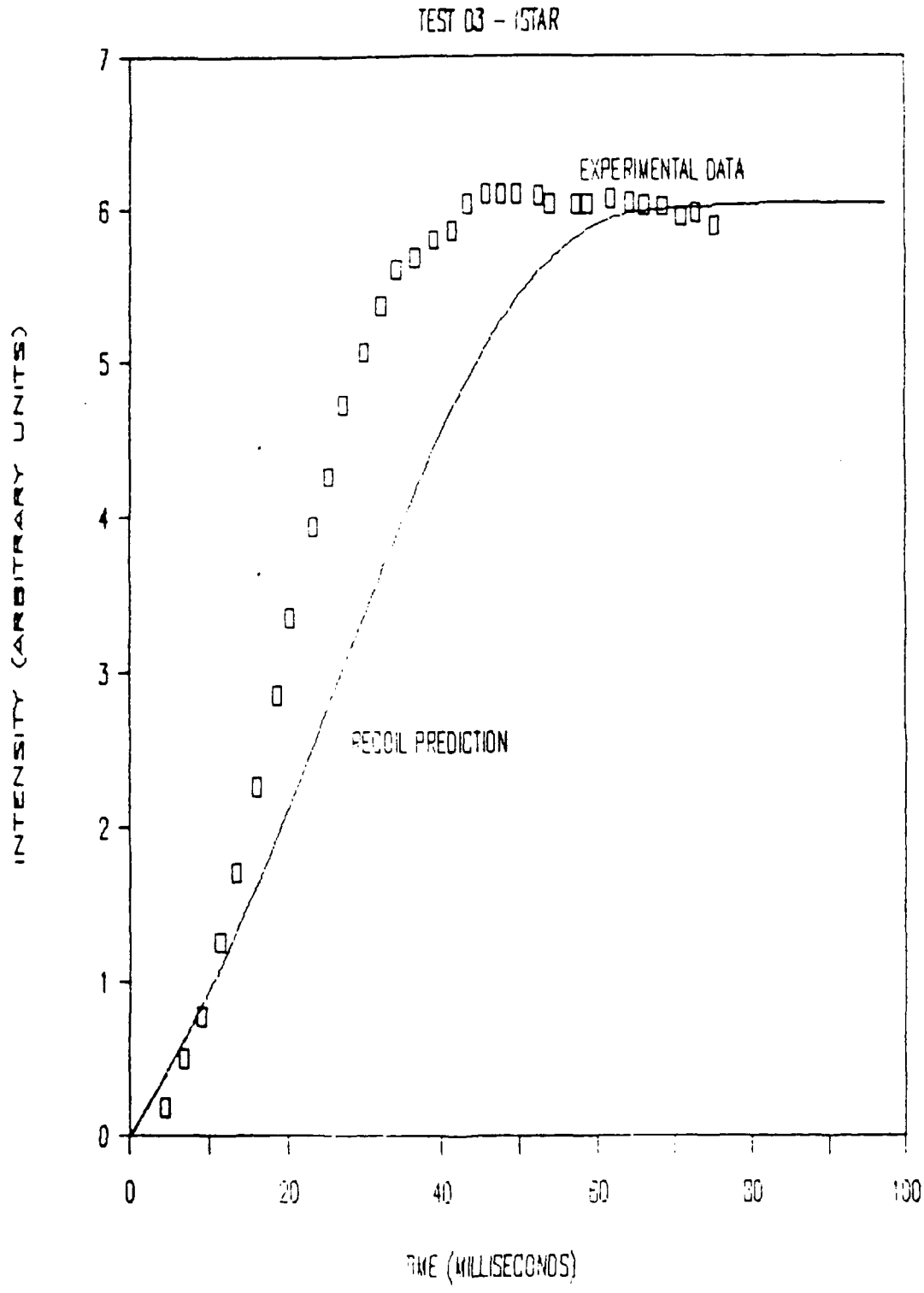

Figure 5. Comparison of 1-D Premixed Model Prediction to Heidner's Experimental Results. (Refs 2 and 14)

similar to Heidner's. Actual laser devices represent a significant scaling in flow velocity, pressure, and number density. Conversely, nozzle designs for optimum laser performance usually employ very complicated 3-D transverse injection. Even simplified representations of these geometries have proven to be very difficult and extremely expensive to accurately model. The more economical 1-D and 2-D models are of only limited value because they can be made to match experimental data only by changing measured kinetics rates. As a result, these methods inspire little confidence when attempting to scale current devices to higher powers.

A combined approach which utilizes the strengths of both modeling and experiment is needed to address the issues concerning poor COIL performance prediction. Properly used, models, analytical or numerical, are very powerful investigative tools. Models allow an investigator to carefully control conditions and mechanisms to slowly increase the complexity of the problem in a way not possible in experiment. Any model, however, is only as valid as the physical models and experimental data base upon which it is built. Development of an accurate model is essential because it implies a detailed understanding of the mechanisms responsible

New Approach

A new combined experimental and numerical effort has been initiated at the AFWL to once again address the iodine dissociation problem. The approach differs from the previous efforts. The objective, at least initially, is not to derive detailed kinetic rate data but to tie modeling employing the low speed flow tube kinetics data base to the laser performance data base. Instead of attempting to develop a more

sophisticated numerical scheme to improve the fluid dynamic modeling of an actual laser nozzle, the approach is to develop a much simpler, well diagnosed, experiment which can be modeled using existing techniques. The experimental device will employ a BHP/Cl_2 $O_2(^1\Delta)$ generator and delivery system to provide high concentrations of $O_2(^1\Delta)$ at low H_2O partial pressures. Unlike the actual laser nozzles however, the iodine will be injected from a two dimensional, subsonic slit injector. Figure 6 shows a comparison between the two geometries. A choke plate downstream of the slit injector insures that the cavity pressures are similar to the pressures encountered in the mixing region of the laser nozzle. A more detailed description of the experiment's design and expected operating performance as they relate to the numerical effort described below is given in Appendix A. Admittedly, the two dimensional mixing scheme will be less efficient but the simpler configuration will be much less difficult and expensive to model. This approach should allow comparison of the overall characteristics of the iodine dissociation mechanism to a numerical simulation when the fluid dynamics are well understood. The results of this comparison will allow for a better evaluation of the currently accepted kinetics rate package and will provide a baseline against which to test future changes.

Numerical Investigation

This thesis describes the development and exercising of a two-dimensional, reactive flow, thin-shear-layer numerical model to support the separate experimental effort described in Appendix A. The starting point for the numerical model was a 2-D boundary layer code developed by Lt Col Eric Jumper at AFIT (15) (16) to study HF/DF chemical kinetics. The code was modified to solve the COIL kinetics

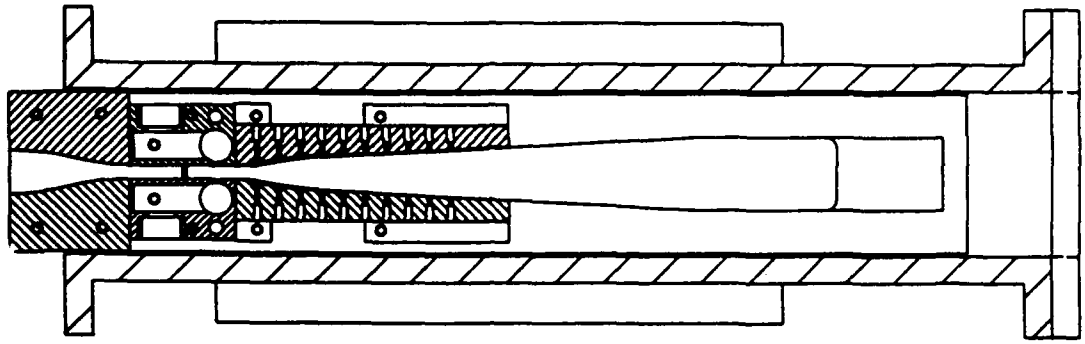

a)

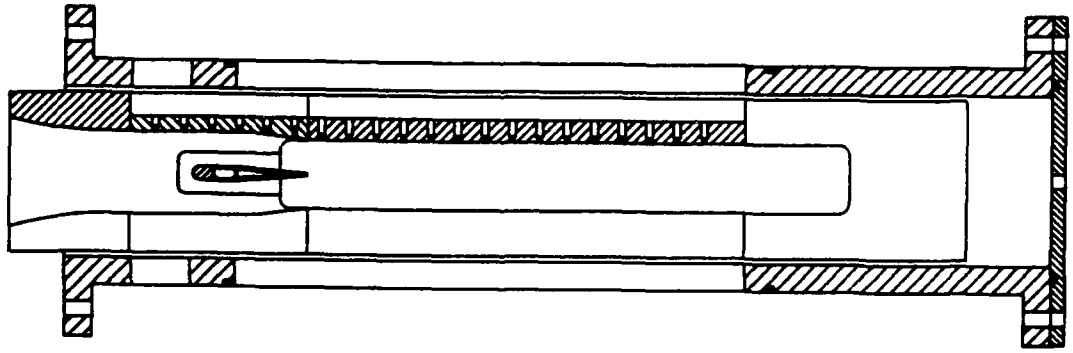

b)

Figure 6. Comparison of the 2-D and 3-D I_2 Nozzle Geometries. a) 3-D, Transonic, Transverse I_2 Nozzle Geometry. (I_2 is injected just upstream of the supersonic throat). b) 2-D, Parallel Jet I_2 Nozzle Geometry.

system for the two dimensional parallel jet problem. The code will eventually be needed for the combined experimental and numerical effort, but no comparisons to experimental data will be made here. Instead, this thesis presents the results of several cases used to verify the performance of the code and to investigate the roles of such important factors as mixing and water vapor in the the dissociation process. Some questions are raised about commonly accepted beliefs about the iodine dissociation in COIL devices. Finally, since the numerical cases were run for conditions similar to those expected in the experiment, the results will provide some insight to the design of the concurrent experiment.

III. Governing Equations

Navier Stokes Equations

The derivation of the differential equations which govern the flow of a two dimensional plane parallel jet begins with the steady-state set of compressible, multispecies Navier-Stokes equations (17).

Continuity:

$$\frac{\partial}{\partial x_j}(\rho u_j) = 0 \tag{3.1}$$

Momentum:

$$\rho u_j \frac{\partial u_i}{\partial x_j} = \frac{\partial \sigma_{ij}}{\partial x_j} \tag{3.2}$$

Mass Diffusion:

$$\rho u_k \frac{\partial W_j}{\partial x_k} = \dot{W}_j + \frac{\partial}{\partial x_k}\left(\gamma_j \frac{\partial W_j}{\partial x_k} \right) \tag{3.3}$$

Energy:

$$\rho u_k \frac{\partial h}{\partial x_k} = \left(u_k \frac{\partial P}{\partial x_k} \right) + \mu\phi + \frac{\partial}{\partial x_k}\left(\sum_j \gamma_j h_j \frac{\partial W_j}{\partial x_k} \right) + \frac{\partial}{\partial x_k}\left(k \frac{\partial T}{\partial x_k} \right) \tag{3.4}$$

where

$$\sigma_{ij} = -\left(P + \frac{2}{3}\mu \frac{\partial u_k}{\partial x_k} \right)\delta_{ij} + \mu\left(\frac{\partial u_i}{\partial x_j} + \frac{\partial u_j}{\partial x_i} \right)$$

$$\gamma_j = \rho D_j$$

$$\phi = \left(\frac{\partial u_i}{\partial x_j} + \frac{\partial u_j}{\partial x_i} - \frac{2}{3}\frac{\partial u_k}{\partial x_k}\delta_{ij} \right)\frac{\partial u_i}{\partial x_j}$$

The set of mass diffusion equations, Eq (3.3), account for the

convection and diffusion of each species across the differential control volume surface and, in the case of reacting flows, the creation of each species due to chemical reactions. The term $\dot{W}_j$ is defined as the mass rate of creation of species j per unit volume.

The energy equation contains two terms due to the presence of multiple species. In the second term on the right hand side of Eq (3.4), ϕ is the dissipation function. This term accounts for the conversion of kinetic energy into thermal energy by the action of viscous stresses. The third term is the change in enthalpy within the control volume due to diffusion of individual species across the control surface. Note, that the convection terms are written in terms of the total enthalpy of the flow where $h = \sum_j W_j h_j$. The conversion of "chemical" energy to thermal energy is, by definition, included in these terms. The energy equation can be rewritten employing the mass diffusion equations to express the addition of chemical energy to the flow in a more explicit form.

Substituting for the enthalpy in terms of the enthalpies of each species, and expanding both the convection and species diffusion terms using the chain rule gives,

$$\rho u_1 \frac{\partial}{\partial x_1}\left(\sum_j W_j h_j \right) - \rho u_1 \sum_j W_j \frac{\partial h}{\partial x_1^j} + \rho u_1 \sum_j h_j \frac{\partial W}{\partial x_1^j} \tag{3.5}$$

$$\frac{\partial}{\partial x_1}\left(\sum_j \gamma_j h_j \frac{\partial W}{\partial x_1^j} \right) - \sum_j \gamma_j \frac{\partial W}{\partial x_1^j} \frac{\partial h}{\partial x_1^j} + \sum_j h_j \frac{\partial}{\partial x_1}\left(\gamma_j \frac{\partial W}{\partial x_1^j} \right) \tag{3.6}$$

The last term in Eq (3.6) can be solved for from the mass diffusion equation (3.3).

$$\sum_j h_j \frac{\partial}{\partial x_1}\left(\gamma_j \frac{\partial W_j}{\partial x_k} \right) - \rho u_k \sum_j h_j \frac{\partial W_j}{\partial x_k} - \sum_j \dot{W}_j h_j \qquad (3.7)$$

The last term in Eq (3.7) is the change in enthalpy due to chemical reactions. Eq (3.7) can be substituted into Eq (3.6) for further simplification. Finally, if each component of the mixture is assumed to behave like an ideal gas, then, by definition of the specific heat,

$$c_{p_j} = \frac{\partial h_j}{\partial T} \qquad \text{and} \qquad c_p = \sum_j W_j c_{p_j}$$

The energy equation becomes:

$$\rho c_p \left(u_1 \frac{\partial T}{\partial x_1} \right) = u_1 \frac{\partial P}{\partial x_1} + \mu\phi - \sum_j \dot{W}_j h_j + \frac{\partial}{\partial x_1}\left(\sum_j \gamma_j \frac{\partial W_j}{\partial x_1} \frac{\partial h_j}{\partial x_1} \right)$$

$$+ \frac{\partial}{\partial x_1}\left(k \frac{\partial T}{\partial x_1} \right) \qquad (3.8)$$

Thin-Shear-Layer Equations

The complexity of the Navier-Stokes equations can be significantly reduced for a commonly occurring class of flows in which the viscous forces are confined to a thin layer relative to the overall flow field. This class is referred to as the boundary-layer approximation in the case of immersed bodies or, more generally, as the thin-shear-layers approximation in the case of jets, wakes, and mixing-layers (18). The plane parallel jet was in fact selected as the mixing scheme to be used in this investigation because it has been extensively studied (19) (20), and because it can be modeled using the thin-shear-layer equations.

The reduced set of governing equations for thin-shear-layers is derived by placing the following constraints on the Navier-Stokes

equations. First, the viscous-layers (including the thermal-layers and diffusion-layers) are thin relative to the characteristic streamwise dimension of the flow field. Let δ be thicknesses of the viscous shear-layer and L be a characteristic streamwise length, then this first constraint implies that $\delta/L \ll 1$. Similar requirements are placed on the thermal and diffusion boundary-layers. The second requirement is that the largest viscous term be of the same order of magnitude as the convective terms. The thin-shear-layer approximations can be applied to the Navier-Stokes equations in a number of ways. An order of magnitude analysis is used here on a term by term basis (See Schlichting (18) for more details). $\delta/L \ll 1$ implies that the streamwise dimension, x, is $O(L)$ while the transverse dimension, y, is $O(\delta)$. The streamwise velocity component must be $O(1)$. The terms of the continuity equation must be of the same order. $\partial u/\partial x \cong O(1)$ so the transverse velocity component, v, must be of $O(\delta/L)$. The pressure gradient term, $\partial P/\partial x$, in the streamwise momentum equation must be balance the convection terms in the inviscid limit, this implies that $\partial P/\partial x \cong O(1)$. The pressure gradient term in transverse momentum equation can not be of higher order than any of the other terms which is $O(\delta/L)$. The streamwise pressure gradient can then be rewritten as dP/dx. In general, for large Reynolds numbers, the terms $\partial^2(\ )/\partial x^2$ are of $O(\delta/L)$ or smaller. Neglecting terms of $O(\delta/L)$ and smaller results in the thin-shear-layer equations.

$$\frac{\partial}{\partial x}(\rho u) + \frac{\partial}{\partial y}(\rho v) = 0 \tag{3.9}$$

$$\rho u \frac{\partial u}{\partial x} + \rho v \frac{\partial v}{\partial y} = - \frac{dp}{dx} + \frac{\partial}{\partial y}\left(\mu \frac{\partial u}{\partial y} \right) \tag{3.10}$$

$$\rho u \frac{\partial W_j}{\partial x} + \rho v \frac{\partial W_j}{\partial y} = + \dot{W}_j + \frac{\partial}{\partial y}\left(\rho D_j \frac{\partial W_j}{\partial y} \right) \qquad (3.11)$$

$$\rho c_p \left(u \frac{\partial T}{\partial x} + v \frac{\partial T}{\partial y} \right) = u \frac{dp}{dx} + \mu \left(\frac{\partial u}{\partial y} \right)^2 - \sum_i \dot{W}_i h_i + \sum_i \rho D_i \frac{\partial W_i}{\partial y} \frac{\partial h_i}{\partial y} + \frac{\partial}{\partial y}\left(k \frac{\partial T}{\partial y} \right) \qquad (3.12)$$

von Mises Transformation

The 2-D, steady, thin-shear-layer equations can be recast into a more convenient form for numerical integration using the compressible stream function, ψ . The stream function is defined as the mass flow (per unit depth) between the origin and any point. By definition, there is no net flow of mass across lines of constant ψ . This does not, however, rule out net transport of individual species. The transformation from cartesian coordinates, x-y, to stream function coordinates, x-ψ, is accomplished using the von Mises transformation (15) (16).

$$\frac{\partial \psi}{\partial x} = -\rho v \qquad \text{and} \qquad \frac{\partial \psi}{\partial y} = \rho u$$

Then for any arbitrary function $f = f(x,y)$,

$$\frac{\partial f}{\partial x} = \frac{\partial f}{\partial \psi}\frac{\partial \psi}{\partial x} + \frac{\partial f}{\partial x}\frac{\partial x}{\partial x} = -\rho v \frac{\partial f}{\partial \psi} + \frac{\partial f}{\partial x}$$

$$\frac{\partial f}{\partial y} = \frac{\partial f}{\partial \psi}\frac{\partial \psi}{\partial y} + \frac{\partial f}{\partial x}\frac{\partial x}{\partial y} = \rho u \frac{\partial f}{\partial \psi}$$

Applying the von Mises transformation to the boundary-layer equations results in,

$$\frac{\partial u}{\partial x} = -\frac{1}{\rho u}\frac{dp}{dx} + \frac{\partial}{\partial \psi}\left(\mu \rho u \frac{\partial u}{\partial \psi}\right) \tag{3.13}$$

$$\frac{\partial W_j}{\partial x} = \frac{1}{\rho u}\dot{W}_j + \frac{\partial}{\partial \psi}\left(\rho D_j \rho u \frac{\partial W_j}{\partial \psi}\right) \tag{3.14}$$

$$\frac{\partial T}{\partial x} = \frac{1}{\rho c_p}\frac{dp}{dx} + \frac{\mu \rho u}{c_p}\left(\frac{\partial u}{\partial \psi}\right)^2 - \frac{1}{\rho u c_p}\sum_i \dot{W}_i h_i + \frac{1}{c_p}\sum_i \rho D_i \rho u \frac{\partial W_i}{\partial \psi}\frac{\partial h_i}{\partial \psi} + \frac{1}{c_p}\frac{\partial}{\partial \psi}\left(k \rho u \frac{\partial T}{\partial \psi}\right) \tag{3.15}$$

Thermodynamic Properties

The density of the mixture of gases was calculated from the ideal gas equation,

$$\rho = \frac{P}{\bar{R}\, T\, M_{mix}} \tag{3.16}$$

where M_{mix} is the molecular weight of the mixture.

$$M_{mix} = \sum_i \chi_i M_i$$

The specific heat and enthalpy for each of the component species of the gas were calculated using fourth order polynomial fits to the data tabulated in the JANAF Thermodynamic Tables (21).

$$c_{p_i} = a_0 + a_1 T + a_2 T^2 + a_3 T^3 + a_4 T^4 \tag{3.17}$$

$$h_i = b_0 + b_1 T + b_2 T^2 + b_3 T^3 + b_4 T^4 + E_i \tag{3.18}$$

The units from the JANAF tables are c_{p_i} [=] (kcal/mole K) and

h_i [-] (kcal/mole). The enthalpy data is referenced at 298.15 K. E_i is the heat of formation of species i (22),

$$E_i = \Delta H_{298} + hcN_A \nu_i$$

where

ΔH^0_{f298} = heat of formation of the ground state

ν_i = excitation energy of the i^{th} excited state (cm^{-1})

The excitation energies for the $O_2(^1\Delta)$ and $O_2(^1\Sigma)$ states of oxygen are 7,882 cm^{-1} and 13,121 cm^{-1}, respectively (20). The excitation energy of the excited iodine atom, I^*, is 7,603 cm^{-1}. As stated in Chapter II, however, the intermediate excited state of the iodine molecule, $I_2^\ddagger$, actually represents a number of vibrational states with $v'' \geq 43$. Little is known about the distribution of energies for the $I_2^\ddagger$ states. Inspection of Eqs (2.8) and (2.9) indicates that the excitation energy should be approximately the same as that of $O_2(^1\Delta)$ or I^*. The excitation energy for $I_2^\ddagger$ is therefore set equal to that for I^*, 7,603 cm^{-1}.

The specific heat of the mixture of gases is

$$c_p = \sum_i \chi_i c_{p_i}$$

The enthalpy of species i per gram is, h_i/M_i. The specific heat and enthalpy are converted to the CGS units (cm^2/s^2K) and (cm^2/s^2) respectively.

Transport Coefficients

The transport coefficients for viscous, thermal, and mass diffusion are derived form the kinetic theory of gases (24). Although expressions

for the transport coefficients can be obtained by modeling the molecules of a gas as rigid spheres, the correlation of the results with experimental data is poor. Better correlation is obtained using the Chapman-Enskog theory which derives the transport coefficients in terms of the potential energy of interaction between two molecules. The potential energy, φ, is related to the force of interaction between molecules by $F = - d\varphi/dr$ where r is the intermolecular distance. Kinetic theory does not provide a formal expression for $\varphi(r)$ however, there is an extensive empirical data base in terms of the Lennard-Jones potential.

$$\varphi = 4\epsilon \left[\left(\frac{\sigma}{r} \right)^2 - \left(\frac{\sigma}{r} \right)^2 \right]$$

σ is a characteristic diameter and ϵ is the maximum energy of attraction. Note that this empirical function displays the expected characteristics of weak attraction at large separations and and strong repulsion at short separations.

Viscosity. The expression for the viscosity of component i from the Chapman-Enskog theory is

$$\mu_i = \frac{2.6693 \times 10^{-5} \sqrt{M_i T}}{\sigma_i^2 \Omega_\mu} \qquad (3.19)$$

The Lennard-Jones parameters were obtained from Refs (24) and (25). Ω_μ, the reduced collision integral, is a slowly varying function of the parameter kT/ϵ. The reduced collision integral represents the departure from rigid sphere behavior. Ω_μ is calculated from a curve fit of data tabulated in Appendix B, Table B-2 of Ref (24).

The viscosity of a mixture of gases is calculated using the relation

$$\mu_{mix} = \sum_{i=1}^{N} \frac{\chi_i \mu_i}{\sum_{j=1}^{N} \chi_i \phi_{ij}} \tag{3.20}$$

where

$$\phi_{ij} = \frac{1}{\sqrt{8}} \left(1 + \frac{M_i}{M_j} \right)^{-1/2} \left[1 + \left(\frac{\mu_i}{\mu_j} \right)^{1/2} \left(\frac{M_j}{M_i} \right)^{1/4} \right]$$

Thermal Conductivity. The Chapman-Enskog formula for the thermal conductivity of a monatomic gas is

$$k_i = \frac{1.9891 \times 10^{-4} \sqrt{T/M_i}}{\sigma_i^2 \Omega_k} \tag{3.21}$$

where $\Omega_k = \Omega_\mu$.

The calculation of the thermal conductivity for a polyatomic gas must account for vibrational and rotational excitation as well as translational energy. The Eucken approximation provides a method to calculate the thermal conductivity of a polyatomic gas.

$$k_i = \left(c_{p_i} + \frac{5}{4} \frac{\bar{R}}{M_i} \right) \mu_i \tag{3.22}$$

The formula for calculating the thermal conductivity of the mixture is similar to Eq (3.20)

$$k_{mix} = \sum_{i=1}^{N} \frac{\chi_i k_i}{\sum_{j=1}^{N} \chi_i \phi_{ij}} \tag{3.23}$$

Diffusivity. The expression for the bimolecular diffusivity of species i into species j is very similar to the expressions for the viscosity and thermal conductivity of of a species.

$$D_{ij} = \frac{0.0018583 \sqrt{T^3 \left(\frac{1}{M_i} + \frac{1}{M_j} \right)}}{P \sigma_{ij}^2 \Omega_D} \tag{3.24}$$

Note that the Lennard-Jones potential is now the intermolecular potential between one molecule of species i and one molecule of species j.

$$\varphi_{ij} = 4\epsilon_{ij} \left[\left(\frac{\sigma_{ij}}{r} \right)^{12} - \left(\frac{\sigma_{ij}}{r} \right)^{6} \right]$$

Ω_D, the reduced collision integral for collisions between unlike molecules, is calculated from a curve fit of data tabulated in Appendix B, Table B-2, (24). The Lennard-Jones parameters are approximated by

$$\epsilon_{ij} = (\epsilon_i \epsilon_j)^{1/2}$$

$$\sigma_{ij} = (\sigma_i + \sigma_j)/2$$

The effective diffusion coefficient of species i into the mixture of gases is obtained by assuming that the diffusional velocities for all of

the species expect i are equal to some constant. The expression for the effective diffusion coefficient is

$$D_i = \frac{1 - \chi_i}{\sum_{\substack{j=1 \\ j \neq i}}^{N} \frac{\chi_i}{D_{ij}}} \tag{3.25}$$

Chemical Reactions

Standard AFWL COIL Rate Package. As discussed in the Introduction, AFWL hosted a conference to review the current state of the Chemical Oxygen-Iodine Laser (COIL) data base in August of 1987 (2). One product of this conference was a new standard reaction set for modeling COIL devices. The standard reaction set includes 50 reactions, many of which appear to have little influence at standard COIL operating conditions. As part of the preparation for the kinetics conference, Captains Glen Perram and Robert Crannage performed a set of sensitivity analyses to identify a reduced set of equations for use in numerical modeling. Their work identified two reduced sets. The first includes 22 reactions and gives excellent agreement with the full reaction set. The second includes the 11 most critical reactions and gives good agreement. In the interest of computational efficiency, the 11 reaction set was used in this investigation. Table 1 lists the reactions along with the accepted empirical rate constants. Note that this is the same set of reactions outlined in Chapter II.

There are several points that should be made about the reactions listed in Table 1. First, note that each reaction is presented in terms of a forward rate constant only. Where the backward reaction is significant, it is listed as a separate reaction with a corresponding

TABLE I

Air Force Weapons Laboratory Reduced COIL Rate Package

11 Reaction Set

	Kinetic Process	Recommended Rate Coefficient (cm^3/molecule-sec)
1.	$O_2(^1\Delta) + O_2(^1\Delta) \longrightarrow O_2(^1\Sigma) + O_2(^3\Sigma)$	$k_1 = 2.7 \times 10^{-17}$
2.	$O_2(^1\Sigma) + H_2O \longrightarrow O_2(^3\Sigma) + H_2O$	$k_2 = 6.7 \times 10^{-12}$
3.	$I_2(X) + O_2(^1\Sigma) \longrightarrow I + I + O_2(^3\Sigma)$	$k_3 = 4.0 \times 10^{-12}$
4.	$I_2(X) + O_2(^1\Delta) \longrightarrow I_2^{\ddagger} + O_2(^3\Sigma)$	$k_4 = 7.0 \times 10^{-15}$
5.	$I_2(X) + I^* \longrightarrow I_2^{\ddagger} + I$	$k_5 = 3.8 \times 10^{-11}$
6.	$I_2^{\ddagger} + O_2(^1\Delta) \longrightarrow I + I + O_2(^3\Sigma)$	$k_6 = 3.0 \times 10^{-10}$
7.	$I_2^{\ddagger} + H_2O \longrightarrow I_2 + H_2O$	$k_7 = 3.0 \times 10^{-10}$
8.	$I + O_2(^1\Delta) \longrightarrow I^* + O_2(^3\Sigma)$	$k_8 = 7.8 \times 10^{-11}$
9.	$I^* + O_2(^3\Sigma) \longrightarrow I + O_2(^1\Delta)$	$k_9 = 2.7 \times 10^{-11}$
10.	$I^* + O_2(^1\Delta) \longrightarrow I + O_2(^1\Sigma)$	$k_{10} = 1.1 \times 10^{-13}$
11.	$I^* + H_2O \longrightarrow I + H_2O$	$k_{11} = 2.0 \times 10^{-12}$

rate constant. For example, reaction 7 is the laser pumping reaction and reaction 8 is the reverse. Second, the rate listed for reaction 2 is not a physically measured rate. For the system of excited oxygen and water vapor, the known rates are for reaction 1 and for the total removal of $O_2(^1\Delta)$ to all products. In this reduced set, the rate for reaction 2 has been set to produce the same overall removal rate. Finally, a limited data base does exist for the temperature dependence of these rates. This data is presented in Table 2.

Chemical Rate Equations. Each of the reactions in Table 1 can be written in the general form (26)

$$\nu_1' X_1 + \nu_2' X_2 + \cdots\cdots \longrightarrow \nu_1'' X_1 + \nu_2'' X_2 + \cdots\cdots \tag{3.25}$$

or as

$$\sum_{s=1}^{l} \nu_s' X_s \longrightarrow \sum_{s=1}^{l} \nu_s'' X_s \tag{3.26}$$

where X_s is any chemical species, ν_s' is the stoichiometric coefficient for the reactant, and ν_s'' is the stoichiometric coefficient for the product. Note that in this notation, X_s appears on both sides of the reaction.

The molar rate of formation of any one of the products can be expressed as

$$\frac{d}{dt}\left[X_s \right] = \nu_s'' k_c N_A \left[X_1 \right]^{z_1} \left[X_2 \right]^{z_2} \cdots\cdots \tag{3.27}$$

where k_c [=] (moles/cm^{3}sec) is the molar rate constant and the product on the right hand side is taken over all of the reactants. For single step reactions or sets of elementary processes, the exponents, z_s's, are equal to the stoichiometric coefficients. Similarly, the disappearance

TABLE II

Available Temperature Dependent Rate Data for the COIL Kinetics

$$k_1 = 9.5 \times 10^{-28}\, e^{(700/T)}$$

$$k_5 = 1.4 \times 10^{-13}\, e^{(1660/T)}$$

$$k_8 = 2.33 \times 10^{-8} / T$$

$$k_9 = \frac{3.1 \times 10^{-8}}{T}\, e^{(-403/T)}$$

$$k_{10} = \frac{4.0 \times 10^{-24}}{T^{3.8}}\, e^{(700/T)}$$

of each of the reactants is

$$\frac{d}{dt}\left[X_s \right] = -\nu_s' k_c N_A \left[X_1 \right]^{z_1} \left[X_2 \right]^{z_2} \cdots \quad (3.28)$$

The total molar rate of creation of each species is the summation of the creation and disappearance terms for that species summed over all of the reactions, N

$$\frac{d}{dt}\left[X_s \right]_{net} = \sum_{n=1}^{N} (\nu_s'' - \nu_s') k_c N_A \left[X_1 \right]^{z_1} \left[X_2 \right]^{z_2} \cdots \quad (3.29)$$

The mass rate of creation of species j is then simply

$$\dot{W}_j = M_j \frac{d}{dt}\left[X_s \right]_{net} \quad (3.30)$$

IV. Numerical Analysis

Integration Scheme

Numerical methods for integrating the boundary-layer equations have been studied extensively over the past four decades. Anderson et al. (27) provides an excellent review of many of the most common methods. Selection of a particular scheme, an explicit or an implicit method, requires careful consideration of such factors as the nature of the problem, efficiency and accuracy of the scheme, and the complexity of the method. For this investigation, a simple explicit marching scheme was selected. It has the advantage of being very straight forward and adapts well to reactive flows. The major draw back of an explicit scheme is the limitation required on the marching step size. While an implicit scheme would be unconditionally stable and usually more efficient, it would be more difficult to implement. In addition, the species creation rates adds a further constraint on the marching step size. This term would tend to increase the number of iterations required to converge each streamwise step in an implicit method, thus decreasing the efficiency advantage.

Finite-Difference Formulas

The finite-difference approximations to the partial derivatives of an arbitrary function, $f(x,\phi)$, are expressed here as truncated Taylor series of $f(x,\psi)$ on a nonuniform grid. Figure 7. shows the configuration and nomenclature of the finite-difference cell in the stream, (a), at the centerline, (b), and at the freestream boundary, (c).

Interior Nodes. The partial of $f(x,\psi)$ with respect to x is

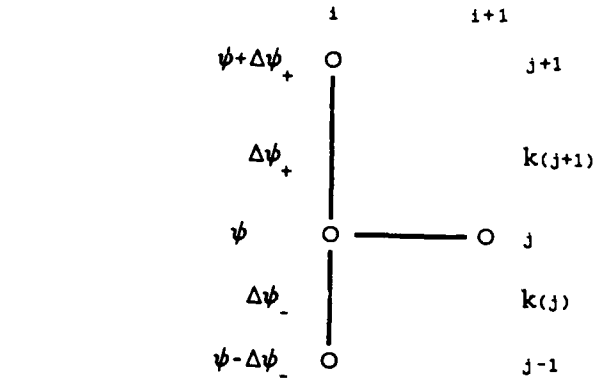

a)

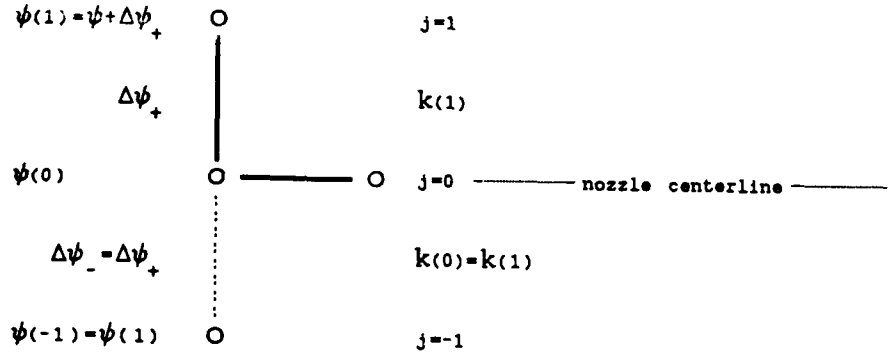

b)

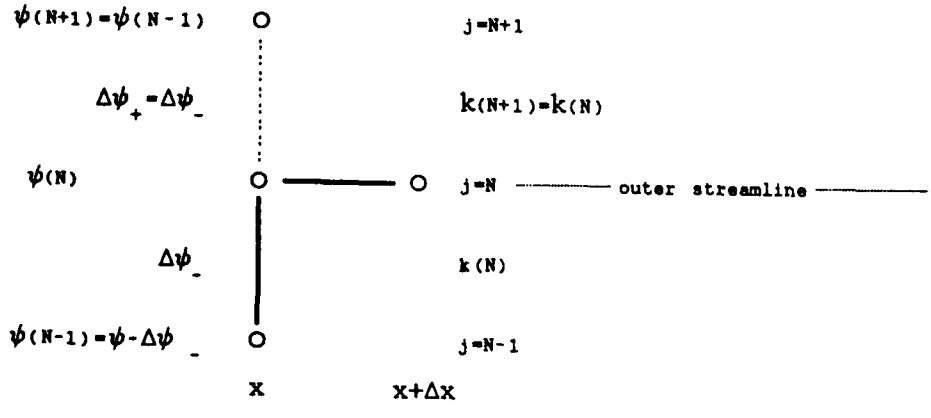

c)

Figure 7. Finite-Difference Grid Notation. a) Interior node. b) Nozzle centerline. c) Outer streamline.

evaluated using a first order forward-difference.

$$\frac{\partial}{\partial x} f(x,\psi) = \frac{f(x+\Delta x,\psi) - f(x,\psi)}{\Delta x} + O(\Delta x) \qquad (4.1)$$

The first and second partials with respect to ψ are evaluated using second order central-differences.

$$\frac{\partial}{\partial \psi} f(x,\psi) = \frac{\Delta\psi_-^2 f(x,\psi+\Delta\psi_+) - (\Delta\psi_-^2-\Delta\psi_+^2) f(x,\psi) - \Delta\psi_+^2 f(x,\psi-\Delta\psi_-)}{(\Delta\psi_-\Delta\psi_+^2 + \Delta\psi_-^2\Delta\psi_+)} + O(\Delta\psi^2) \qquad (4.2)$$

$$\frac{\partial^2}{\partial \psi^2} f(x,\psi) = 2\left[\frac{\Delta\psi_- f(x,\psi+\Delta\psi_+) - (\Delta\psi_-+\Delta\psi_+) f(x,\psi) + \Delta\psi_+ f(x,\psi-\Delta\psi_-)}{(\Delta\psi_-\Delta\psi_+^2 + \Delta\psi_-^2\Delta\psi_+)}\right] + O(\Delta\psi^2) \qquad (4.3)$$

Boundary Nodes. The problem of interest here is a two dimensional parallel jet. For these initial numerical investigations, it is further assumed that the jet is a free jet, that is a jet in an unconfined free stream. The jet is symmetric about the centerline which implies that there are no transverse gradients at the centerline. If the centerline is selected as the origin for ψ,

$$\frac{\partial}{\partial \psi} f(x,0) = 0 \qquad (4.4)$$

Approximating $\partial f/\partial\psi$ with a central-difference, Eq (4.2), about the centerline (see Figure 7 (b)), Eq (4.4) is satisfied for $\Delta\psi_- = \Delta\psi_+$ and $f(x,\psi-\Delta\psi_-) = f(x,\psi+\Delta\psi_+)$. When this result is substituted into the central-difference for $\partial^2 f/\partial x^2$, an expression for the second partial

with respect to ψ at the centerline is obtained.

$$\frac{\partial^2}{\partial\psi^2} f(x,0) = 2\left[\frac{f(x,\Delta\psi_+) - f(x,0)}{\Delta\psi_+^2}\right] \tag{4.5}$$

As stated, the freestream for a free jet is unconfined. If a streamline is selected (line of constant ψ) sufficiently far away from the jet, one would expect the gradients transverse to the streamline to be zero.

$$\frac{\partial}{\partial\psi} f(x,\psi_{fs}) = 0 \tag{4.6}$$

A similar expression to Eq (4.5) can be derived at the outer streamline, $\psi = \psi_{fs}$ (see Figure 7 (c)).

$$\frac{\partial^2}{\partial\psi^2} f(x,\psi_{fs}) = 2\left[\frac{f(x,\psi_{fs}-\Delta\psi_-) - f(x,\psi_{fs})}{\Delta\psi_-^2}\right] \tag{4.7}$$

Explicit Finite-Difference Equations

The finite-difference formulas for $\partial f/\partial\psi$ and $\partial^2 f/\partial\psi^2$ defined above can be rewritten in terms of general difference operators.

$$\frac{\Delta}{\Delta\psi} f(x,\psi) = \frac{A_1 f(x,\psi_A) + B_1 f(x,\psi_B) + C_1 f(x,\psi_C)}{D} \tag{4.8}$$

$$\frac{\Delta^2}{\Delta\psi^2} f(x,\psi) = 2\left[\frac{A_2 f(x,\psi_A) + B_2 f(x,\psi_B) + C_2 f(x,\psi_C)}{D}\right] \tag{4.9}$$

Details of the values for the coefficients A_1, B_1, C_1, A_2, B_2, C_2, D, ψ_A, ψ_B, and ψ_C are given in Appendix B.

The thin-shear-layer equations in Eqs (3.13), (3.14), and (3.15) were approximated using the finite-difference formulas defined above. In terms of the finite-difference operators, the governing equations become,

$$u(x+\Delta x) = u(x) + \Delta x \left[- \frac{1}{\rho u} \frac{dp}{dx} + \frac{\Delta}{\Delta \psi} (\mu \rho u) \frac{\Delta u}{\Delta \psi} + \mu \rho u \frac{\Delta^2 u}{\Delta \psi^2} \right] \tag{4.10}$$

$$W_j(x+\Delta x) = W_j(x) + \Delta x \left[\frac{1}{\rho u} \dot{W}_j + \frac{\Delta}{\Delta \psi} (\rho D_j \rho u) \frac{\Delta W}{\Delta \psi}_j + \rho d \, \rho u \frac{\Delta^2 W}{\Delta \psi^2}_j \right] \tag{4.11}$$

$$T(x+\Delta x) = T(x) + \Delta x \left[\frac{1}{\rho c_p} \frac{dp}{dx} + \frac{\mu \rho u}{c_p} \left(\frac{\Delta u}{\Delta \psi} \right)^2 - \frac{1}{\rho u c_p} \sum_j \rho \dot{W}_j h_j \right.$$

$$\left. + \frac{1}{c_p} \left[\sum_j \rho D_j \rho u \frac{\Delta W}{\Delta \psi}_j \frac{\Delta h}{\Delta \psi}_j \right] + \frac{1}{c_p} \left[\frac{\Delta}{\Delta \psi} (k \rho u) \frac{\Delta T}{\Delta \psi} + k \rho u \frac{\Delta^2 T}{\Delta \psi^2} \right] \right] \tag{4.12}$$

Numerical Stability

One disadvantage of explicit finite-difference formulations is that a maximum step size limitation must be imposed in order to obtain a stable solution. Determining the exact criteria for the step size limitation for Eqs (4.10), (4.11), and (4.12) is difficult due to the nonlinear nature of the equations. Normally, in the absence of chemical reactions, stability of the finite-difference equations will be controlled by one of the diffusive terms (viscous, thermal, or mass). In reacting flows, however, an additional difficulty is encountered. The formation of each of the species is a chemical rate process with a corresponding time scale. If the time scale of the streamwise marching,

$(\Delta x/u)$, is larger than the time scale of the chemical rate process, the solution of the chemical kinetics can become unstable; however, even "fast" chemical processes tend to be rapidly modulated by the ability of the reactant species to diffuse to the reaction front.

The stability of a finite-difference equation is determined by examining the effect of introducing small errors (from numerical round off for instance) into the numerical solution. If the error is amplified, the equations are unstable. The most common approach used to investigate stability is the von Neumann error analysis. If the numerical solution to a finite-difference equation is expressed as the sum of the exact solution plus an error, it can be shown that any numerical error must also satisfy the deference equation. The error distribution is then expressed in terms of a Fourier series with a wave number which is dependent on the grid spacing. The amplification of an arbitrary Fourier component is determined by substituting into the finite-difference equation.

In order to examine the stability of the finite-difference formulation employed here, the effect of the diffusion terms on the stability of the mass diffusion equations is addressed by ignoring the species creation term.

$$\frac{\partial W}{\partial x} = \frac{\partial}{\partial \psi}\left[\alpha \frac{\partial W}{\partial \psi}\right] \tag{4.13}$$

where $\alpha = \rho D \rho u$. Application of the von Neumann stability analysis to Eq (4.13) can be simplified by recasting the finite-difference approximation for the diffusion term in a slightly different form. Instead of expanding the diffusion term using the chain rule, the diffusion term is evaluated as follows.

$$\frac{\partial}{\partial \psi}\left[\alpha \frac{\partial W}{\partial \psi^j}\right] = \frac{\left(\alpha \frac{\partial W}{\partial \psi^j}\right)\Big|_{j+1/2} - \left(\alpha \frac{\partial W}{\partial \psi^j}\right)\Big|_{j-1/2}}{\left(\frac{(\Delta\psi_+ + \Delta\psi_-)}{2}\right)} \tag{4.14}$$

where,

$$\left(\alpha \frac{\partial W}{\partial \psi^j}\right)\Big|_{j+1/2} = \left(\frac{\alpha_{j+1} + \alpha_j}{2}\right)\left(\frac{W_{j+1} - W_j}{\Delta\psi_+}\right) \tag{4.15}$$

$$\left(\alpha \frac{\partial W}{\partial \psi^j}\right)\Big|_{j-1/2} = \left(\frac{\alpha_j + \alpha_{j-1}}{2}\right)\left(\frac{W_j - W_{j-1}}{\Delta\psi_-}\right) \tag{4.16}$$

The finite-difference approximation to Eq (4.13) is then

$$W_{i+1} = W_i + 2\,\Delta x\left[\frac{\alpha_{j+1/2}(W_{j+1} - W_j)}{\Delta\psi_+(\Delta\psi_+ + \Delta\psi_-)} + \frac{\alpha_{j-1/2}(W_j - W_{j-1})}{\Delta\psi_-(\Delta\psi_+ + \Delta\psi_-)}\right] \tag{4.17}$$

The von Neumann stability analysis can then be applied to Eq (4.17) by approximating the error as

$$\epsilon(x,\psi) = e^{ax}e^{ik\psi}$$

and requiring the absolute magnitude of the amplification be less than or equal to one. The resulting stability criteria for Eq (4.17) is

$$\Delta x \le \frac{\Delta\psi_-\Delta\psi_+(\Delta\psi_- + \Delta\psi_+)}{2(\Delta\psi_-\alpha_{j+1/2} + \Delta\psi_+\alpha_{j-1/2})} \times C \tag{4.18}$$

The stability criteria for momentum or thermal diffusion is identical

with $\alpha = \mu\rho u$ and $\alpha = k\rho u$, respectively. In the absence of large velocity or temperature gradients, mass diffusion usually controls the stability.

This analysis is only approximate and does not provide an absolute stability criteria. Coupling between the equations, the presence of artificially large gradients in the initial conditions, and the stability of the chemical rate processes are not addressed. The constant C ($0.0 < C < 1.0$) in Eq (4.18) allows the diffusion limit to be further reduced in order to obtain a stable solution. Experience has shown that C 0.05 is required for the problem under investigation here. In addition, for the initial starting conditions where the species gradients are set to step functions at the jet boundary, C is further reduced to 0.01 and allowed to increase linearly with streamwise position to 0.05.

V. Results and Discussion

Introduction

The COIL kinetic rate package was combined with the thin-shear-layer equations and a simple explicit integration scheme (Chapters III and IV) to create a numerical model to be used in concert with the planned two dimensional jet experiment to investigate I_2 dissociation. The resulting code, COILFT, is listed in Appendix C. This section presents the results of several numerical investigations conducted to validate this code and demonstrate its capabilities as an investigative tool. The first case presented is a comparison with the results of a nonequilibrium chemistry code to validate the chemistry model installed in COILFT. The next series of cases compares a set of premixed cases (i.e., the O_2 and I_2 are uniformly mixed) and simple jet-mixed cases (i.e., a secondary jet of I_2 is injected in a parallel sheet into the O_2 primary flow) in order to investigate the influence of "mixing" on the dissociation process. The last set of cases are intended to demonstrate the role that water vapor plays in the dissociation process for both the premixed and jet-mixed cases. The intent is to perform some simple, well-defined numerical experiments (simulations) that will aid in building some rational feel for and raise questions about common perceptions concerning the performance of COIL lasers (c.f., preceding chapters). Finally, although this work is intended to stand on its own, the jet dimensions and velocity range were chosen to bear some resemblance to the concurrent experimental program. In this regard, then, the results of this study will be useful in guiding the eventual experimental design of the concurrent effort (c.f.,

previous chapters).

Validation of COIL Chemistry Package

Figure 8 shows a comparison of the time dependent concentration profiles of $O_2(^1\Delta)$, I_2, and I^* calculated using COILFT and those from the presently accepted "canonical" nonequilibrium chemistry code, SENCHEM (28). SENCHEM calculates the concentrations of various mixtures due to the eleven reaction set referred to earlier (c.f., Table I, Chapter III) as a function of time at constant pressure and temperature. It should be noted the SENCHEM is purely a kinetics code and is incapable of describing fluid mechanic coupling. In order to compare to the SENCHEM results, COILFT was set up with a uniformly mixed (i.e. no mixing) initial condition for the same mixture, pressure, and temperature as SENCHEM and a uniform initial velocity. The resulting concentration of each species verses position downstream was then transformed to time by dividing the position by the velocity. The initial conditions used for this comparison are listed in Table III. This comparison between the two computational models was used to trouble shoot the installation of the COIL chemistry package into the thin-shear-layer code and to validate the results. Reference to Figure 8 shows that essentially no differences exist between the results of the two codes, i.e., we can have high confidence that the kinetics in COILFT function properly.

Mixing Studies

The next six cases presented here are intended to provide insight into the role mixing plays in the I_2 dissociation process. The first three runs were for parallel jet cases with varying ratios of the secondary jet (I_2 and diluent) velocity to the primary freestream (O_2

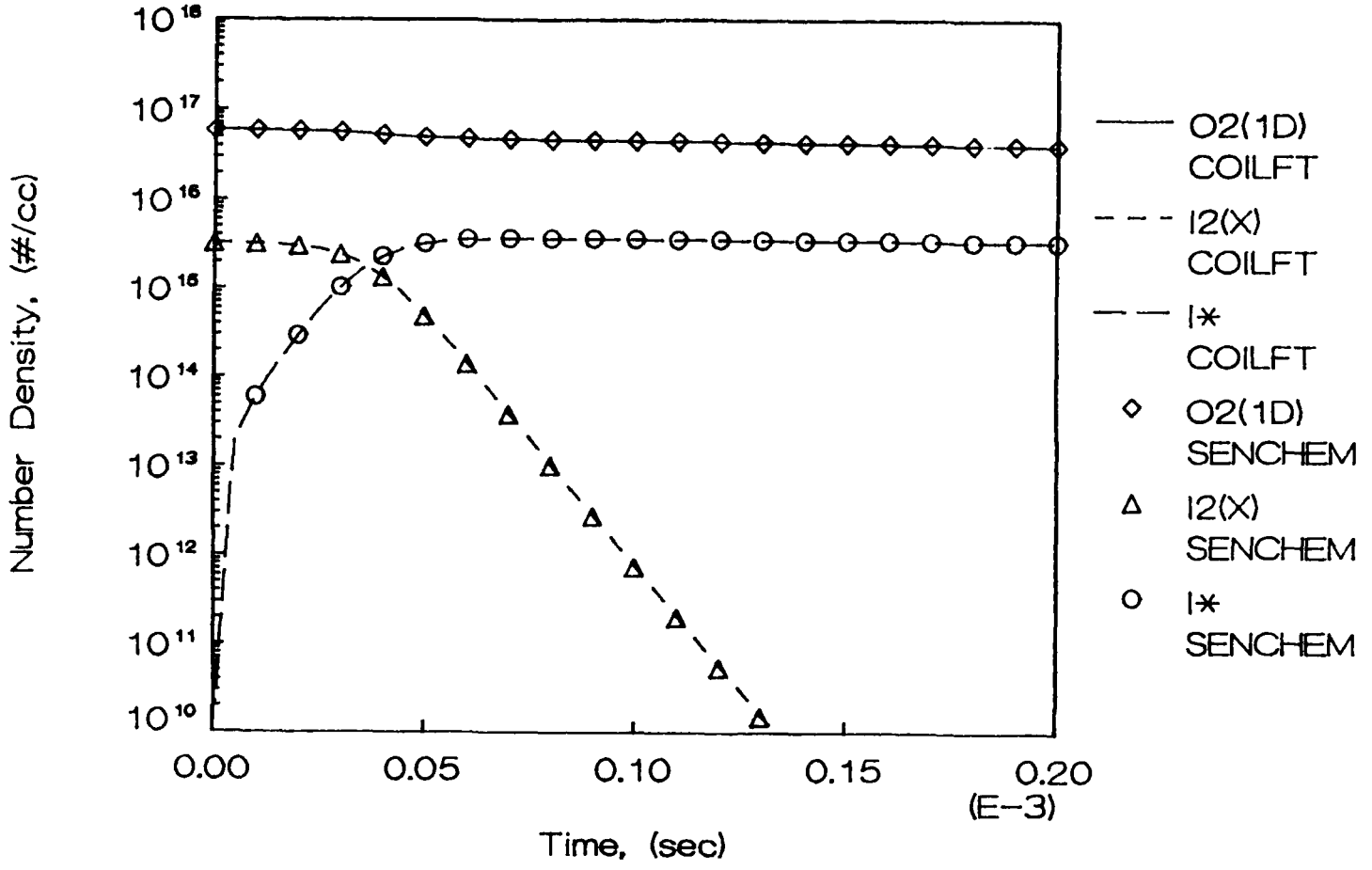

Figure 8. Comparison of the O_2, I_2, and I^* Profiles Predicted by the Codes SENCHEM and COILFT.

TABLE III

Initial Conditions for COIL Chemistry Validation Case

Temperature	300.0 K	
Pressure	3.33×10^4 dyne/cm^2	(25.0 torr)
Velocity	5,550.0 cm/sec	

Concentrations

Species	Number Density (molecule/cm^3)	Mole Fraction
$O_2(^3\Sigma)$	8.85×10^{16}	0.1100
$O_2(^1\Delta)$	5.91×10^{16}	0.0734
$O_2(^1\Sigma)$	8.05×10^{13}	0.0001
$I_2(x)$	3.22×10^{15}	0.0040
$I_2^{\ddagger}$	0.0	0.0
I	0.0	0.0
I^*	0.0	0.0
He	6.39×10^{17}	0.7936
H_2O	3.22×10^{15}	0.0440
Cl_2	1.12×10^{16}	0.0149

and diluent) velocity. At the lower limit, this ratio is set to one and mixing between the two streams is due solely to molecular diffusion of the species. As the jet velocity increases relative to the freestream velocity, the oxygen stream becomes "entrained" into the iodine stream resulting in increased mixing. Entrainment is used here to describe the process by which the higher velocity secondary jet accelerates the primary flow through shear; the increasing velocity of the primary flow gives rise to a component of velocity in the primary flow toward the secondary jet, thereby adding a convective transport mechanism for the $O_2(^1\Delta)$ in the direction of the I_2. This transport tends to increase the concentration gradient for molecular transport, thus enhancing the rate of molecular mixing. The next three are "premixed" cases representing the ideal instantaneous mixing of the oxygen and iodine streams of the three jet cases at the initial plane, not unlike the chemistry verification run of the previous section.

Geometry and Initial Conditions. The geometry and flow conditions for the jet-mixed cases were chosen to approximate those of the concurrent experimental study discussed in Chapter II. The configuration and expected performance of both the oxygen generator and iodine injection nozzle are discussed briefly Appendix A. Figure 9 is a schematic of the computational domain for the parallel jet cases (simplified from the experimental test section diagram in Figure A1, Appendix A) which illustrates the setup of the numerical cases. The solutions were begun at the nozzle exit plane where the velocity, temperature, and species mole fractions were taken to be uniform "slug" profiles for both the jet and freestream flows. The pressure was specified. Taking advantage of the symmetry, the numerical solutions

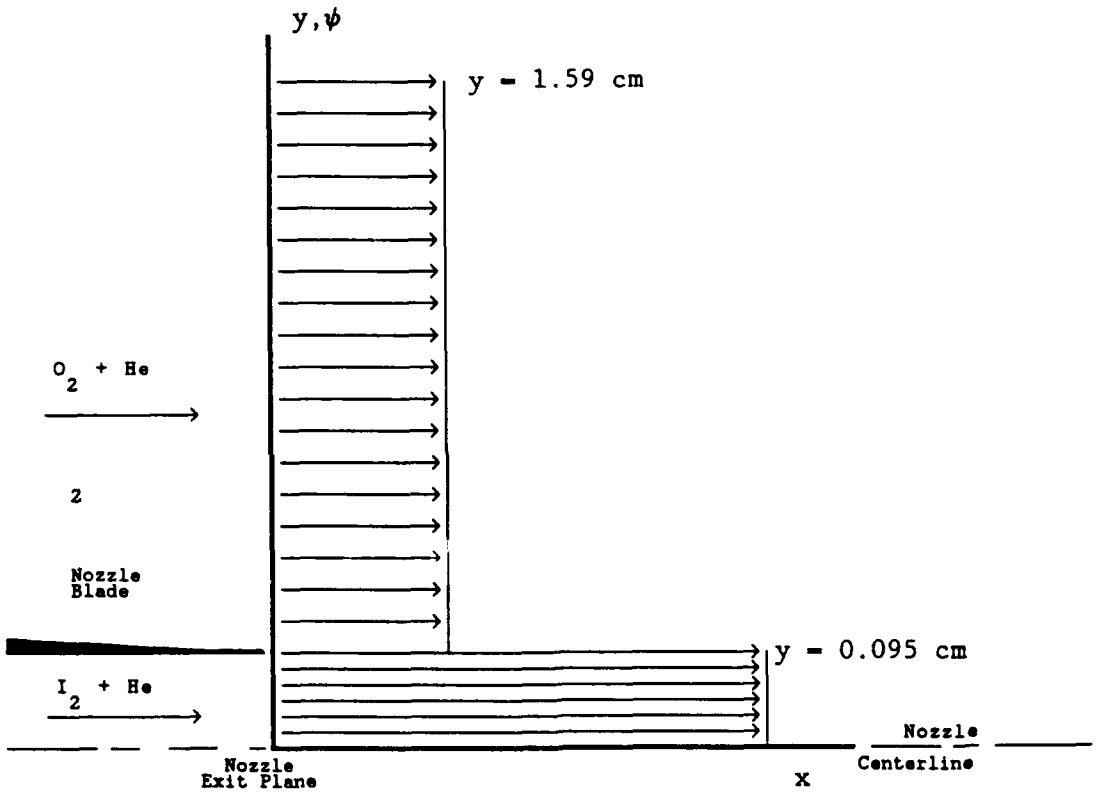

Figure 9. Schematic of the Computational Domain for the Parallel Jet Cases.

were calculated from the nozzle centerline to the "wall" (the wall itself was not modeled). The combined height (cavity half height) of the jet and freestream flows was 0.625 inches (1.59 cm) and the nozzle height for the secondary jet alone was 0.0375 inches (0.095 cm). Six finite-difference nodes (in the y/ψ direction) were placed in jet with twenty-seven in the freestream.

Three jet-mixed cases with ratios between the jet velocity and the freestream velocity of 1/1, 3/1, and 6/1 were run. The jet Mach Numbers ranged from 0.1 to 0.4. The freestream Mach Number was approximately 0.1. The velocity ratio of the jet was changed by changing the amount of diluent (helium carrier in this case) in the jet. Note, the flow rate of iodine was held constant although the the iodine mole fraction

changed with increasing diluent. The freestream flows were held constant. The initial conditions for these three cases are listed in Table IV.

For comparison, three premixed cases were also run. These cases were created by uniformly mixing the freestream and jet flows for each of the jet-mixed cases. In order to allow for some rational basis of comparison between the premixed and jet-mixed cases, the velocities for the premixed cases were set equal to the corresponding jet velocity. By comparing premixed and jet-mixed cases in this way, the common factor was the time that the I_2 was exposed to the $O_2(^1\Delta)$. The criteria was not strictly adhered to however, since the secondary jet did lose velocity with time. The initial conditions for these premixed cases are listed in Table V.

Assumptions and Simplifications. Before examining the results of these test cases, it is important to be aware of the assumptions and simplifications made in selecting both the initial conditions and boundary conditions for these numerical cases. Some of the caveats placed on these results are implicit in the solution while others have been made in order to isolate the specific influence of mixing and water vapor and to make the results easier to interpret. Where prudent, the boundary conditions have been simplified to reduce the computational complexity.

An implicit assumption in the discussion to this point is that the chemical kinetics package employed in COILFT accurately reflects the actual physical processes. Confirming the accuracy of the current COIL kinetics package is, in fact, the purpose of the synergistic concurrent experimental and computational program of which this effort is a part.

TABLE IV

Initial Conditions for the Jet Mixing Cases

Freestream	1/1 Velocity Ratio		3/1 Velocity Ratio		6/1 Velocity Ratio	
Temperature	300.0 K		300.0 K		300.0 K	
Pressure	2.9795×10^4 dyne/cm^2		3.1449×10^4 dyne/cm^2		3.3635×10^4 dyne/cm^2	
Velocity	6228.4 cm/sec		5900.8 cm/sec		5518.9 cm/sec	
Species	Flow Rate (mmole/sec)	Mole Fraction	Flow Rate (mmole/sec)	Mole Fraction	Flow Rate (mmole/sec)	Mole Fraction
$O_2(^3\Sigma)$	18.0	0.15	18.0	0.15	18.0	0.15
$O_2(^1\Delta)$	12.0	0.10	12.0	0.10	12.0	0.10
$O_2(^1\Sigma)$	0.0	0.0	0.0	0.0	0.0	0.0
He	90.0	0.0	90.0	0.0	90.0	0.0
H_2O	0.0	0.0	0.0	0.0	0.0	0.0
Cl_2	0.0	0.0	0.0	0.0	0.0	0.0
Jet						
Temperature	400.0 K		400.0 K		400.0 K	
Pressure	2.9795×10^4 dyne/cm^2		3.1449×10^4 dyne/cm^2		3.3635×10^4 dyne/cm^2	
Velocity	6228.4 cm/sec		17702.5 cm/sec		31273.8 cm/sec	
Species	Flow Rate (mmole/sec)	Mole Fraction	Flow Rate (mmole/sec)	Mole Fraction	Flow Rate (mmole/sec)	Mole Fraction
I_2	0.6	0.111	0.6	0.037	0.6	0.02
He	4.8	0.889	15.6	0.963	30.0	0.98

TABLE V

Initial Conditions for the 1-D, Premixed Cases

Associated Jet-Mixed Case	1/1	3/1	6/1
Temperature (K)	400.0	400.0	400.0
Pressure (dyne/cm^2)	2.9795×10^4	3.1449×10^4	3.3635×10^4
Velocity (cm/sec)	6228.4	17702.5	31273.8
Concentrations (mole fraction) Species			
$O_2(^3\Sigma)$	0.1435	0.1322	0.1195
$O_2(^1\Delta)$	0.0957	0.0881	0.0797
$O_2(^1\Sigma)$	0.0	0.0	0.0
$I_2(x)$	0.0048	0.0044	0.0040
$I_2^{\ddagger}$	0.0	0.0	0.0
I	0.0	0.0	0.0
I^*	0.0	0.0	0.0
He	0.7560	0.7753	0.7968
H_2O	0.0	0.0	0.0
Cl_2	0.0	0.0	0.0

Even if the individual kinetic rates are correct, the reduced eleven reaction set is not necessarily valid. Note, for instance, that the initial concentrations of H_2O and $O_2(^1\Sigma)$ are set to zero for all of the cases in Table IV and V. In an actual device, it is essentially impossible to eliminate all of the H_2O vapor. Even at low concentrations, H_2O vapor is the strongest quenching mechanism for $O_2(^1\Sigma)$, $I_2^{\ddagger}$, and I^*. This fact allowed the removal of all other quenching mechanisms from the eleven reaction set. In the absence of H_2O, other loss mechanisms not included in Table I could become important. Furthermore, assuming that our knowledge of the complete reaction set is sound, we know that in the presence of H_2O, $O_2(^1\Sigma)$ reaches an equilibrium value between production from $O_2(^1\Delta)$ pooling (Eq 2.3) and quenching with H_2O (Eq 2.4). In the absence of H_2O, the $O_2(^1\Sigma)$ concentration would slowly rise to unrealistic concentrations. Since $O_2(^1\Sigma)$ plays a role in initiating the dissociation of I_2 (Eq 2.6), the dissociation rates would be accelerated. Ignoring H_2O in the initial conditions effectively slows this affect. The assumption of no H_2O in the initial conditions does, however, allow for a clearer interpretation and makes understanding of the results presented here possible. The role of H_2O is treated independently in a separate set of numerical cases.

The most important assumption made here is that the jet flow is laminar. The available transition data base is sparse. Finding clear transition data for this problem is further complicated by the presence of temperature and concentration gradients, chemical reactions, and, in the case of the concurrent experiment, a confining wall. The Reynolds number based on the jet height, R_d, for the 6/1 jet case is

approximately 200. Birkhoff et. al. (16) suggest that for $R_d < 1000$ (round, free jets), the jet should remain laminar (molecular transport only), however, for $R_d > 100$ the development of periodic large scale structure is certainly a possibility. The whole issue is further complicated by the use of the words laminar and turbulent, where in many cases large scale vortical structure are not considered turbulent because they have not cascaded down to the higher frequency, small scale eddies. The assumption of laminar flow, however, is pragmatic from a computational point of view and may, in fact, be correct. Ultimately, the validity of this key assumption must be confirmed or rejected based on experimental evidence.

It should also be stressed that this study represents a set of "numerical experiments," and as such, is not meant to simulate an actual experiment in anymore than a general way. This is apparent from the initial conditions. Reference to Figure A1, Appendix A, clearly demonstrates that an actual experiment would involve the growth of boundary layers on the inner and outer walls of the nozzle. The no-slip condition requires that the velocity at the edge of the nozzle blade (the interface between the two streams) be zero although concentration gradients would be large. In the numerical model the initially large gradients between the freestream and jet "slug" profiles are smeared out over the two adjacent grid nodes between the jet and the freestream.

One would also expect the growth of a boundary layer on the cavity walls. This viscous shear loss coupled with heat release due to chemical reaction should cause some pressure gradient in the streamwise direction. Since the freestream Mach number is small ($M \approx 0.1$) and the amount of heat released is also small (near resonant energy transfers),

the pressure gradient would be due to the shear on the wall. As mentioned in Chapter 4, no attempt has been made in this numerical study to model the streamwise pressure gradient. The pressure gradient instead was set to zero for all of the cases. Because the solution is being calculated along lines across which no net mass flows, i.e., constant ψ, the error due to this assumption can be qualitatively evaluated by examining the variation in the y-coordinate of the outer streamline. The maximum change was 8% for the 6/1 jet-mixed case. If required, a streamwise pressure gradient could be specified based on measured wall pressure data (See Figure A1, Appendix A). The boundary layer at the wall could also be modeled by imposing a no-slip condition.

General Results. The output of the numerical code, COILFT, provides information on both the flow field properties and species concentrations. Figures 10 and 11 show the development of the transverse velocity and temperature profiles for the 6/1 velocity ratio jet case as a function of ψ. The slug profile initial conditions at the nozzle exit plane quickly develop into a series of profiles which may be compared with a self-similar free jets (19). Although the comparison is complicated by dissimilar species, chemical diffusion, and reactions, the evolution of the velocity and temperature profiles closely mimic those of the self-similar jet (19), and give high confidence that the code performed properly with regard to simulating the fluid-mechanic environment. Figure 12 shows the development of the species profiles transverse to the flow, three centimeters downstream of the nozzle exit plane. Note that the freestream profiles are undisturbed confirming that ignoring the influence of the cavity walls was a reasonable

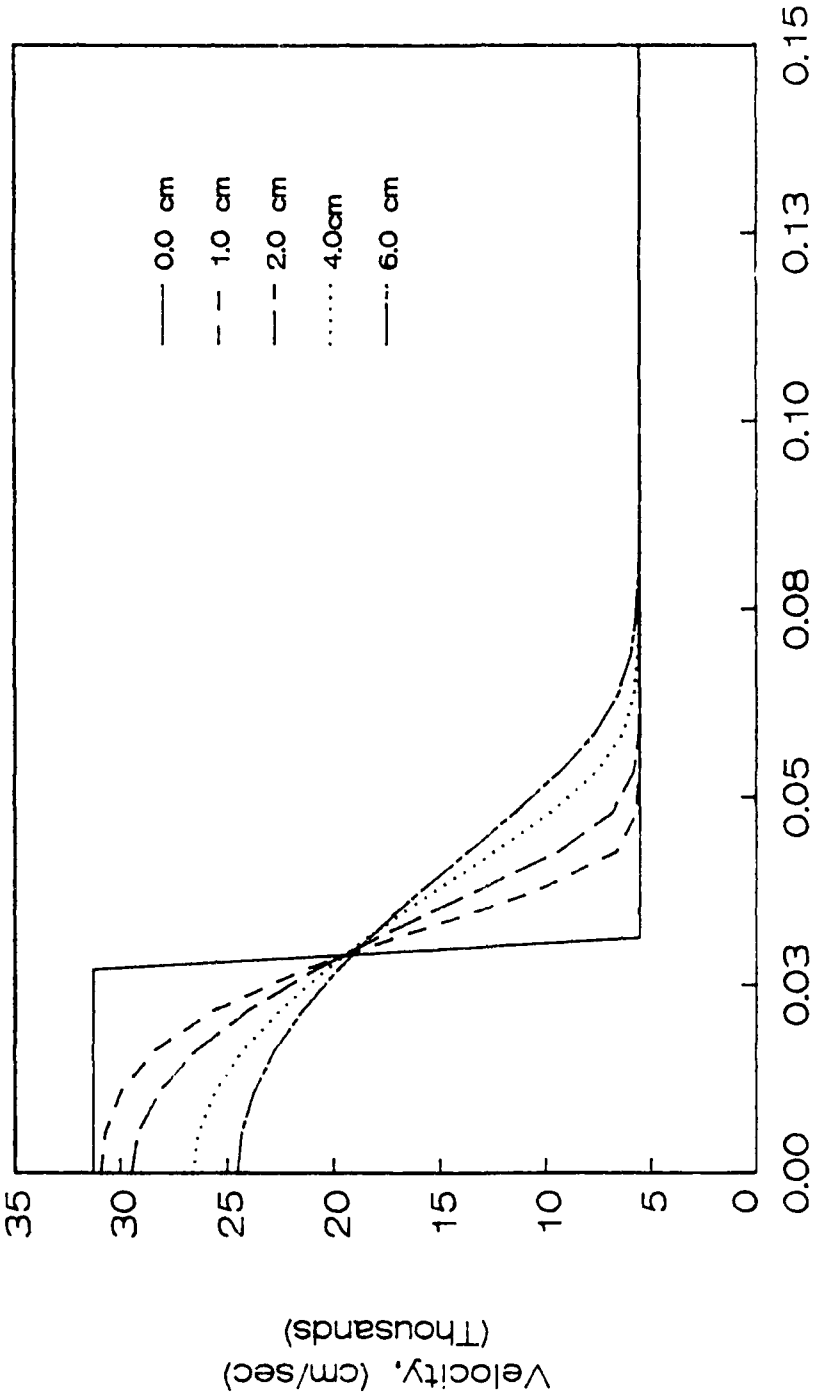

Figure 10. Development of the Transverse Velocity Profiles as a Function of ψ.

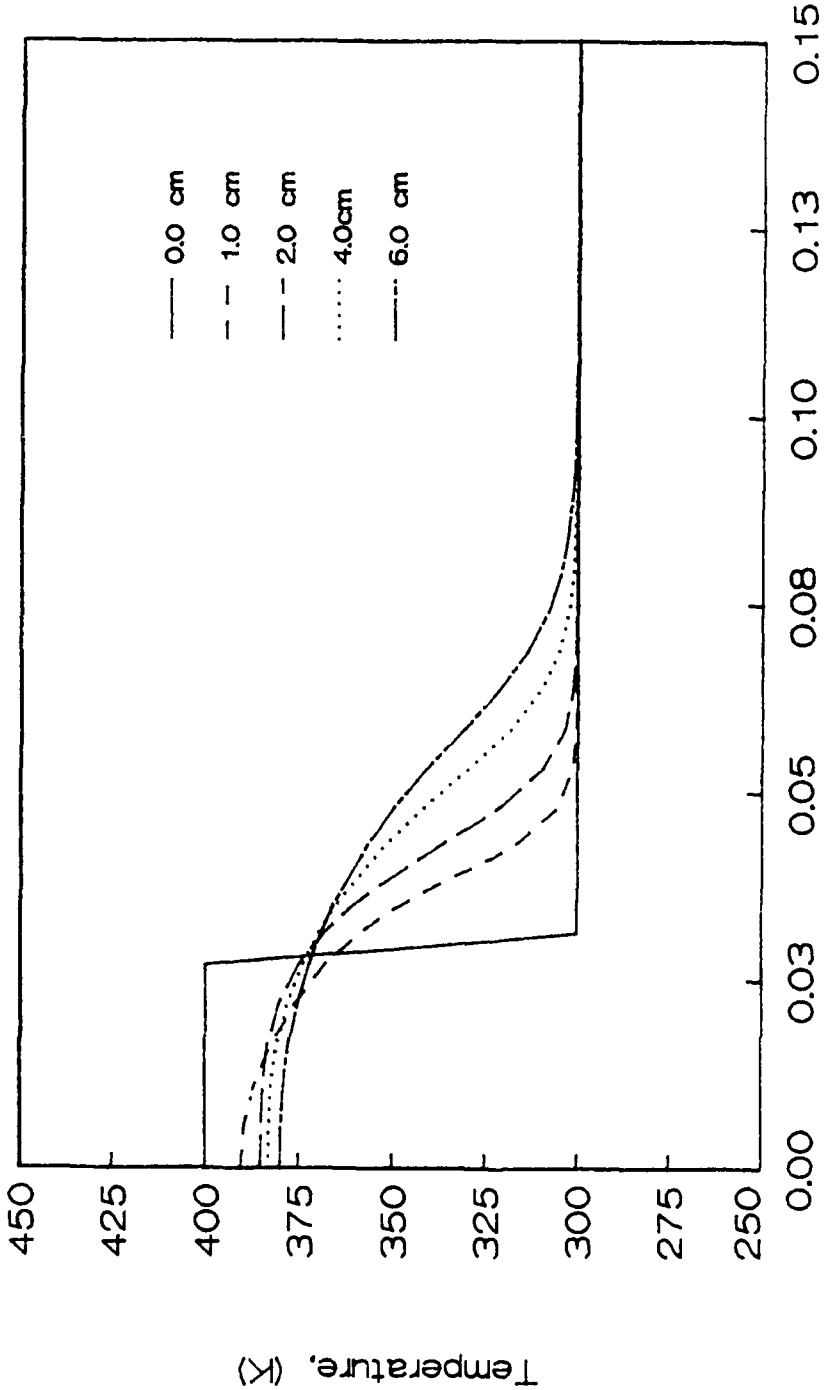

Figure 11. Development of the Transverse Temperature Profiles as a Function of ψ.

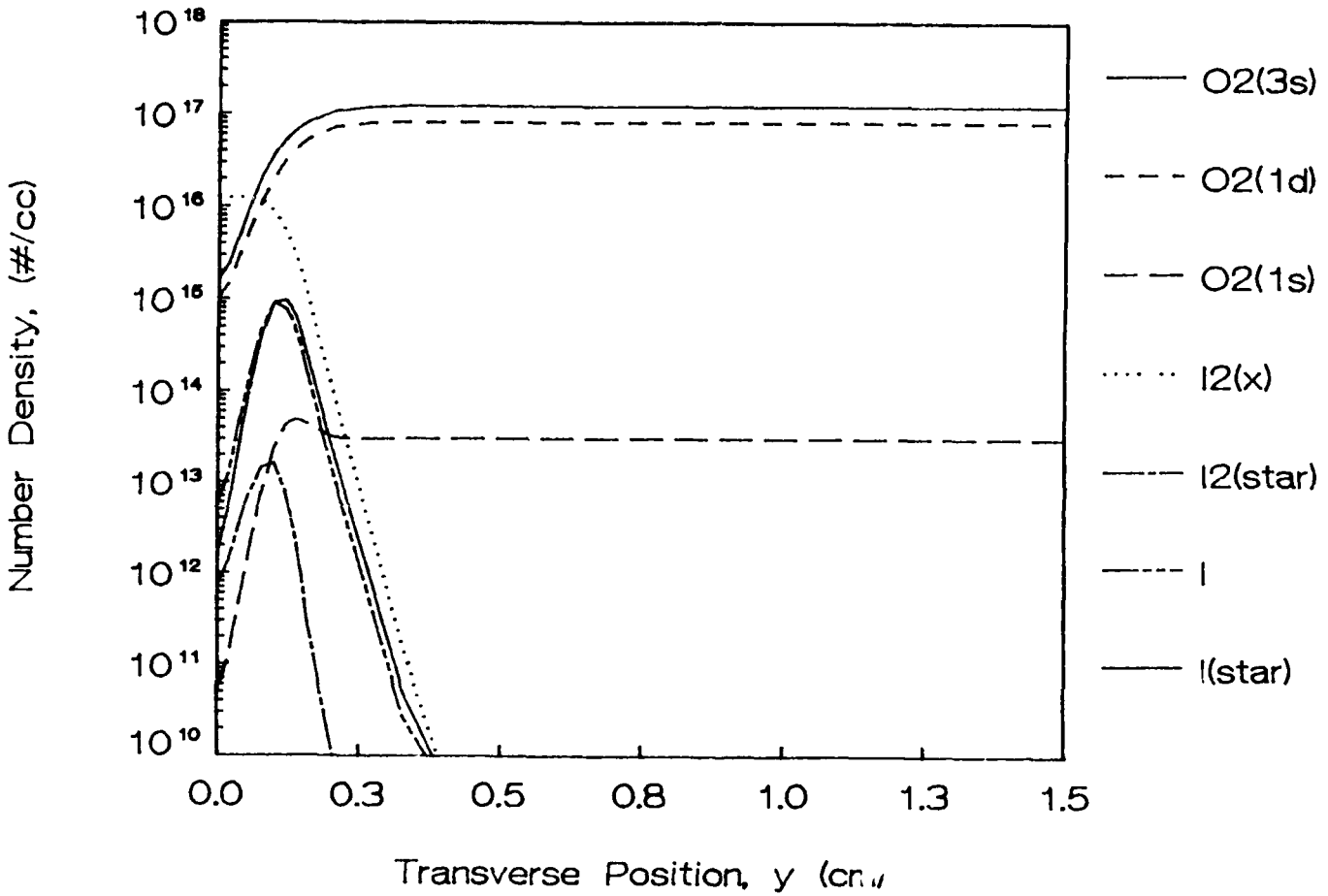

Figure 12. Transverse Species Concentration Profiles for the 6/1 Jet Case 3 cm Downstream from the Nozzle Exit Plane.

assumption. Figure 13 shows the development along the nozzle centerline in the streamwise direction. Close inspection of Figures 12 and 13 shows the diffusion of O_2 into the jet and the rise of both I and I^* as the dissociation process proceeds. Although these detailed maps of the individual species concentrations will become important when attempting to compare numerical results with experimental data, developing a "feel" for the dissociation process from these profiles alone is often difficult because it requires examining the changes in several different species as a function of both the streamwise and transverse position at the same time. To aid in developing a "feel" for the process the flow field properties and the species concentrations were manipulated to form integrated parameters which are more characteristic of the overall product of the dissociation process.

Streamwise Comparisons. The two questions of most concern to this investigation were what is the rate of I_2 dissociation and how efficiently does the dissociation occur. Integration of the transverse profiles of both the O_2 and I_2 as the flow develops in the streamwise direction provided a means of addressing both of these questions.

The fraction of the I_2 dissociated can be defined in terms of the total mass flow rates of iodine through a plane perpendicular to the nozzle centerline as

$$\text{Diss} = \frac{\Delta\dot{m}(I_2)}{\dot{m}(I_2)_{TOT}} = 1 - \frac{\dot{m}(I_2)}{\dot{m}(I_2)_{TOT}} \tag{5.1}$$

where

$$\dot{m}(I_2) = \dot{m}(I_2) + \dot{m}(I_2^{\ddagger})$$

and

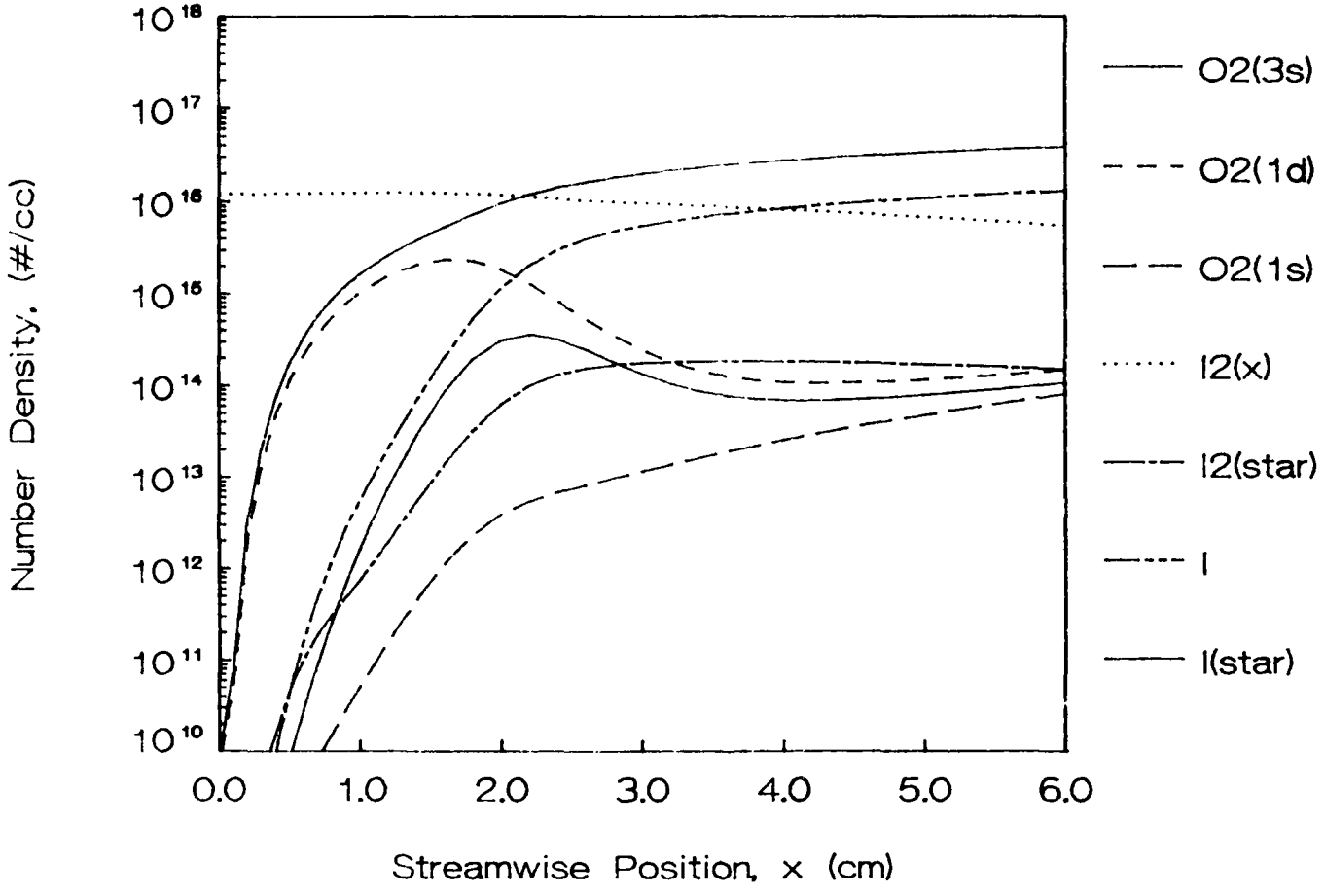

Figure 13. Streamwise Species Concentration Profiles for the 6/1 Jet Case on the Nozzle Centerline.

$$\dot{m}(I_2)_{TOT} = \dot{m}(I_2) + \dot{m}(I_2^{\ddagger}) + \dot{m}(I) + \dot{m}(I^*)$$

Total dissociation corresponds to Diss = 1. The total mass flow rate of species i through a plane was found by integrating the product of the mass flow rate (ψ) and the mass fraction of species i across the flow. This integral was approximated on the finite-difference grid as

$$\dot{m}(i) = \sum_{j=1}^{N} \frac{\left(W(i)_{j+1} + W(i)_j \right)}{2} \Delta\psi_j \qquad (5.2)$$

where N is the total number of nodes transverse to the flow.

Figure 14 shows the I_2 dissociation fraction for the three jet-mixed cases and the corresponding premixed cases as a function of the streamwise position. Note that initially, just as for the RDA results, Figure 4, Chapter II, the rate of dissociation for the premixed cases is slower than for the jet-mixed cases. Comparison of the species concentrations as a function of the distance downstream for the premixed case in Figure 15 with those at the jet boundary for the 6/1 jet-mixing case in Figure 16 shows a higher initial I_2 concentration with a corresponding rapid rise in the concentrations of I, I^*, and, most importantly, $I_2^{\ddagger}$. The result is a much more rapid rate of dissociation at the jet boundary. The drop off in $I_2^{\ddagger}$ concentration near the 2 cm point occurs simply because the I_2 is being depleted. Because in the premixed case, all species are completely mixed, the initial concentration of I_2 is lower for the premixed case. The rate of formation of all of the excited species in the premixed case shows a much more gradual rise. As the I^* concentration builds, however, the rate of dissociation increases due to a hand off between the slower

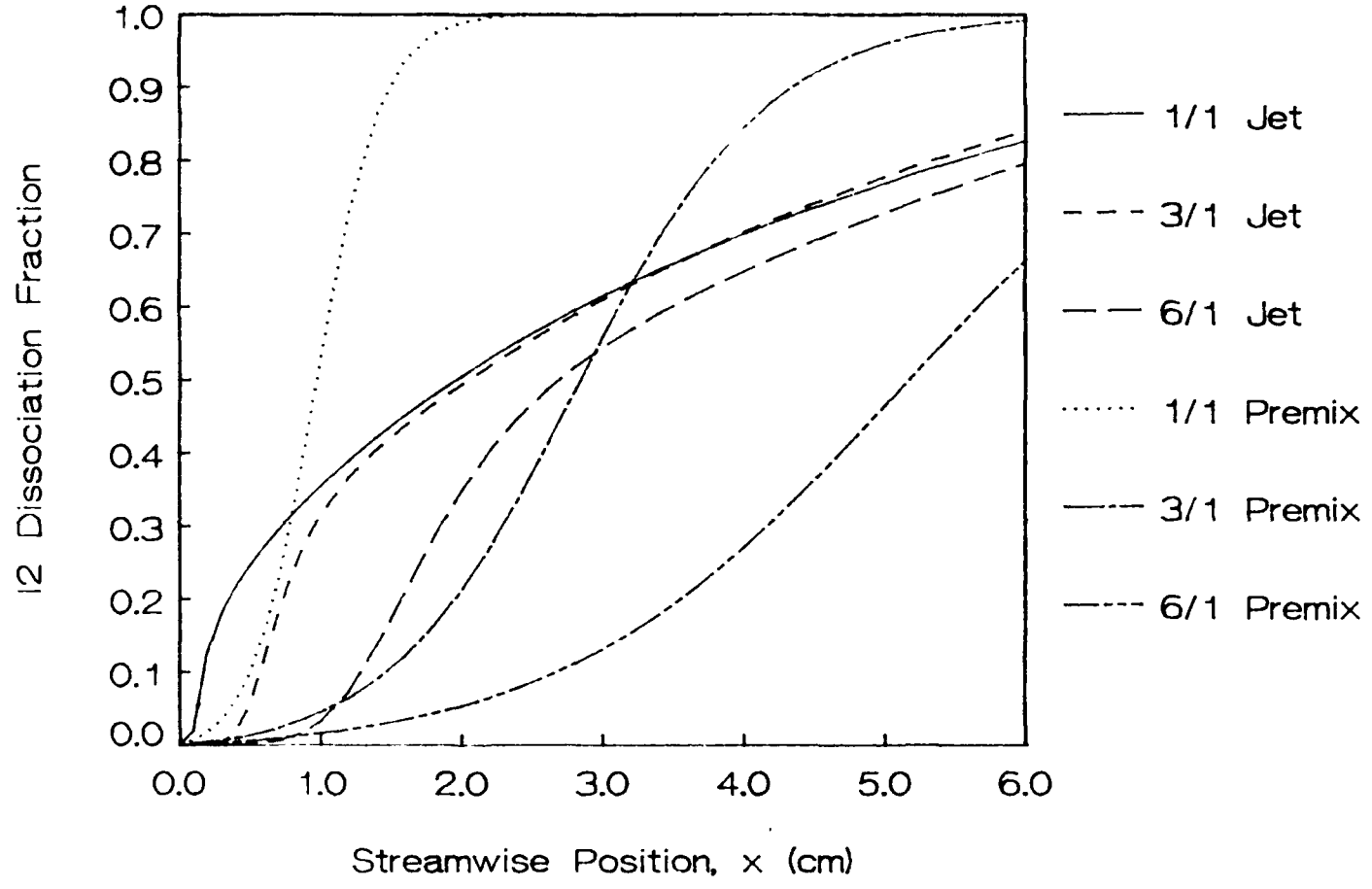

Figure 14. Comparison of the Streamwise Variation in I_2 Dissociation for the 1-D, Premixed and Jet-Mixed Cases.

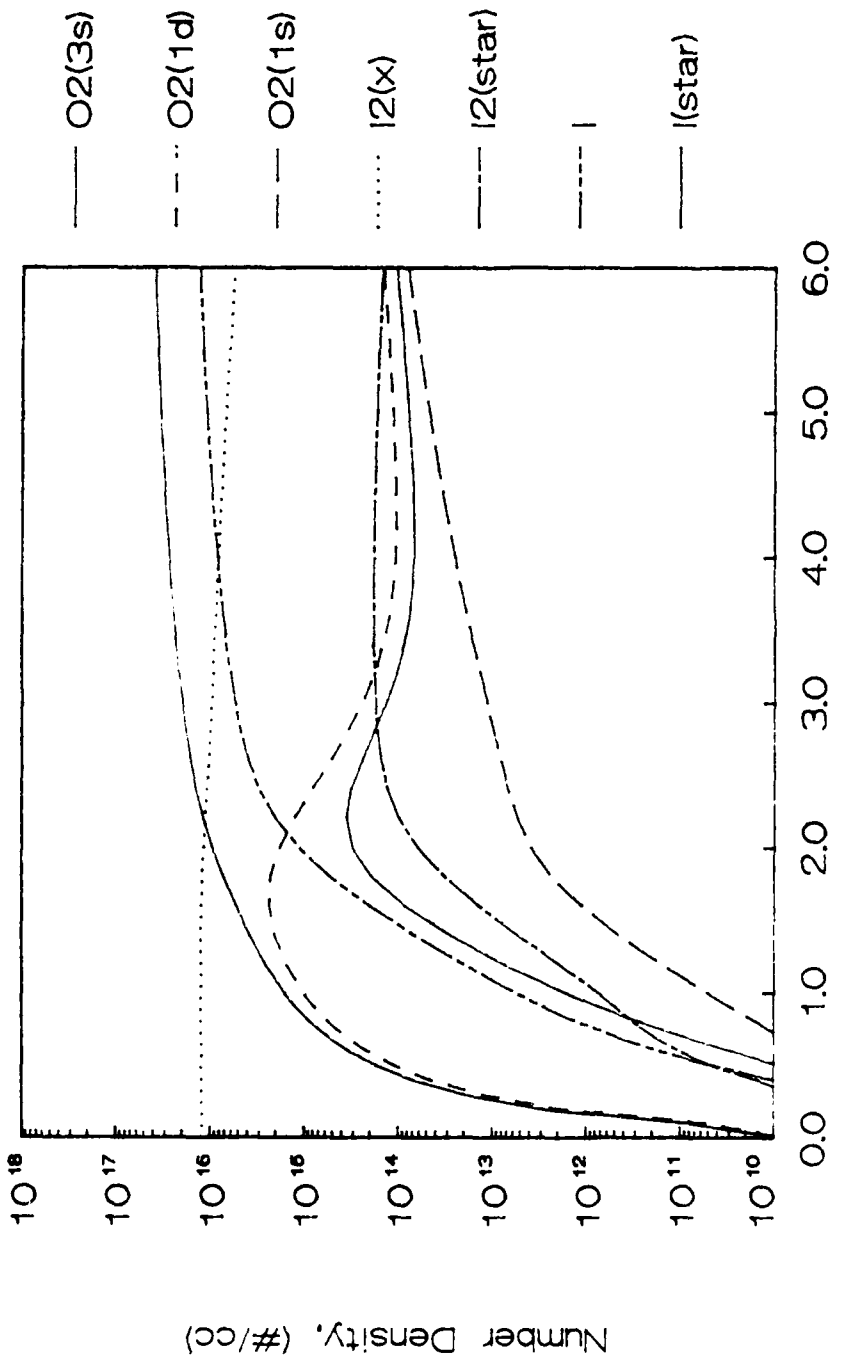

Figure 15. Streamwise Development of the Species Concentration Profiles for the "6/1" Premixed Case.

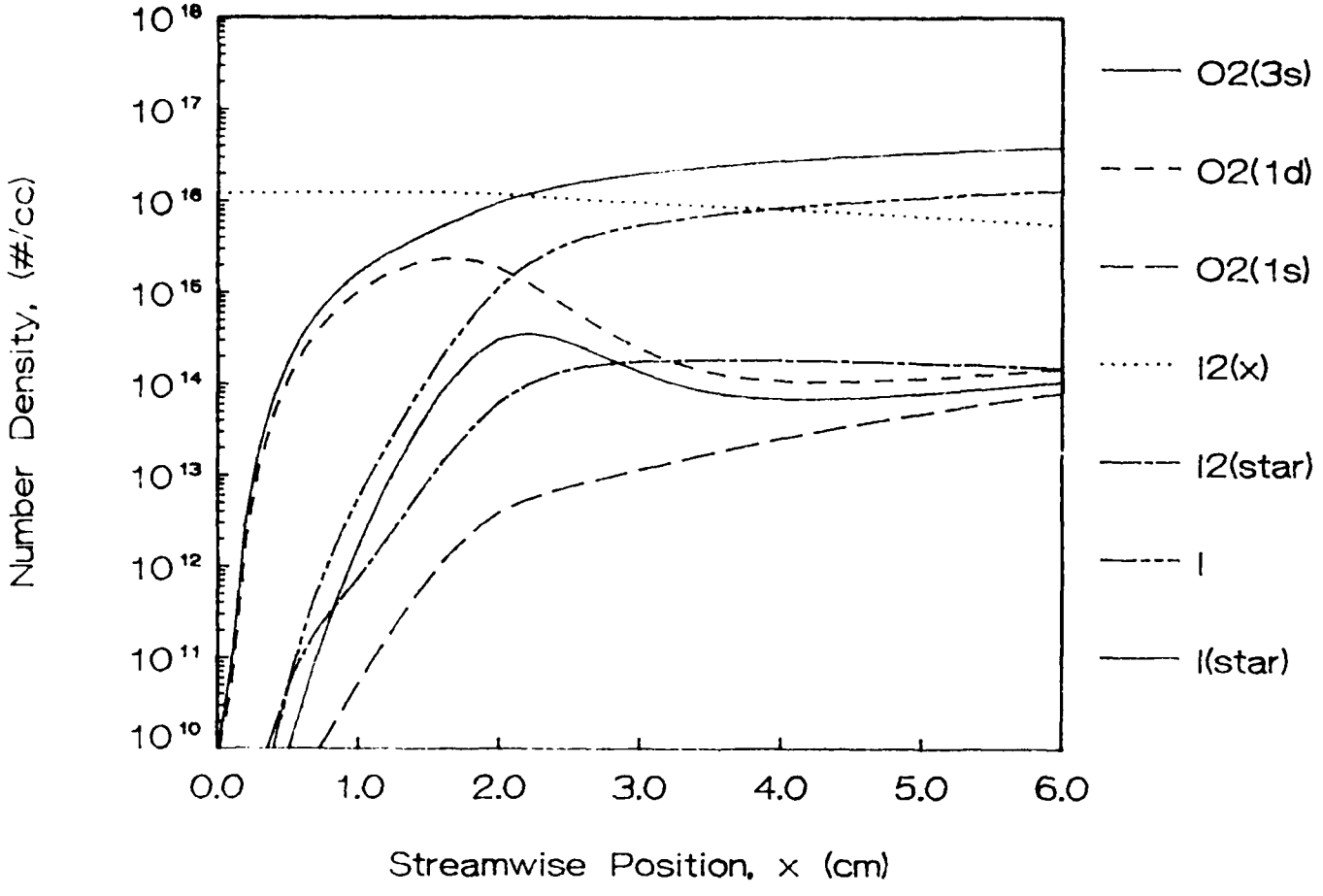

Figure 16. Streamwise Development of the Species Concentration Profiles at the Jet Boundary for the 6/1 Jet Case.

dissociation mechanisms, Eqs (2.6) or (2.12), and (2.14), and the faster mechanism of Eqs (2.13) and (2.14) as discussed in Chapter II. All of the jet-mixed cases display a slow roll off in the dissociation rate and the premixed cases eventually overtake the jet cases. Note, that the 6/1 case which corresponds to highest entrainment rate stays ahead of the premixed case for the longest period of time.

In Chapter I, the efficiency of the I_2 dissociation process was defined in terms of the parameter N, the number of $O_2(^1\Delta)$ molecules required to dissociate one I_2 molecule. An efficiency parameter similar to N can be defined for the numerical results in terms of the total (integrated across the flow) loss of the excited "chemical energy" in the flow divided by the change in the flow rate of I_2. Initially, all of the chemical energy in the flow is in $O_2(^1\Delta)$.

$$\dot{E}_{IN} - \dot{E}\left(O_2(^1\Delta) \right)_{IN} - \dot{n}\left(O_2(^1\Delta)\right)_{IN} \epsilon\left(O_2(^1\Delta)\right) \qquad (5.3)$$

$\dot{E}$ is the total energy flux [=] (kJ/sec) in the flow, $\dot{n}$ is the total molar flow rate [=] (mole/sec), and ϵ is the energy per mole [=] (kJ/mole). ϵ corresponds to the excitation energy in Eq (2.18), Chapter II (also, see Figure 1). The subscript IN refers to the initial plane. At any streamwise location, the energy still available in the flow is defined as the energy in both $O_2(^1\Delta)$ and I^*. Any energy that transfers to $O_2(^1\Sigma)$ or $I_2^{\ddagger}$ is considered as a loss.

$$\dot{E} = \dot{E}\left(O_2(^1\Delta) \right) + \dot{E}\left(I^* \right)$$

$$= \dot{n}\left(O_2(^1\Delta) \right) \epsilon\left(O_2(^1\Delta) \right) + \dot{n}\left(I^* \right) \epsilon\left(I^* \right) \qquad (5.4)$$

The total energy loss between the initial plane and any streamwise location is then

$$\Delta\dot{E} = \dot{E}_{IN} - \dot{E}$$

which can be expressed in terms of the transition energy of $O_2(^1\Delta)$.

$$\frac{\Delta\dot{E}}{\epsilon\left(O_2(^1\Delta) \right)} = \dot{n}\left(O_2(^1\Delta) \right)_{IN} - \dot{n}\left(O_2(^1\Delta) \right) - \frac{\epsilon\left(I^* \right)}{\epsilon\left(O_2(^1\Delta) \right)} \dot{n}\left(I^* \right) \qquad (5.5)$$

The total loss of I_2 to dissociation can be computed by accounting for both I_2 and $I_2^{\ddagger}$ as

$$\Delta\dot{n}\left(I_2 \right) = \dot{n}\left(I_2 \right)_{IN} - \dot{n}\left(I_2 \right) - \dot{n}\left(I_2^{\ddagger} \right) \qquad (5.6)$$

The efficiency can then be defined as

$$N(x) = \frac{\Delta\dot{E} \Big/ \epsilon\left(O_2(^1\Delta) \right)}{\Delta\dot{n}\left(I_2 \right)} \qquad (5.7)$$

Note, that the lower this number is, the more efficient the dissociation process is (less energy lost). The theoretical limit based on energy required to dissociate I_2 is 2 (See the energy level diagram in Figure 1, Chapter I). For initially very small dissociation fractions, the denominator of Eq (5.7) is near zero, which causes erratic behavior in computed efficiencies from the code; these, however, settle out

rapidly as $\Delta\dot{n}(I_2)$ becomes sufficiently large to overcome the roundoff errors involved in subtracting nearly equal numbers.

Figure 17 shows the streamwise variation of the efficiency factor defined in Eq (5.7) for the six cases with the curves beginning after the calculated error has settled out. The slight difference in efficiency between the premixed and jet-mixed cases can be seen in Figure 17. The slight increase in N(x) (i.e., decrease in efficiency, c.f. above) in the streamwise direction is due to the relatively slow $O_2(^1\Delta)$ and I^* pooling reactions, Eqs (2.2) and (2.4). Keep in mind that with no H_2O in the initial conditions, there are no other loss mechanisms, so that the value of the efficiency factor should be close to the minimum limit of 2. Although defined similarly, the efficiency factor from Eq (5.7) illustrates an important point about the N commonly used in Eq (1.1); N is defined as the number of $O_2(^1\Delta)$'s required to dissociate one I_2 at 100% dissociation. N is then an asymptotic limit of the factor, N(x) in Figure 17 as the dissociation proceeds to completion. Difficulty arises, however, in defining N precisely. Examination of Eq (5.7) and Figure 17 shows that even after the dissociation has reached 100% the loss mechanisms will continue to cause the apparent N to increase. This example points out that N, as defined and used in Eq (1.1), is not a universal constant for COIL devices but tied to a specific device and, in fact, to a specific run condition. Clearly, N will be of little value when making large excursions from the current baseline designs and operating conditions.

Transverse Comparisons. For thin shear layers, gradients transverse to the flow direction are more important to the development of the flow than gradients in the streamwise direction, since the

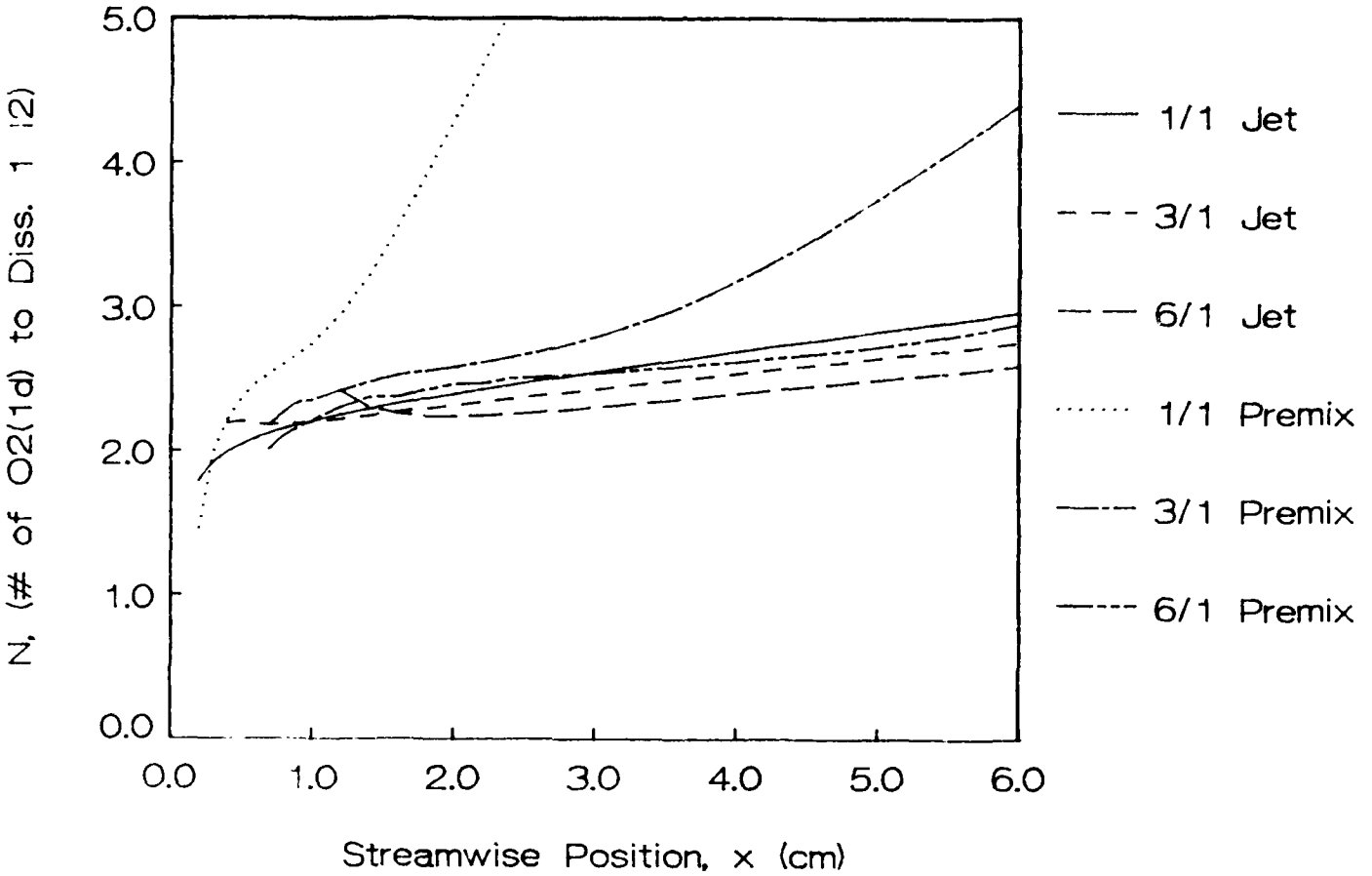

Figure 17. Comparison of the Streamwise Variation of the I_2 Dissociation Efficiency for the 1-D, Premixed and Jet-Mixed Cases.

transverse profiles provide an indication of the structure of the jet . Once again, combined parameters which characterize COIL system performance provide a clearer picture than attempting to look at the individual profiles. The first parameter of interest is the local I_2 dissociation fraction. The local dissociation fraction is the mass fraction of atomic iodine at any point in the flow divided by the total mass fraction of iodine (atomic or molecular) at the point.

$$I_2 \text{ Diss} = \frac{W(I)_{TOT}}{W(I_2)_{TOT}} \tag{5.8}$$

where W is the mass fraction and

$$W(I)_{TOT} = W(I) + W(I^*) \tag{5.9}$$

and

$$W(I_2)_{TOT} = W(I_2) + W(I_2^{\ddagger}) + W(I) + W(I^*) \tag{5.10}$$

Complete dissociation corresponds to I_2 Diss = 1. As before, some confusion arises because the I_2 dissociation is not defined where the total mass fraction of iodine is zero or well behaved where it is small. Plotting the total mass fraction of I_2 aids in interpreting the I_2 dissociation fraction.

The $O_2(^1\Delta)$ "yield", fraction of O_2 that is $O_2(^1\Delta)$, along with the total mass fraction of O_2 provides means of tracing the "entrainment" of the O_2 from the primary freestream. The yield (c.f., above) is defined as the fraction of $O_2(^1\Delta)$ in the total O_2

$$\text{YIELD} = \frac{W(O_2(^1\Delta))}{W(O_2)_{TOT}} \tag{5.11}$$

where

$$W(O_2)_{TOT} = W(O_2(^3\Sigma)) + W(O_2(^1\Delta)) + W(O_2(^1\Sigma)) \tag{5.12}$$

Finally, the "gain" provides an indication of where the atomic iodine has reached an inverted population. As discussed in Chapter II, Eq (2.7), inversion occurs when

$$\frac{[I^*]}{[I]} \geq 0.5 \tag{5.13}$$

The gain is defined as

$$g = \sigma \left([I^*] - 0.5 [I] \right) \tag{5.14}$$

where σ is the stimulated emission cross section, $\sigma = 5.7X10^{-18}$ cm^2.

Figure 18 shows the transverse profiles for the total I_2 mass fraction, Eq (5.10), local I_2 dissociation fraction, Eq (5.8), total O_2 mass fraction, Eq (5.12), $O_2(^1\Delta)$ fraction, Eq (5.11), and gain, Eq (5.14), at a streamwise position 1 cm from the nozzle exit plane for the 6/1 jet case. The origin for the y coordinate is the nozzle centerline, and the initial boundary between the jet and freestream flows is at y = 0.09 cm; the profiles are displayed out to y = 0.8 cm, approximately half of the computational domain. The remaining freestream flow is undisturbed by the jet expansion. Figure 18 shows that the O_2 and I_2 streams have only just began to mix by the 1 cm location. The I_2 dissociation fraction has been deliberately set to

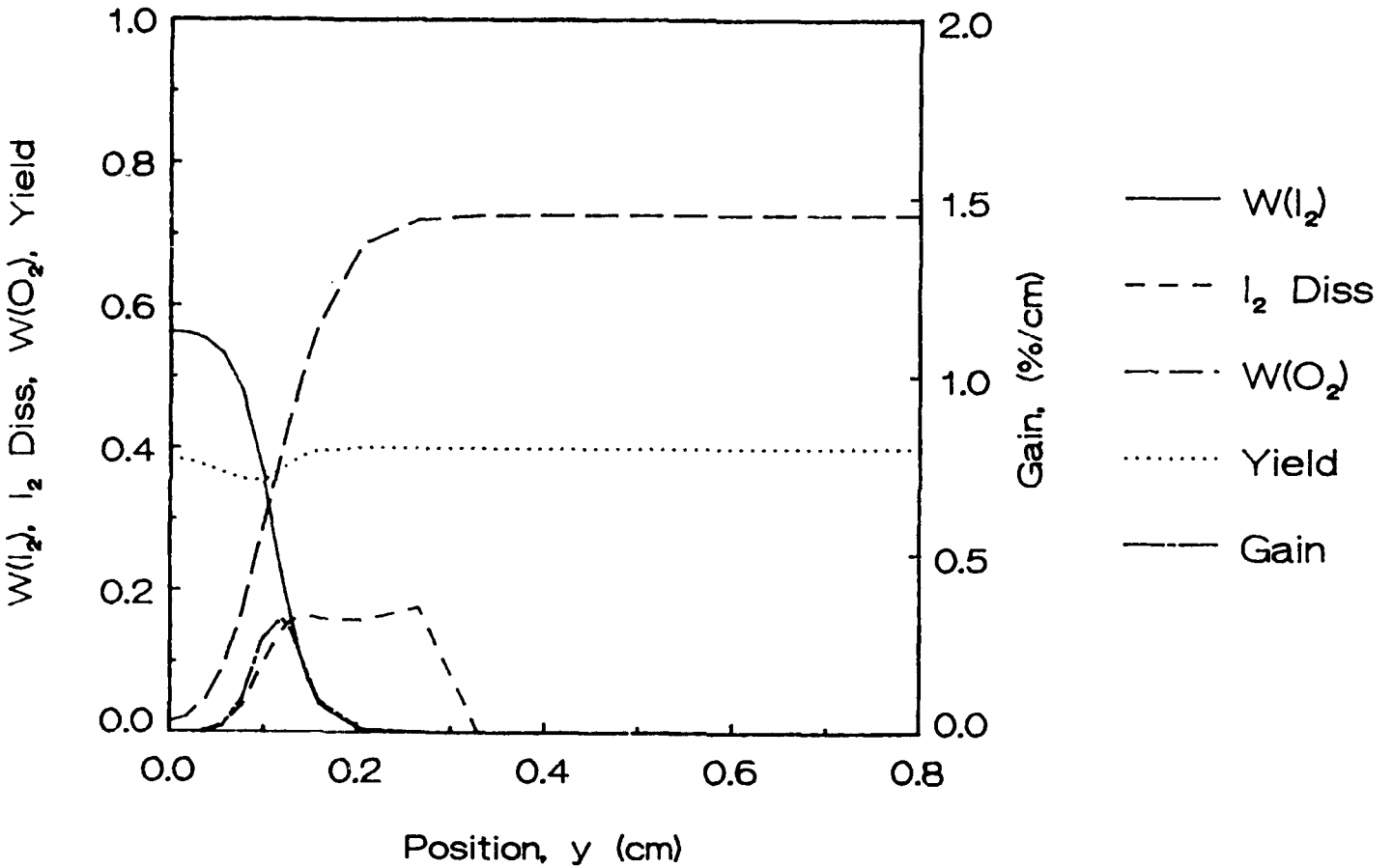

Figure 18. Transverse O_2 Mixing, I_2 Dissociation, Gain Profiles for the 6/1 Jet Case at x = 1 cm.

zero for total I_2 mass fractions less than 0.01 to avoid any confusion from artificially high dissociation fractions in regions where the iodine concentrations are numerically very small. This accounts for the dramatic drop off in the dissociation fraction near y = 2.5 cm. The I_2 is only slightly dissociated in the mixing region ($\approx$ 0.15). No dissociation has occurred in the core of the jet by the this point. Note, gain occurs, according to the arguments in Chapter 2 and by examination of the definition in Eq (2.14), only where I_2 has dissociated to create I atoms and where the $O_2(^1\Delta)$ fraction, Eq (5.11) is greater than 0.15. The gain profile in Figure 18 illustrates this point.

Figures 19 and 20 repeat the profiles of Figure 18 for the 6/1 jet case at the x = 3 cm and x = 6 cm planes respectively. As the flow progresses downstream, the I_2 in the jet diffuses outward while the O_2 in the jet diffuses inward aided by convective transport as the O_2 is "entrained" into the faster moving jet flow. Although the O_2 concentration on the jet centerline increases rapidly, the $O_2(^1\Delta)$ fraction drops quickly to zero in the jet core. The I_2 which diffuses into the $O_2(^1\Delta)$ rich freestream is dissociated rapidly. The largest concentration of I_2, however, remains in the jet core even at x = 6 cm and nearly one half of the I_2 in the core is still undissociated. Note the location of the gain regions. Once again, gain occurs only where the I_2 is dissociated and where the $O_2(^1\Delta)$ fraction is greater than 0.15. Unfortunately, in this case, much of the I atom population is in the $O_2(^1\Delta)$ poor jet core. This illustrates an important design consideration for COIL devices. Although nonideal mixing may result in faster dissociation (c.f. previous section), the resulting I atoms must

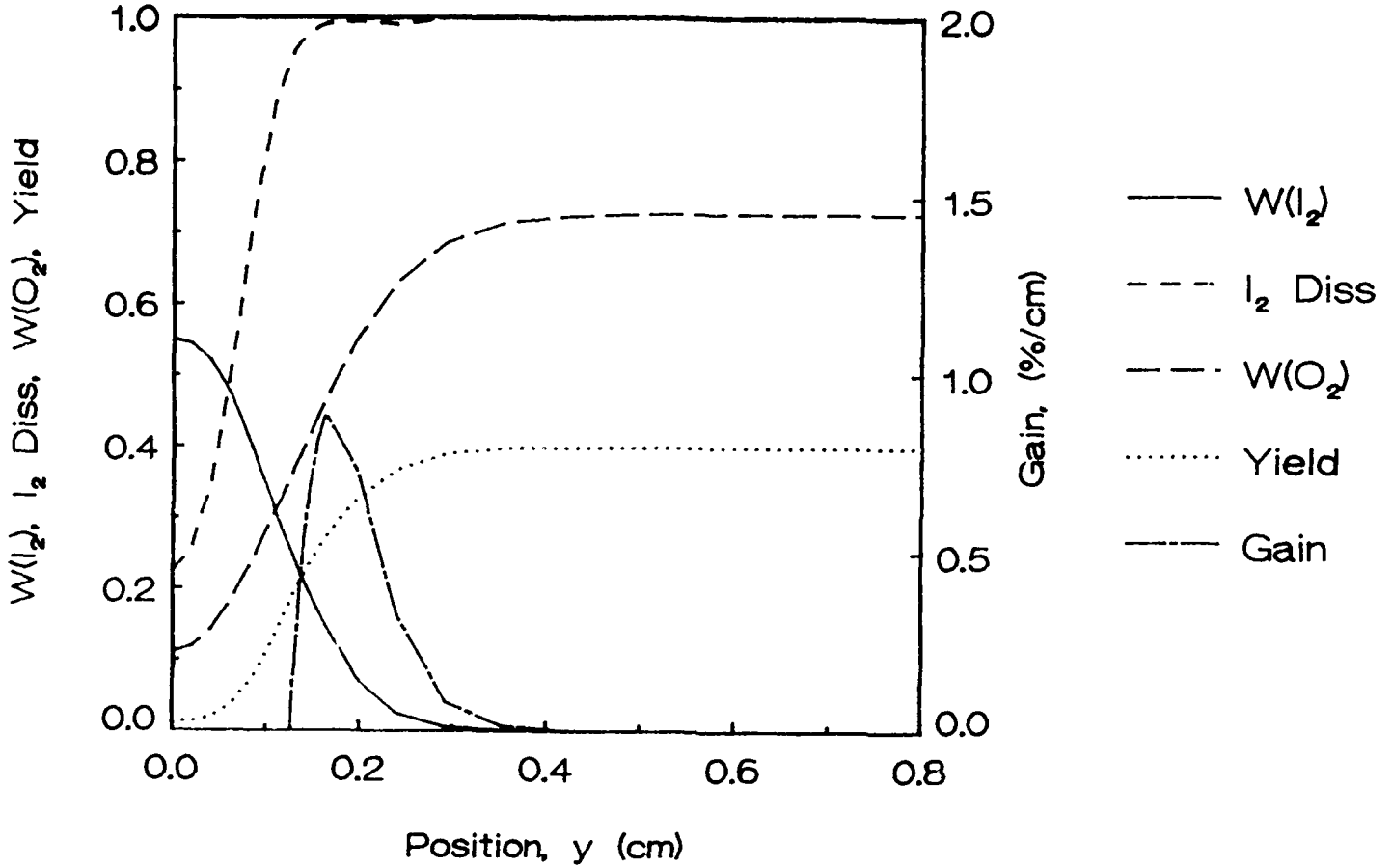

Figure 19. Transverse O_2 Mixing, I_2 Dissociation, and Gain Profiles for the 6/1 Jet Case at x = 3 cm.

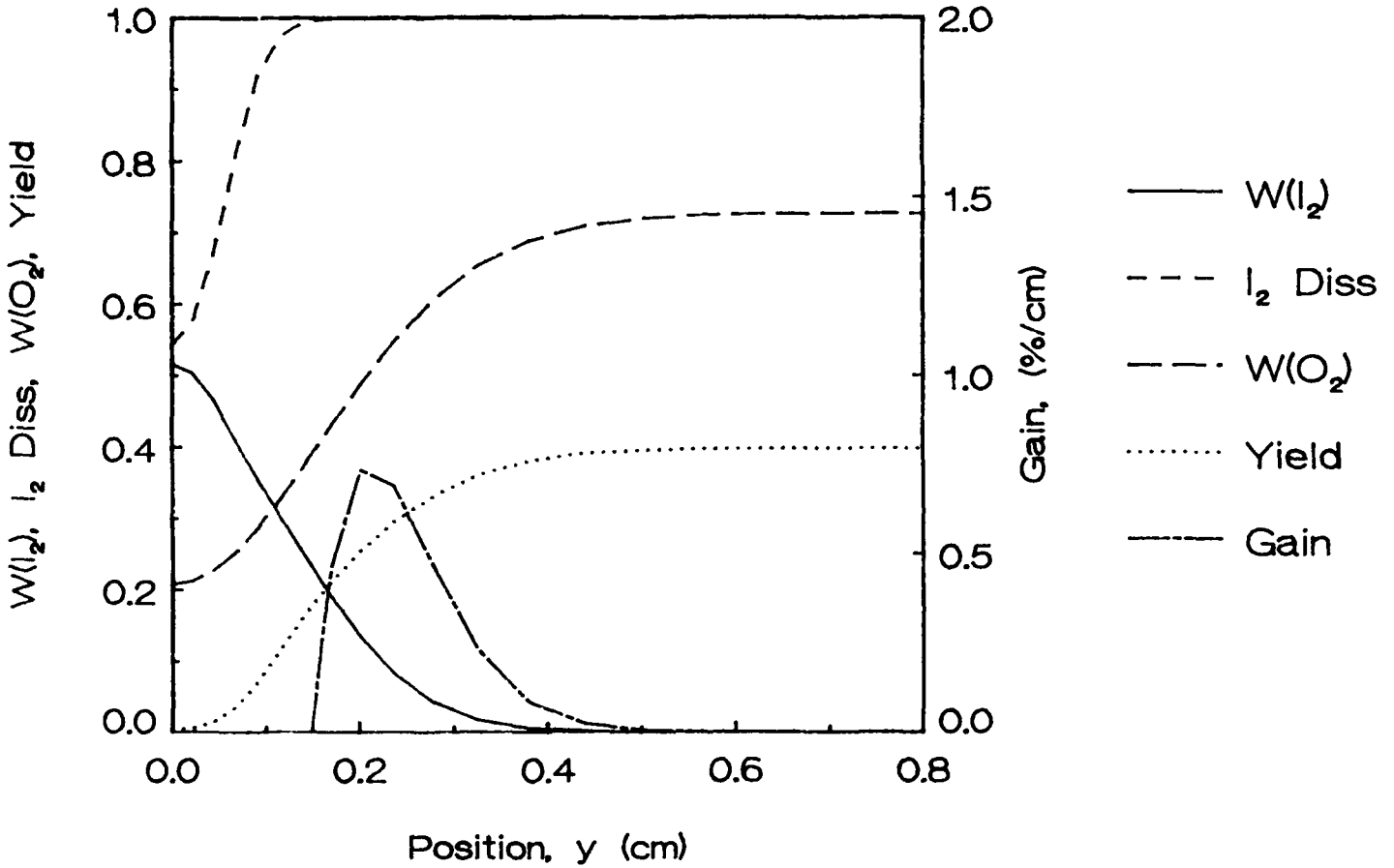

Figure 20. Transverse O_2 Mixing, I_2 Dissociation, and Gain Profiles for the 6/1 Jet Case at x = 6 cm.

be well mixed with the $O_2(^1\Delta)$ stream to obtain good power extraction.

Note how the gain region moves outward toward the O_2 freestream as the jet expands, even though most of the I atom concentration is in the jet core. It now seems clear that the drop off in the streamwise direction of the dissociation rate for the jet cases in Figure 14 occurs because the I_2 in the jet core becomes isolated from the $O_2(^1\Delta)$ in the freestream by a layer of completely dissociated iodine atoms. $O_2(^1\Delta)$ is removed rapidly by the I atom pumping reaction, Eq (2.1), as it diffuses toward the jet. The dissociation rate becomes limited by the rate of transport of I_2 into the $O_2(^1\Delta)$ stream.

These observations suggest that the most efficient laser nozzle design should result in regions of high I_2 concentrations initially to promote dissociation and then rapidly mix the O_2 and I streams to obtain good extraction characteristics. This, in fact, seems to be the reason why the the transverse, transonic I_2 injection nozzle configuration (Figures 3 and 6a, Chapter 2) employed on the most recent COIL devices was much more successful than other configurations.

We now compare the structure of the 3/1 and 1/1 jet-mixed cases with the 6/1 case in order to examine the effect the varying velocity ratio has on the mixing and dissociation processes. In order to do so, we need to first establish a common basis for comparison. The most obvious would be to compare the profiles at the same streamwise locations, but, as in comparisons with the premixed cases discussed in the proceeding section, the results are confused by the differing time scales for the jets. For the 1/1 jet case, the jet flow propagates approximately a factor of six slower than the flow for the 6/1 case. The iodine will be exposed to the $O_2(^1\Delta)$ for six times as long (time and

distance being approximately linearly relatable, c.f. previous section). For any chemical rate process, time is clearly an important variable. Based on this argument, the transverse structure of the jets are compared at similar times where the jet velocity is employed to relate time and distance. Figures 21, 22, and 23 compare the transverse profiles for the 6/1 jet at x = 6 cm to the 3/1 jet at x = 3 cm the 1/1 jet at x = 1 cm. Admittedly, scaling the distances by the jet velocity is an over simplification of the development of the jet, however, this first order comparison does provide some insight.

The difference in the total O_2 mass fraction, Eq (5.12), and the $O_2(^1\Delta)$ fraction, Eq (5.11), profiles for the lower velocity ratio cases can be seen in Figure 21. In the 6/1 jet case, molecular diffusion is aided by convection (entrainment) due to the large velocity difference producing the largest O_2 mass fraction on the jet centerline. Transport in the 1/1 case is due solely to diffusion which results in a much lower O_2 concentration in the jet core. For all of these cases, very little of the $O_2(^1\Delta)$ transported toward the centerline survives the combination of the dissociation and I_2/I pumping processes. The corresponding comparison of the total I_2 mass fraction, Eq (5.10), and I_2 dissociation fraction, Eq (5.8) is shown in Figure 22. Note that the higher initial I_2 mass fraction on the centerline for the 1/1 and 3/1 case are due to a lower secondary helium flow rate for the slower jets (c.f. Table IV). The expansion of the I_2 jets for all three cases is nearly the same. Nearly all of the I_2 which diffuses into the O_2 primary freestream is dissociated. The higher entrainment rates for the 6/1 and 3/1 jet velocity ratios, however, lead to much higher dissociation levels in the jet core. As a result, the total dissociation rate is faster for

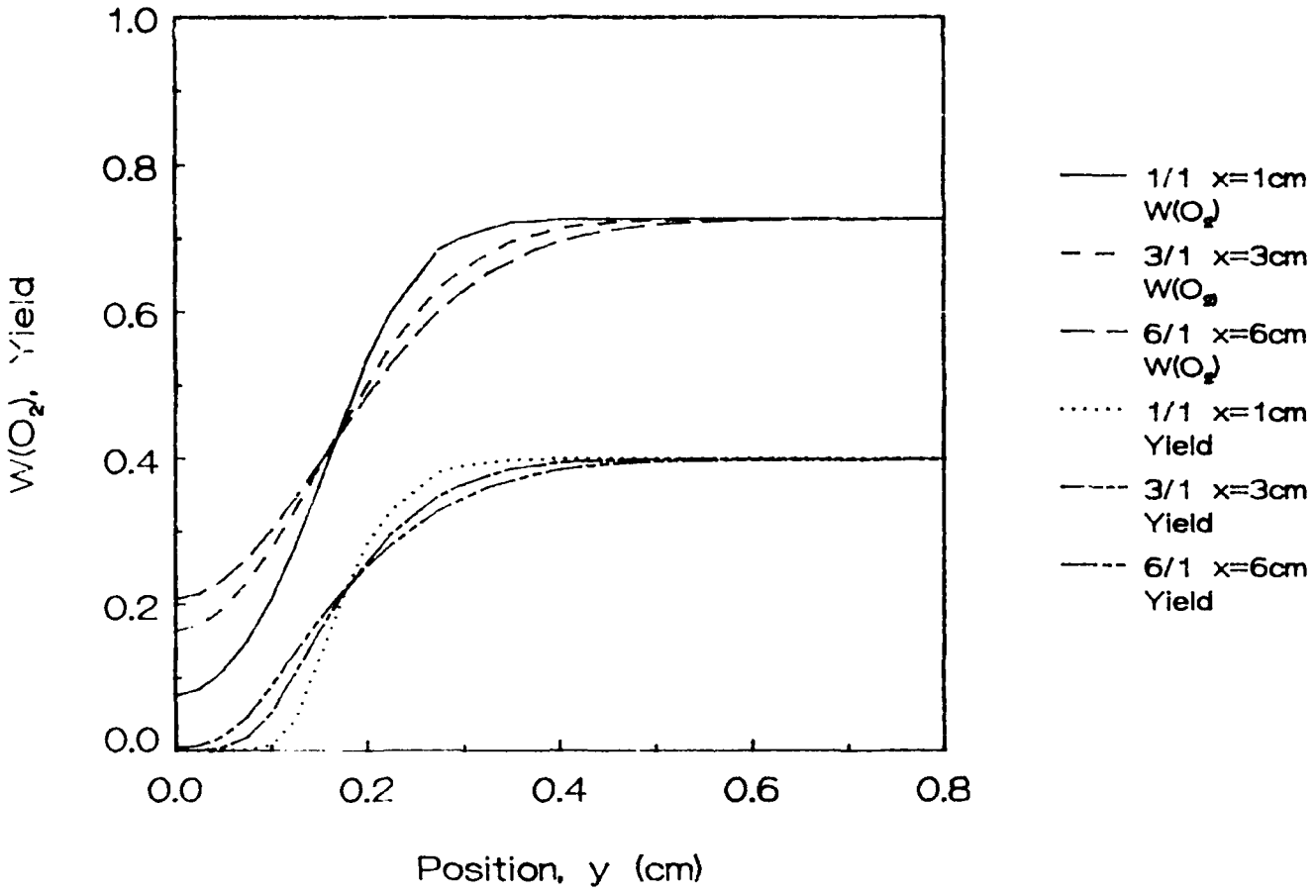

Figure 21. Comparison of the Transverse O_2 Mixing Profiles between the 1/1 Jet Case at x = 1cm, the 3/1 Jet Case at x = 3cm, and the 6/1 Jet Case at x = 6cm.

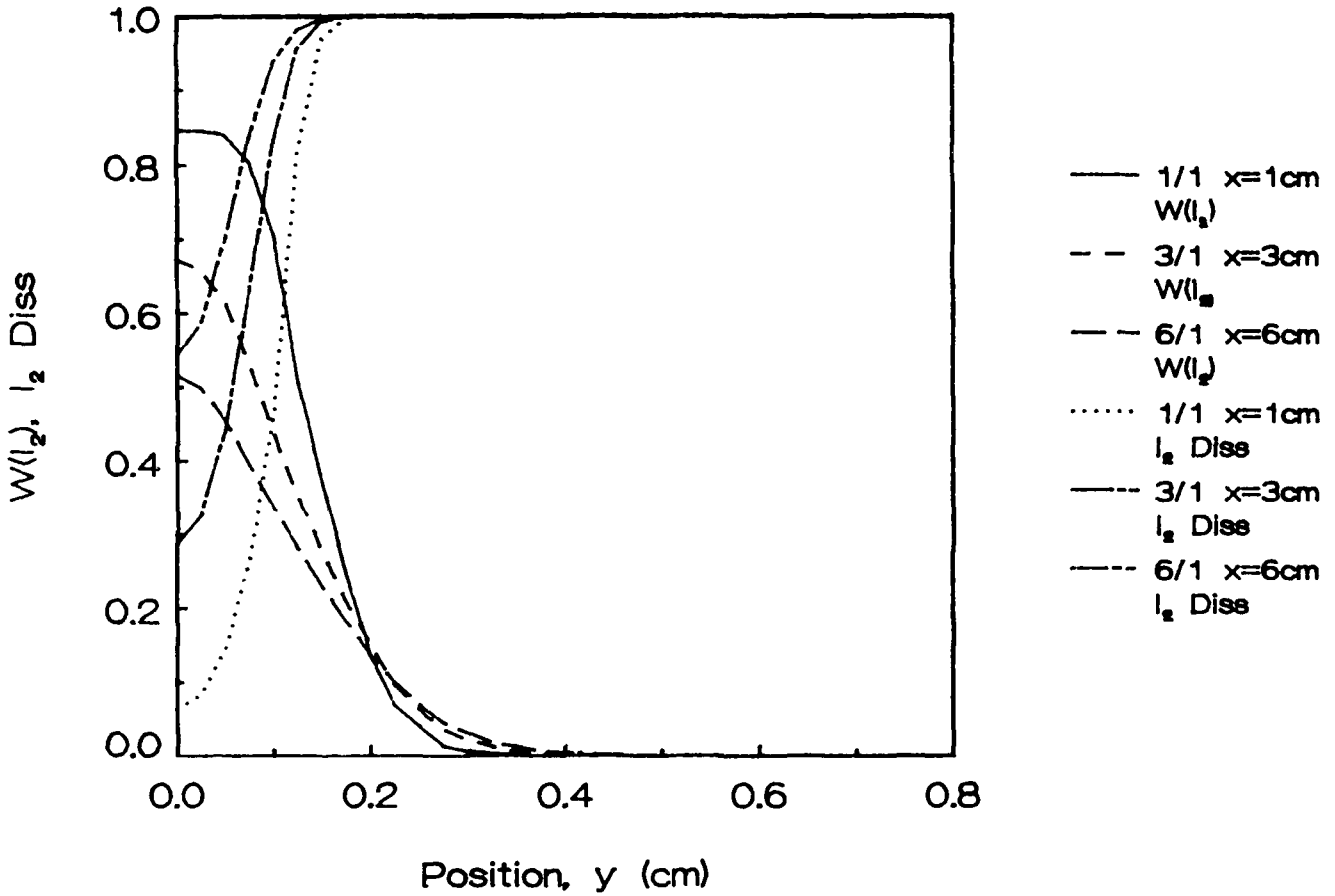

Figure 22. Comparison of the Transverse I_2 Dissociation Profiles between the 1/1 Jet Case at x = 1cm, the 3/1 Jet Case at x = 3cm, and the 6/1 Jet Case at x = 6cm.

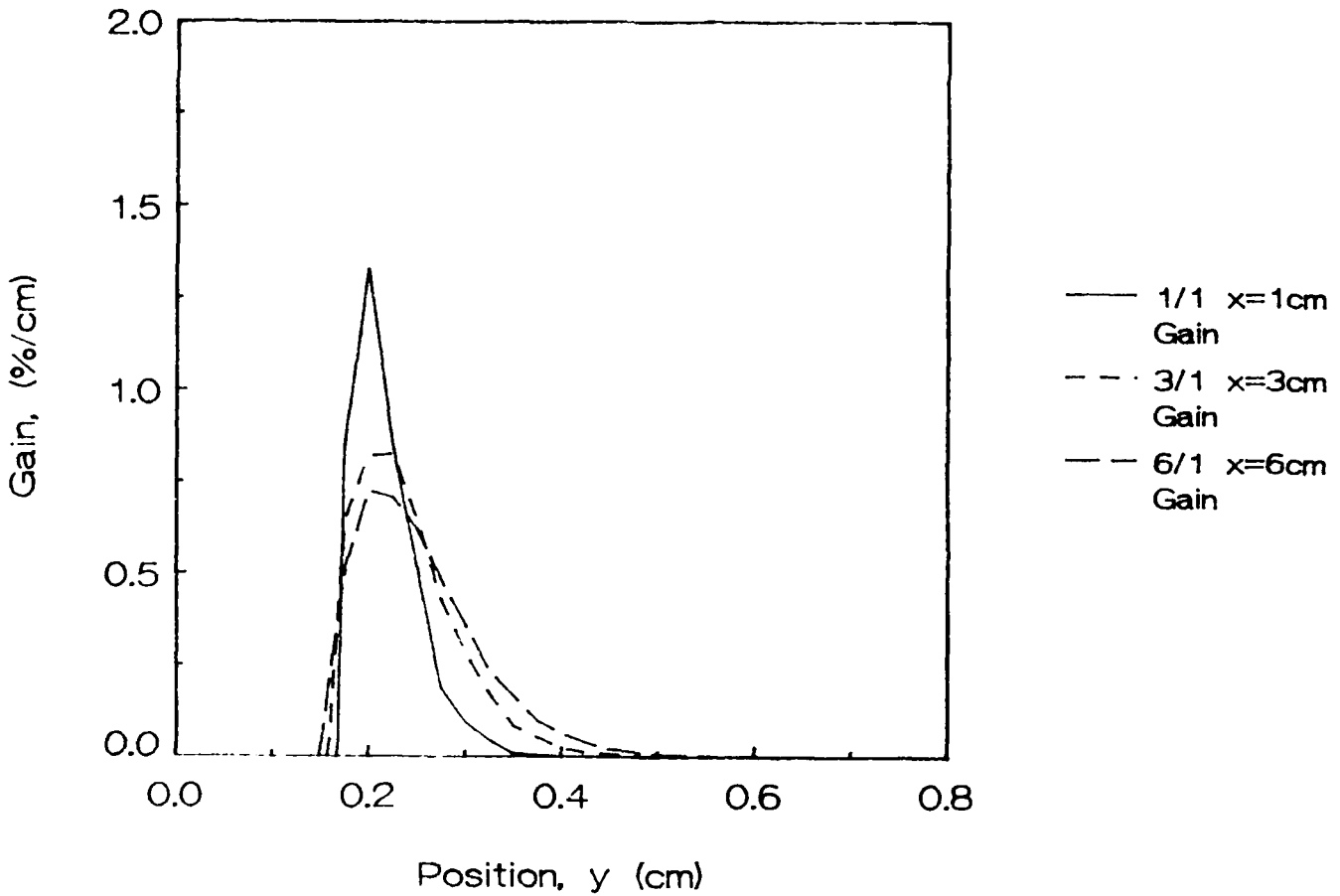

Figure 23. Comparison of the Transverse Gain Profiles between the 1/1 Jet Case at x = 1cm, the 3/1 Jet Case at x = 3cm, and the 6/1 Jet Case at x = 6cm.

the higher jet velocity ratio cases (c.f. Figure 14 for 1/1 at 1 cm, 3/1 at 3 cm, and 6/1 at 6cm). The gain profiles for these three cases, Figure 23, show an interesting trend. The gain for the 6/1 case is low even though the total dissociation is high. This is true because more of the $O_2(^1\Delta)$ near the mixing region was consumed in creating a higher level of dissociation. This reinforces the point that the I_2 must be both dissociated and thoroughly mixed to produce good power extraction qualities.

Effect of Water Quenching

One of the simplifying assumptions made for the mixing cases reviewed in the preceding section was that no H_2O vapor was included in the initial conditions. As discussed earlier, this eliminates all of the quenching (loss) reactions for the reduced eleven reaction set (Table I, Chapter III) employed for these calculations. In order to demonstrate the role that H_2O vapor (higher loss rates) has on the dissociation process, 2% H_2O vapor (% of the O_2 flow) was added to the initial conditions for the 6/1 case and the associated premixed case. For the 6/1 jet-mixed case, the H_2O vapor was added to the O_2 freestream only. This is physically realistic because H_2O vapor is introduced by the BHP/Cl_2 $O_2(^1\Delta)$ generator in actual devices. The integrated effect of H_2O on the I_2 dissociation fraction, Eq (5 1), for both of these cases is seen in Figure 24. As expected, H_2O interferes with the dissociation process (by quenching $O_2(^1\Sigma)$ and I^*, the initiators, and $I_2^\ddagger$, the intermediate) resulting in slower dissociation rates for both the premixed and the jet-mixed cases. The H_2O appears to have a more detrimental effect in the jet case. This is probably due to the higher concentration of H_2O in the primary freestream than in the premixed case

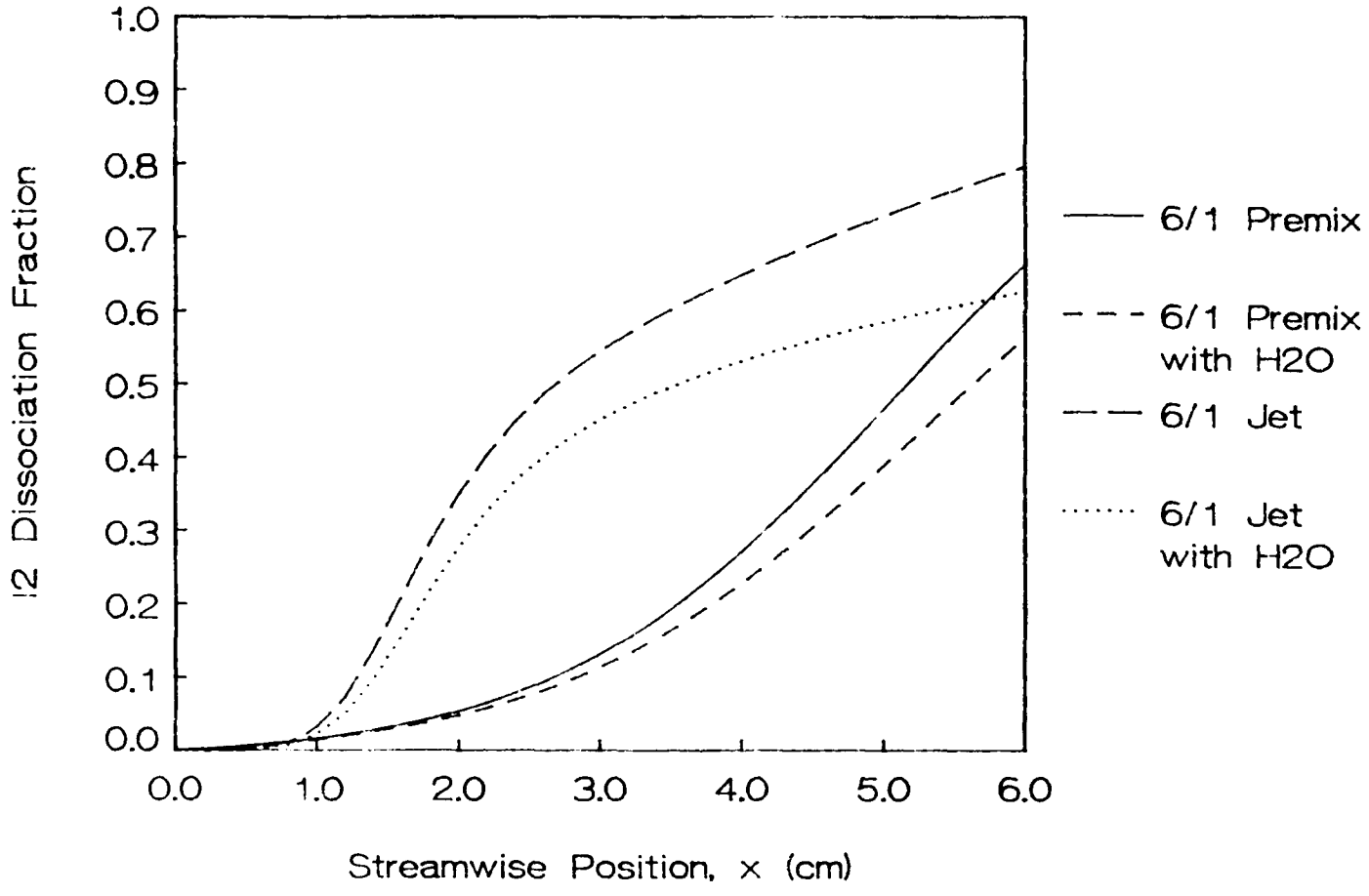

Figure 24. Effect of 2% (of the O_2 Flow) H_2O Vapor on the I_2 Dissociation for the 6/1 Premixed and Jet-Mixed Cases.

(i.e., H_2O is spread over a larger volume in the premixed case). Elimination of H_2O vapor from the O_2 flow has always been recognized as important to COIL performance; however, this was attributed to the fast quenching rate for I^*, the lasing species. Figure 24 shows that H_2O plays an important role in retarding the I_2 dissociation process as well.

The dissociation efficiency parameter, Eq (5.7), is plotted in Figure 25 for these H_2O cases. As discussed in an earlier section, the higher loss rate due to the H_2O quenching reactions results in less efficient (higher N) dissociation. Note, the impact on the jet-mixed case is more severe; however, this is due to the higher H_2O concentration in the primary freestream in the mixing case. With H_2O, the value of the efficiency factor begins to approach the often used range of from 5 to 7 at 100% dissociation. Figures 17 and 25 raise some important questions about the use of the empirical factor N for COIL performance prediction. These numerical cases point out that N is clearly not a constant. The apparent value of N varies with both the loss rates (H_2O concentration) and the dwell time between iodine injection and power extraction. N is, therefore, dependent on both device geometry and operating conditions. The practice of using a fixed N (which is derived from a demonstrated device design) to make large design excursions is, therefore, extremely suspect.

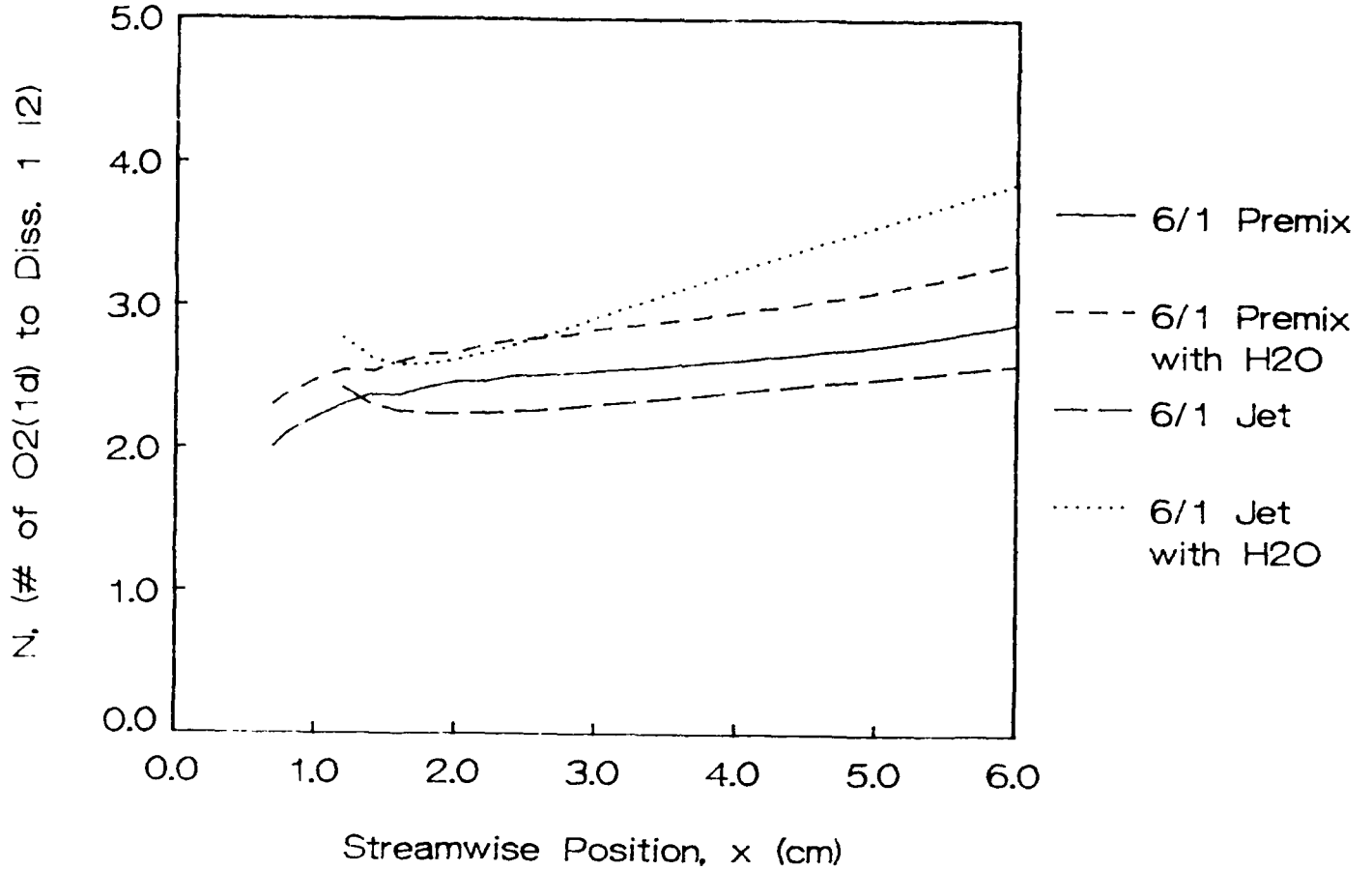

Figure 25. Effect of 2% (of the O_2 Flow) H_2O Vapor on the I_2 Dissociation Efficiency for the 6/1 Premixed and Jet-Mixed Cases.

VI. Conclusion

The observations made from the numerical results of the previous section provide some insight into the nature of the iodine mixing and dissociation process and its impact on the performance of COIL systems. One common belief is that better mixing of the oxygen and iodine streams will result in faster, more efficient dissociation. This is true only indirectly. Comparison of the one-dimensional, premixed cases with the jet-mixed cases in Figure 14 clearly showed that, due to hand off in rate control from $O_2(^1\Sigma)$ and $O_2(^1\Delta)$ to the faster $I^* \longrightarrow I_2^\ddagger$ mechanism, the less than perfectly mixed jet cases resulted in higher dissociation rates, at least initially. Conversely, the gain profiles in Figures 18-20 and 23 illustrate the need to achieve complete mixing in order to obtain high gains (and power extraction). Obviously, a compromise design is required which results in regions of high initial iodine concentrations to initiate the dissociation and then in thorough mixing of oxygen and atomic iodine streams. This in fact, seems to be the case for the highly successful transverse injection nozzle currently being employed.

As should be expected, the magnitude of the loss mechanisms (due to H_2O in this case) have the strongest influence on the efficiency of the dissociation process. Dissociation is slowed by the quenching of $O_2(^1\Sigma)$, I^*, and $I_2^\ddagger$. Mixing plays a role only to the extent that more losses are incurred as the rate of dissociation is limited by the mixing of the two streams. Figures 17 and 25 illustrate the fact that the efficiency of the combined iodine mixing and dissociation process as defined by N, the number of $O_2(^1\Delta)$'s required to dissociate one I_2, is

very much dependent on the individual device design and operating conditions. Larger dwell times (the flow time between the I_2 injection and power extraction) and greater losses (due to H_2O) result in a higher apparent N.

The recent Roto-COIL experience discussed in Chapter I reinforces the unacceptability of using empirical factors like N to predict the performance of off-baseline designs. Experience with one-dimensional, premixed models has proven to be just as unsatisfying. As demonstrated here, the premixed results display a very different character altogether from the mixing cases. This effect may become even more pronounced when attempting to model the performance of a highly three-dimensional laser nozzle. Clearly, COIL performance prediction will require a more sophisticated numerical approach. The modeler, however, must never forget that the accuracy of any prediction is only as valid as the data base supporting it.

The most basic question to be addressed by the proposed experimental and computational effort is; are the current COIL kinetics mechanism and rates accurate? Because dissociation of iodine in an $O_2(^1\Delta)$ stream is so highly dependent on the mixing as well as the kinetics, neither the simple experiments from which the kinetics data were derived nor the laser device experiments have been able to provide an answer to this question. The planned parallel jet experiment described in Appendix A is intended to shed some light on this subject; however, just as the results of an unanchored code are of little value, the experimental results will be of little value if they can not be accurately modeled using the code developed here or a more sophisticated one. Several issues concerning this question were raised in Chapter V.

Certainly, the most critical is whether the flow will remain truly laminar. The modeling difficulty will obviously increase dramatically if this is not so.

The numerical experience of Chapter V does provide some useful guidance. One effect not anticipated in the design of the experiment can be seen in Figure 14. Note that although the comparisons made of the dissociation rates for the three jet cases based on time did provide some insight, the spatial profiles display very similar character. This will make diagnosing the experimental flows much more difficult. On a more promising note, the gain profiles in Figures 18-20 and 23 show a much more distinct behavior. Gain mapping is a promising diagnostic technique because it provides information not only on the dissociation, but, also on the mixing of the atomic iodine with the $O_2(^1\Delta)$.

The most immediate goals of the proposed experimental and computational effort are to acquire a strong dissociation data base and validate the current AFWL COIL kinetics data set. The ultimate success of the combined experimental and computational effort lies in identifying new techniques for determining fundamental rate information. This combined approach is not so different from the techniques employed to measure the original rate data (9) (11). Analytical models for possible mechanisms were compared to overall creation and depletion rates measured on simple flow tube experiments. Figure 5, Chapter II, points to some possible difficulties with this method which may have resulted from attempting to oversimplify the problem. It remains to be shown that all of the important influences can indeed be modeled in the more complicated experiments.

Appendix A

Concurrent Experiment: Configuration and Expected Operating Conditions

Figure A1 is a schematic of the COIL device which will be used in planned experiments. The major components of the excited oxygen delivery system include a BHP/Cl_2 sparger, liquid separator, transition and vacuum bypass, H_2O cold trap. The nozzle cavity allows optical diagnostic access to both the side and top of the two dimensional slit injector. Pressure taps spaced at half inch intervals along the top and bottom walls allow for an experimental measurement of the streamwise pressure gradient. The initial conditions of the oxygen stream are measured in a diagnostic duct located just upstream of the slit injector. Iodine is supplied by passing heated helium over a heated iodine bed. The concentration of the entrained iodine is measured optically just before injection. The transverse injection supersonic slit nozzle shown in Figure 6a exists and can be mated to the same $O_2(^1\Delta)$ delivery system for comparison with the two dimensional results.

Figure A2 shows the detailed geometry of the two-dimensional iodine nozzle and the optical cavity. The cross section of the test section is 1.25 X 2.0 inches (3.175 X 5.08 cm) The height of the two dimensional nozzle is 0.075 inches (0.190 cm). The baseline flow rates through the BHP/Cl_2 reactor are 30 mmole/sec of chlorine at a 3/1 diluent ratio (90 mmole/sec of helium) and 100% chlorine utilization (complete conversion of chlorine to oxygen). The generator is expected to deliver an excited oxygen fraction ($O_2(^1\Delta)/O_2$(total)) of 0.40. The temperature of the oxygen stream will be approximately 300 K as it exits the cold trap. The nominal iodine to oxygen ratio is 0.02 (0.6 mmole/sec of I_2). The

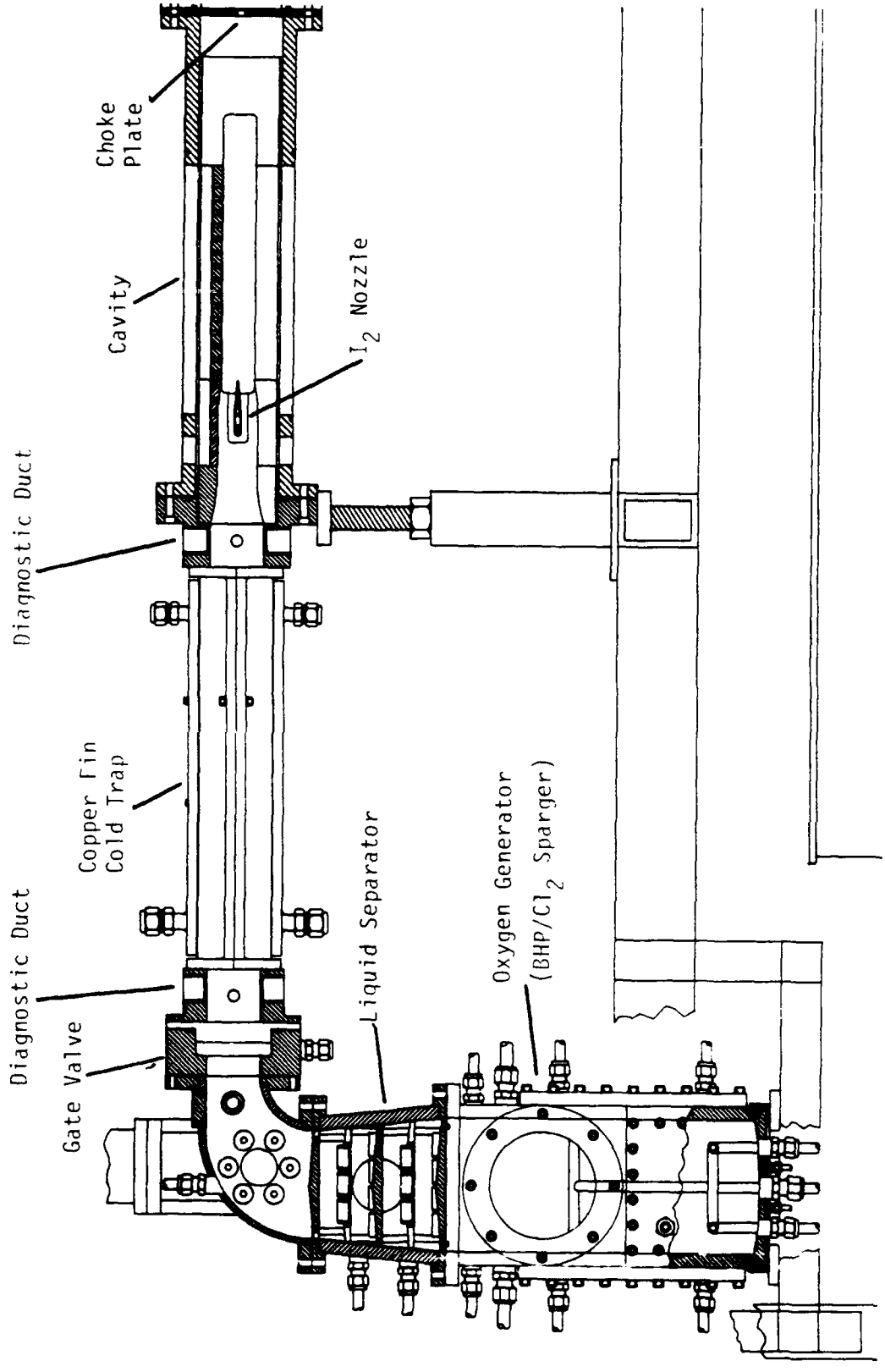

Figure A1. COIL Diagnostic Flow Tube Assembly

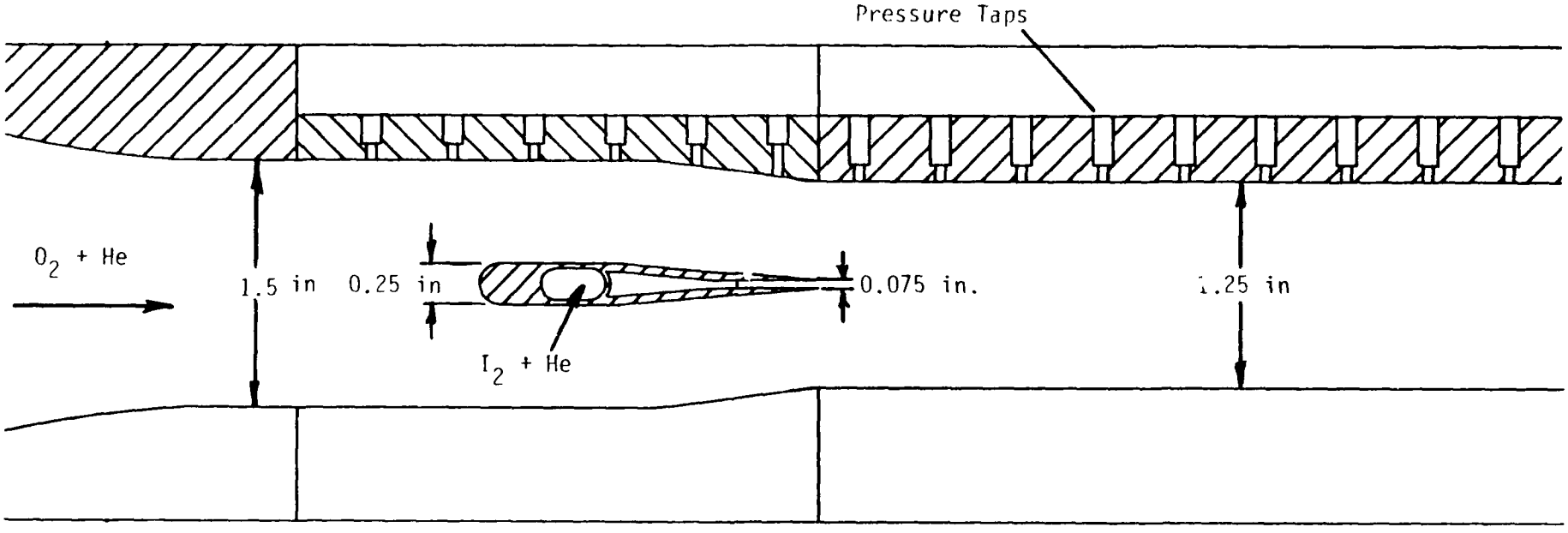

Figure A2. COIL Diagnostic Flow Tube I_2 Injection Nozzle

velocity of the iodine jet is controlled by varying the secondary diluent (helium in this case). The nozzle was designed for a 6/1 velocity ratio for a secondary diluent flow rate of 30 mmole/sec of helium. The iodine flow is heated to 400 K to avoid condensing iodine vapor on the flow surfaces. The pressure in the cavity is set by a 0.25 X 2.0 inch (0.635 X 5.08 cm) choke plate located well downstream of the nozzle exit plane. The cavity pressure is approximately 25 torr (3.33×10^4 dyne/cm^2). The velocity of the freestream at these flow conditions is 5,550 cm/sec ($M \cong 0.1$) and the velocity of the jet is 33,000 cm/sec ($M \cong 0.4$).

The basic array of diagnostics for this experiment include a number of flow and media diagnostics of increasing complexity. Flow visualization using one of two techniques will be used to provide a qualitative picture of the flow field and mixing region. The first technique, Laser Induced Fluorescence (LIF), uses an Argon Ion (Ar^+) laser to excite an electronic transition in the I_2 molecule during cold flows (no $O_2(^1\Delta)$).

$$I_2(X) + 5145nm \longrightarrow I_2(B) \qquad (A.1)$$

This same transition is also pumped in the $O_2(^1\Delta)/I_2$ system giving off a characteristic yellow flame. Infrared spectroscopy using spatially filtered intrinsic germanium photo diode detectors will be used to monitor $O_2(^1\Delta)$ and I^* species concentrations. Residual (unreacted) chlorine is measured by absorption using a Helium-Cadmium laser in the diagnostic duct. I and I_2 can also be measured by absorption using an I^* probe laser (or diode laser) and an Ar^+ laser, respectively.

Appendix B

Coefficients for Generalized Finite-Difference Operators

The general finite-difference operators for $\partial f/\partial\psi$ and $\partial^2 f/\partial\psi^2$ defined in Chapter IV, Eqs (4.8) and (4.9) are repeated here for convenience.

$$\frac{\Delta}{\Delta\psi} f(x,\psi) = \frac{A_1 f(x,\psi_A) + B_1 f(x,\psi_B) + C_1 f(x,\psi_C)}{D} \tag{B.1}$$

$$\frac{\Delta^2}{\Delta\psi^2} f(x,\psi) = 2 \left[\frac{A_2 f(x,\psi_A) + B_2 f(x,\psi_B) + C_2 f(x,\psi_C)}{D} \right] \tag{B.2}$$

The values for the coefficients A_1, B_1, C_1, A_2, B_2, C_2, D, ψ_A, ψ_B, and ψ_C are given in Table B. The notation used is shown to the right of the schematics in Figure 7, Chapter IV.

TABLE B

Coefficients for the Generalize Finite-Difference Operators

	Centerline j=0	Interior 0<j<N	Freestream j=N
ψ_A	$\psi(2)$	$\psi(j+1)$	$\psi(N-2)$
ψ_B	$\psi(1)$	$\psi(j)$	$\psi(N-1)$
ψ_C	$\psi(0)$	$\psi(j-1)$	$\psi(N)$
A_1	0.0	$k(j)$	0.0
B_1	0.0	$-(k(j)^2-k(j+1)^2)$	0.0
C_1	0.0	$-k(j+1)^2$	0.0
A_2	0.0	$k(j)$	0.0
B_2	1.0	$-(k(j)+k(j+1))$	1.0
C_2	- 1.0	$k(j+1)$	-1.0
D	$k(1)^2$	$(k(j)^2k(j+1)-k(j)k(j+1)^2)$	$k(N)^2$

Appendix C

COILFT Program Listing

```
      PROGRAM COILFT
*
*  PROGRAM SPECIES WRITTEN BY:
*
*      JOHN S. LAWRENCE, GAE-83D
*
*  MIXING WRITTEN BY:
*
*      CAPT. DAVID BJURSTROM
*      CAPT. DENISE PEREZ
*      LT. JEFFREY MILLER
*      GAE 84D
*
*  COILFT WRITTEN BY:
*
*      CAPT JEFFREY A. MILLER
*      MASTERS MARCH, 1989
*
*
*  THE PURPOSE OF THIS PROGRAM IS TO CALCULATE THE PROPERTIES OF A
*  MULTI-SPECIES FLOW AS IT PROPAGATES DOWNSTREAM, TAKING INTO ACCOUNT
*  TRANSPORT PHENOMENA DUE TO MOMENTUM, ENERGY, AND MASS OF SPECIES
*  (INCLUDING CHEMICAL REACTION).  THE USER MUST SPECIFY THE INITIAL
*  VELOCITY AND TEMPERATURE PROFILES AND THE INITIAL MOLE FRACTIONS
*  OF EACH SPECIES.
*
*  IN USER'S REFERENCES THROUGHOUT THE PROGRAM, THE FOLLOWING
*  ABBREVIATIONS APPLY:
*    BS&L - BIRD, STEWART, AND LIGHTFOOT, TRANSPORT PHENOMENA, 1960.
*    V&K - VINCENTI AND KRUGER, PHYSICAL GAS DYNAMICS, 1965.
*    JANZ - JANZ, THERMODYNAMIC PROPERTIES OF ORGANIC COMPOUNDS, 1967.
*
*  SYMBOLOGY WITHIN THE PROGRAM IS AS FOLLOWS:
*    X - POSITION VARIABLE TANGENT TO THE FREE-STREAM FLOW. (CM)
*    DX - INCREMENT IN THE X-DIRECTION.(CM)
*    Y - POSITION VARIABLE NORMAL TO THE FREE-STREAM FLOW. (CM)
*    DY - INCREMENT IN THE Y-DIRECTION. (CM)
*    PSI - POSITION VARIABLE NORMAL TO THE STREAMWISE VELOCITY (PSI).
*       (G/CM*S)
*    K - INCREMENT BETWEEN LINES OF CONSTANT PSI. (G/CM*S)
*    I AND ICOUNT - INTEGER COUNTERS IN THE X-DIRECTION.
*    J AND L - INTEGER COUNTERS IN THE Y-DIRECTION.
*    M AND N - NUMBER OF DESIRED STEPS IN THE X- AND Y-DIRECTIONS.
*    NS - NUMBER OF SPECIES.
*    Q AND S - INTEGER COUNTERS FOR SPECIES.
*    U - VELOCITY. (CM/S)
*    D1U AND D2U - 1ST AND 2ND DERIVATIVES OF U WRT PSI.
*    T - TEMPERATURE. (K)
*    D1T AND D2T - 1ST AND 2ND DERIVATIVES OF T WRT PSI.
```

```
*     PR - PRESSURE. (DYNE/CM**2)
*     DPDX - PRESSURE DERIVATIVE WRT X.
*     R - DENSITY (RHO). (G/CM**3)
*     MU - VISCOSITY. (G/CM*S)
*     MUS - VISCOSITY OF SPECIES. (G/CM*S)
*     KT - THERMAL CONDUCTIVITY. (DYNE/S*K)
*     KTS - THERMAL CONDUCTIVITY OF SPECIES. (DYNE/S*K)
*     CP - SPECIFIC HEAT AT CONSTANT PRESSURE. (DYNE*CM/K)
*     CPS - SPECIFIC HEAT OF SPECIES. (DYNE*CM/MOLE*K)
*     H AND HT - ENTHALPY OF SPECIES. (DYNE*CM/G)
*     D1H AND D1HT - 1ST DERIVATIVE OF ENTHALPY WRT PSI.
*     DIF - DIFFUSIVITY OF SPECIES. (CM**2/S)
*     DIFS - BINARY DIFFUSION COEFFICIENT. (CM**2/S)
*     MW - MOLECULAR WEIGHT. (GM/MOLE)
*     RBAR AND RCA - UNIVERSAL GAS CONSTANT. (DYNE*AM/MOLE*K) OR
*        (CAL/MOLE*K)
*     EPSK AND SIG - LENNARD-JONES PARAMETERS (EPSILON/K AND SIGMA).
*     OM - CHAPMAN-ENSKOG PARAMETER (OMEGA).
*     MRU AND KRU - MUXRXU AND KTXRXU, TREATED AS SEPARATE VARIABLES.
*     D1MRU AND D1KRU - CORRESPONDING 1ST DERIVATIVES WRT PSI.
*     W AND WT - MASS FRACTION OF SPECIES.
*     D1W, D2W, D1WT, AND D2WT - 1ST AND 2ND DERIVATIVES OF W WRT PSI.
*     MF - MOLE FRACTION OF SPECIES.
*     WD - CREATION OF MASS (RATE) TERM FROM CHEMICAL REACTION.
*     MWM - MOLECULAR WEIGHT OF THE MIXTURE. (G/MOLE)
*     PHI - SPECIES TRANSPORT COEFFICIENT.
*     XPHI - SUMMATION OF MFXPHI OVER SPECIES.
*     GRU AND GRT - DIFX(R**2)XU, TREATED AS A SEPARATE VARIABLE.
*     D1GRU  - CORRESPONDING 1ST DERIVATIVE WRT PSI.
*     TTABLE - TEMPERATURE TABLE FOR CP AND H INTERPOLATION. (K)
*     CPTBLE - CP TABLE ENTRIES. (CAL/MOLE*K)
*     HTABLE - H TABLE ENTRIES. (KCAL/MOLE)
*     C - CONSTANT 0.0<C<=1.0.  USED FOR DETERMINATION OF DX.
*
      INTEGER I,J,M,N,ICOUNT,S,NS
      PARAMETER (NS=10,N=32)
      REAL*4 C
C     PARAMETER (C=0.05)
      REAL*4 RBAR
      PARAMETER (RBAR=8.3143E+07)
      REAL*8 U(0:N),R(0:N),T(0:N),W(NS,0:N)
      REAL*8 UIP1(0:N),TIP1(0:N),WIP1(NS,0:N)
      REAL*8 WD(NS,0:N)
      REAL*8 X,DX,DXP,PR,DPDX,TIME(0:N)
      REAL*8 Y(0:N),DY(N),K(N),PSI(0:N)
      REAL*8 MW,MWM,MF
      REAL*8 SIG,EPSK
      REAL*8 A,B,HFORM
      REAL*8 MU(0:N),CP(0:N),H(NS,0:N),KT(0:N),DIF(NS,0:N)
      INTEGER IA(0:N),IB(0:N),IC(0:N)
      REAL*8 A1(0:N),B1(0:N),C1(0:N)
      REAL*8 A2(0:N),B2(0:N),C2(0:N),D(0:N)
      REAL*8 D1U,D2U,MRU,D1MRU
      REAL*8 D1T,D2T,KRU,D1KRU
```

```
      REAL*8 D1W,D2W,D1H,GRU,D1GRU
      REAL*8 TERM1,TERM2,DENOM
      INTEGER SSAVE,JSAVE
      COMMON /PROP1/ MW(NS),MWM(0:N),MF(NS,0:N)
      COMMON /LENJONES/ SIG(NS),EPSK(NS)
      COMMON /SPHT1/ A(NS,0:4),B(NS,0:4),HFORM(NS)
*
*  ESTABLISH INPUT (MIXIN) AND OUTPUT (MIXOUT) FILES.  THE INPUT FILE
*  IS UNFORMATTED , AND SHOULD BE CONSTRUCTED AS FOLLOWS:
*    FIRST LINE
*      M - NUMBER OF STREAMWISE STEPS
*      C - STABILITY FACTOR
*    SECOND LINE
*      X - INITIAL X
*      PR - PRESSURE
*      DPDX - PRESSURE GRADIENT
*    NEXT NS*3 LINES
*      (MW, ESPK, SIG) - MOLECULAR WEIGHT, LENNARD-JONES POTENTIALS
*      (A(S,I),I=0,4)  - COEFFICIENTS FOR FOURTH ORDER POLYNOMIAL FITS FOR
*      (B(S,I),I=0,4)  - CP AND H.  DATA FROM JANAF TABLES
*    NEXT N LINES - ONE LINE ENTRY FOR EACH PSI STEP STARTING AT THE
*       BOTTOM BOUNDRY.  EACH LINE CONTAINS Y(I),U(I),T(I),MF(1,I)-
*       MF(NS,I).
*
      OPEN(UNIT=15,FILE='coilin.dat')
      REWIND 15
      OPEN(UNIT=16,FILE='coilout.dat')
      REWIND 16
*
      NM1=N-1
      PSI(0)=0.0
      SSAVE=0
      JSAVE=0
*
*  EXTRACT DATA FROM INPUT FILE.
*
      READ(15,*) M,C
      READ(15,*) X,PR,DPDX
      READ(15,*) IPRINT,XPRINT,DXPRNT
      DO 5 S=1,NS
        READ(15,*) MW(S),EPSK(S),SIG(S)
        READ(15,*) (A(S,I),I=0,4)
        READ(15,*) (B(S,I),I=0,4),HFORM(S)
5     CONTINUE
      DO 10 J=0,N
        READ(15,*) Y(J),U(J),T(J),(MF(II,J),II=1,NS)
        Y(J)=Y(J)*2.54
10    CONTINUE
*
*  DENSITY AND MASS FRACTIONS ARE COMPUTED BY FIRST OBTAINING THE
*  MOLECULAR WEIGHT OF THE MIXTURE (MWM = SUMMATION OF MFXMW OVER
*  ALL SPECIES), COMPUTING DENSITY OF THE MIXTURE BY THE PERFECT GAS
*  LAW, AND TAKING THE APPROPRIATE RATIO FOR MASS FRACTION.  SEE
*  BS&L, TABLE 16.1-1, P498.
```

```
*
      DO 25 J=0,N
        MWM(J)=0.0
        DO 15 S=1,NS
          MWM(J)=MWM(J)+MF(S,J)*MW(S)
 15     CONTINUE
        R(J)=MWM(J)*PR/(RBAR*T(J))
        DO 20 S=1,NS
          W(S,J)=MF(S,J)*MW(S)/MWM(J)
 20     CONTINUE
 25   CONTINUE
*
*  THE VON MISES TRANSFORMATION, D(PSI)/DY=RHO*U, IS USED TO COMPUTE
*  VALUES FOR PSI AND K, WHERE RHO AND U ARE AVERAGED OVER EACH STEP
*  OUTWARD FROM THE WALL, AND THE DERIVATIVE IS APPROXIMATED BY THE
*  RATIO OF INCREMENTAL VALUES.
*
      DO 30 J=1,N
        DY(J)=Y(J)-Y(J-1)
        K(J)=DY(J)*(R(J)+R(J-1))*(U(J)+U(J-1))/4.
        PSI(J)=PSI(J-1)+K(J)
 30   CONTINUE
*
*  SET GENERALIZED FINITE-DIFFERENCE COEFFICIENTS.  WALL BOUNDARY
*  CONDITIONS ARE COMMENTED OUT IN FAVOR OF REFLECTION BOUNDARY
*  CONDITIONS.
*
      DO 31 J=0,N
        IF(J.EQ.0)THEN
          IA(0)=2
          IB(0)=1
          IC(0)=0
C         A1(0)=-K(1)*K(1)
C         B1(0)=(K(1)+K(2))*(K(1)+K(2))
C         C1(0)=(-A1(0)-B1(0))
C         A2(0)=K(1)
C         B2(0)=-(K(1)+K(2))
C         C2(0)=K(2)
C         D(0)=K(1)*K(1)*K(2)+K(1)*K(2)*K(2)
          A1(0)=0.0
          B1(0)=0.0
          C1(0)=0.0
          A2(0)=0.0
          B2(0)=1.0
          C2(0)=-1.0
          D(0)=K(1)*K(1)
        ELSE IF(J.EQ.N)THEN
          IA(N)=N-2
          IB(N)=N-1
          IC(N)=N
          A1(N)=0.0
          B1(N)=0.0
          C1(N)=0.0
          A2(N)=0.0
```

```
            B2(N)=1.0
            C2(N)=-1.0
            D(N)=K(N)*K(N)
C           A1(N)=K(N)*K(N)
C           B1(N)=-(K(N)+K(N-1))*(K(N)+K(N-1))
C           C1(N)=-(A1(J)+B1(J))
C           A2(N)=K(N)
C           B2(N)=-(K(N)+K(N-1))
C           C2(N)=K(N-1)
C           D(N)=(K(N)*K(N)*K(N-1)+K(N)*K(N-1)*K(N-1))
          ELSE
            IA(J)=J+1
            IB(J)=J
            IC(J)=J-1
            A1(J)=K(J)*K(J)
            B1(J)=-(K(J)*K(J)-K(J+1)*K(J+1))
            C1(J)=-K(J+1)*K(J+1)
            A2(J)=K(J)
            B2(J)=-(K(J)+K(J+1))
            C2(J)=K(J+1)
            D(J)=(K(J)*K(J)*K(J+1)+K(J)*K(J+1)*K(J+1))
          END IF
   31   CONTINUE
*
*  COMPUTE INITIAL VISCOSITY, SPECIFIC HEAT, ENTHALPY, THERMAL
*  CONDUCTIVITY, DIFFUSIVITY, AND MASS CREATION TERM.
*
       CALL PROP(PR,T,MU,CP,H,KT,DIF)
       CALL RATE(W,R,T,WD,MW)
*
*  RECORD INITIAL PROPERTIES OF THE FLOW.
*
       I=0
       WRITE(16,200) N,NS,M,C
       WRITE(16,210) I,X,DX,PR,DPDX
       DO 35 J=0,N
         TIME(J)=0.0
         WRITE(16,220) PSI(J),Y(J),TIME(J),R(J),U(J),T(J),MWM(J),
     +     MU(J),CP(J),KT(J)
   35  CONTINUE
       DO 36 J=0,N
         WRITE(16,220) (MF(S,J),S=1,NS)
   36  CONTINUE
       DO 37 J=0,N
         WRITE(16,220) (WD(S,J),S=1,NS)
   37  CONTINUE
       DO 38 J=0,N
         WRITE(16,220) (H(S,J),S=1,NS)
   38  CONTINUE
       DO 39 J=0,N
         WRITE(16,220) (DIF(S,J),S=1,NS)
   39  CONTINUE
*
*  THIS LOOP STEPS THE ENTIRE SOLUTION FORWARD BY AN INCREMENT IN THE
```

```
*  X-DIRECTION.
*
        ICOUNT=0
        DO 85 I=1,M
*
*  ESTABLISH DESIRED SIZE OF INCREMENTAL STEP IN X-DIRECTION.
*
          DX=0.1
C          IF(X.GT.1.0)C=0.05
          ICOUNT=ICOUNT+1
          DO 45 S=1,NS
            DO 40 J=1,NM1
              AMPH=(DIF(S,J)*R(J)**2*U(J)+DIF(S,J+1)*R(J+1)**2
     +         *U(J+1))/2.0
              AMMH=(DIF(S,J)*R(J)**2*U(J)+DIF(S,J-1)*R(J-1)**2
     +         *U(J-1))/2.0
              IF(AMPH.NE.0.0.AND.AMMH.NE.0.0)THEN
                DXP=C*(K(J)*K(J+1)*(K(J)+K(J+1)))/(2.0*(K(J)*AMPH
     +           +K(J+1)*AMMH))
                IF(DXP.LT.DX)THEN
                  SSAVE=S
                  JSAVE=J
                  DX=DXP
                END IF
              END IF
  40        CONTINUE
  45      CONTINUE
          DO 55 J=0,N
*
*  COMPUTE NEW VALUES FOR VELOCITY, TEMPERATURE, AND MASS FRACTION.
*  THESE DIFFERENCE EQUATIONS ARE DERIVED FROM A CONTROL VOLUME
*  ANALYSIS OF CONTINUITY, MOMENTUM, AND ENERGY, WITH BOUNDARY LAYER
*  ASSUMPTIONS.  SEE ACCOMPANYING DERIVATIONS.
*
*
*  SOLVE THE MOMENTUM EQUATION.
*
            MRU=MU(J)*R(J)*U(J)
            D1U=(A1(J)*U(IA(J))+B1(J)*U(IB(J))+C1(J)*U(IC(J)))/D(J)
            D1MRU=(A1(J)*MU(IA(J))*R(IA(J))*U(IA(J))+
     +       B1(J)*MU(IB(J))*R(IB(J))*U(IB(J))+
     +       C1(J)*MU(IC(J))*R(IC(J))*U(IC(J)))/D(J)
            D2U=(A2(J)*U(IA(J))+B2(J)*U(IB(J))+C2(J)*U(IC(J)))*2./D(J)
            UIP1(J)=U(J)+DX*(-DPDX/(R(J)*U(J))+D1MRU*D1U+MRU*D2U)
*
*  SOLVE EACH OF THE SPECIES EQUATIONS AND COMPUTE TERMS OF THE ENERGY
*    EAUTION.
*
            TERM1=0.0
            TERM2=0.0
            DO 50 S=1,NS
              GRU=DIF(S,J)*U(J)*R(J)**2
              D1H=(A1(J)*H(S,IA(J))+B1(J)*H(S,IB(J))+
     +         C1(J)*H(S,IC(J)))/D(J)
```

```
              D1W=(A1(J)*W(S,IA(J))+B1(J)*W(S,IB(J))+
     +         C1(J)*W(S,IC(J)))/D(J)
              D1GRU=(A1(J)*DIF(S,IA(J))*R(IA(J))**2*U(IA(J))+
     +         B1(J)*DIF(S,IB(J))*R(IB(J))**2*U(IB(J))+
     +         C1(J)*DIF(S,IC(J))*R(IC(J))**2
     +         *U(IC(J)))/D(J)
              D2W=(A2(J)*W(S,IA(J))+B2(J)*W(S,IB(J))+
     +         C2(J)*W(S,IC(J)))*2./D(J)
              WIP1(S,J)=W(S,J)+DX*(WD(S,J)/(R(J)*U(J))+D1GRU*D1W
     +         +GRU*D2W)
              TERM1=TERM1+WD(S,J)*H(S,J)
              TERM2=TERM2+GRU*D1W*D1H
   50       CONTINUE
*
*  SOLVE THE ENERGY EQUATION.
*
              KRU=KT(J)*R(J)*U(J)
              D1T=(A1(J)*T(IA(J))+B1(J)*T(IB(J))+C1(J)*T(IC(J)))/D(J)
              D1KRU=(A1(J)*KT(IA(J))*R(IA(J))*U(IA(J))+
     +         B1(J)*KT(IB(J))*R(IB(J))*U(IB(J))+
     +         C1(J)*KT(IC(J))*R(IC(J))*U(IC(J)))/D(J)
              D2T=(A2(J)*T(IA(J))+B2(J)*T(IB(J))+C2(J)*T(IC(J)))*2./D(J)
              TIP1(J)=T(J)+DX*(DPDX/(R(J)*CP(J))+MRU*D1U**2/CP(J)
     +         +(D1KRU*D1T+KRU*D2T)/CP(J))
              TIP1(J)=TIP1(J)-DX*(TERM1/(R(J)*U(J)*CP(J))-TERM2/CP(J))
              TIME(J)=TIME(J)+DX/U(J)
   55       CONTINUE
            X=X+DX
*
*  THE MOLE FRACTIONS ARE COMPUTED BY TAKING THE RATIO OF W/MW
*  TO THE SUMMATION OF W/MW OVER ALL SPECIES.  THE DENSITY IS
*  THEN COMPUTED IN THE SAME MANNER AS PREVIOUSLY, AND Y AND DY ARE
*  BACKED OUT OF THE SAME EQUATION USED TO CALCULATE PSI AND K.
*
            DO 70 J=0,N
              U(J)=UIP1(J)
              T(J)=TIP1(J)
              DENOM=0.0
              DO 60 S=1,NS
                W(S,J)=WIP1(S,J)
                DENOM=DENOM+W(S,J)/MW(S)
   60         CONTINUE
              MWM(J)=1./DENOM
              DO 65 S=1,NS
                MF(S,J)=W(S,J)*MWM(J)/MW(S)
   65         CONTINUE
              R(J)=MWM(J)*PR/(RBAR*T(J))
   70       CONTINUE
            DO 75 J=1,N
              DY(J)=4.*K(J)/((R(J)+R(J-1))*(U(J)+U(J-1)))
              Y(J)=Y(J-1)+DY(J)
   75       CONTINUE
*
*  COMPUTE VISCOSITY, SPECIFIC HEAT, ENTHALPY, THERMAL CONDUCTIVITY,
```

```
*  DIFFUSIVITY, AND MASS CREATION TERM.
*
          CALL PROP(PR,T,MU,CP,H,KT,DIF)
          CALL RATE(W,R,T,WD,MW)
*
*  RECORD PROPERTIES OF THE FLOW.  THE ICOUNT PROCEDURE IS DETERMINED
*  BY HOW OFTEN THE USER WISHES A PRINT OUT OF RESULTS.
*
          IF(ICOUNT.EQ.IPRINT.OR.X.GT.XPRINT)THEN
            ICOUNT=0
            IF(X.LT.1.0)THEN
              XPRINT=XPRINT+DXPRNT/2.0
            ELSE
              XPRINT=XPRINT+DXPRNT
            END IF
            WRITE(16,210) I,X,DX,PR,DPDX
            DO 80 J=0,N
              WRITE(16,220) PSI(J),Y(J),TIME(J),R(J),U(J),T(J),MWM(J),
     +          MU(J),CP(J),KT(J)
   80       CONTINUE
            DO 81 J=0,N
              WRITE(16,220) (MF(S,J),S=1,NS)
   81       CONTINUE
C            DO 82 J=0,N
C              WRITE(16,220) (WD(S,J),S=1,NS)
C   82       CONTINUE
C            DO 83 J=0,N
C              WRITE(16,220) (H(S,J),S=1,NS)
C   83       CONTINUE
C            DO 84 J=0,N
C              WRITE(16,220) (DIF(S,J),S=1,NS)
C   84       CONTINUE
          END IF
   85   CONTINUE
  200   FORMAT(' ',3(I10),E13.5)
  210   FORMAT(' ',I5,4(E13.5))
  220   FORMAT(' ',10(E13.5))
        STOP
        END
*****************************************************************************
*                                                                           *
*  THIS SUBROUTINE COMPUTES THE THERMODYNAMIC PROPERTIES AND THE            *
*  TRANSPROT COEFFICIENTS.                                                  *
*                                                                           *
*****************************************************************************
*
*  NOTE:  1 (CAL) = 4.186E+07 (DYNE*CM)
*         1 (DYNE/CM**2) = 9.869E-07 (ATM)
*         RBAR = 8.3143E+07 (ERG/MOLE*K)
*
        SUBROUTINE PROP(PR,T,MU,CP,H,KT,DIF)
        INTEGER L,N,Q,NS,QS
        PARAMETER (NS=10,N=32)
        REAL*4 RBAR
```

```
      PARAMETER (RBAR=8.3143E+07)
      REAL*8 T(0:N),PR,PRESS
      REAL*8 MU(0:N),CP(0:N),H(NS,0:N),KT(0:N),DIF(NS,0:N)
      REAL*8 MW,MWM,MF
      REAL*8 SIG,EPSK
      REAL*8 A,B,HFORM
      REAL*8 MUS(NS),OMEGA,PHI,XPHI
      REAL*8 CPS,KTS
      REAL*8 DIFS,DIFSUM,EPSKT,SIGT
      COMMON /PROP1/ MW(NS),MWM(0:N),MF(NS,0:N)
      COMMON /LENJONES/ SIG(NS),EPSK(NS)
      COMMON /SPHT1/ A(NS,0:4),B(NS,0:4),HFORM(NS)
*
      PRESS=PR*9.869E-07
      DO 20 L=0,N
        MU(L)=0.0
        CP(L)=0.0
        KT(L)=0.0
*
*  COMPUTE THE VISCOSITY OF THE MIXTURE AND VISCOSITIES
*  OF THE INDIVIDUAL SPECIES BY EMPLOYING THE CHAPMAN-ENSKOG FORMULAS.
*  THE VALUE FOR OMEGA IS DETERMINED FROM AN ALGEBRAIC CURVE-FIT
*  ANALYSIS OF TABULATED DATA FOR OMEGA AS A FUNCTION OF EPSK AND T.
*  SEE BS&L; EQNS 1.4-18, 1.4-19, 1.4-20, PP22-25, AND TABLES B1 AND
*  B2, PP744-746.
*
      DO 5 Q=1,NS
        OMEGA=.588+1./((1./EPSK(Q))*T(L)+.125)**.6666
        MUS(Q)=.000026693*SQRT(MW(Q)*T(L))/(OMEGA*SIG(Q)**2)
 5    CONTINUE
      DO 15 Q=1,NS
        XPHI=0.0
        DIFSUM=0.0
        DO 10 QS=1,NS
          PHI=((1.+((MUS(Q)/MUS(QS))**.5)*(MW(QS)/MW(Q))**.25)
     +      **2)/(8.*(1.+MW(Q)/MW(QS)))**.5
          XPHI=XPHI+MF(QS,L)*PHI
          IF(Q.EQ.QS)THEN
            DIFS=0.0
          ELSE
            EPSKT=SQRT(EPSK(Q)*EPSK(QS))
            SIGT=(SIG(Q)+SIG(QS))/2.
            OMEGA=.488+1./((1./EPSKT)*T(L)+.125)**.6666
            DIFS=.0018583*SQRT((1./MW(Q)+1./MW(QS))*T(L)**3)/
     +       (PRESS*OMEGA*SIGT**2)
            DIFSUM=DIFSUM+MF(QS,L)/DIFS
          END IF
 10     CONTINUE
        MU(L)=MU(L)+MF(Q,L)*MUS(Q)/XPHI
*
*  COMPUTE THE SPECIFIC HEAT AT CONSTANT PRESSURE OF
*  VALUES FOR THE SPECIES ARE LINEAR INTERPOLATED BETWEEN INPUT VALUES
*  SUPPLIED BY A JANAF TABLE.  NOTE: UNITS FOR INPUT ARE CP (CAL/MOLE*
*  K) AND H(KCAL/MOLE).  THESE UNITS ARE CHANGED TO CGS UNITS IN THE
```

```
*  SUBROUTINE.  CP OF THE MIXTURE IS A SUM OF THE PRODUCT OF MOLE
*  FRACTION AND CP OF THE SPECIES DIVIDED BY THE MOLECULAR WEIGHT OF
*  MIXTURE.
*
            CPS=(A(Q,0)+T(L)*(A(Q,1)+T(L)*(A(Q,2)+T(L)*(A(Q,3)+
     +       T(L)*A(Q,4)))))*4.186E+07
            CP(L)=CP(L)+CPS*MF(Q,L)
            CPS=CPS/MW(Q)
            H(Q,L)=((B(Q,0)+T(L)*(B(Q,1)+T(L)*(B(Q,2)+T(L)*(B(Q,3)+
     +       T(L)*B(Q,4)))))+HFORM(Q))/MW(Q)*4.186E+07*1000.0
*
*  COMPUTE THE THERMAL CONDUCTIVITY OF THE MIXTURE
*  AND THERMAL CONDUCTIVITIES OF SPECIES BY UTILIZATION OF THE
*  EUKEN FORMULAS.  SEE BS&L; EQNS 8.3-15, 8.3-17, 8.3-18, PP253-260.
*
            KTS=(CPS+1.25*RBAR/MW(Q))*MUS(Q)
            KT(L)=KT(L)+MF(Q,L)*KTS/XPHI
*
*  COMPUTE THE DIFFUSIVITY OF SPECIES BY CALCULATING
*  RELATIVE DIFFERENCES OF MOLE FRACTIONS, CALCULATING THE BINARY
*  DIFFUSION COEFFICIENTS, AND THEN EMPLOYING THESE IN A FORMULA
*  DERIVED FROM THE STEFAN-MAXWELL EQUATIONS.  SEE BS&L;
*  EQNS 16.4-13, 16.4-15, 16.4-16, PP508-513, EQN 18.4-25, PP569-572.
*
            IF(DIFSUM.EQ.0.0)THEN
              DIF(Q,L)=0.0
            ELSE
              DIF(Q,L)=(1.0-MF(Q,L))/DIFSUM
            END IF
 15       CONTINUE
          CP(L)=CP(L)/MWM(L)
 20     CONTINUE
        RETURN
        END
*
```

```
**********************************************************************
*                                                                    *
*                                                                    *
*  THIS SUBROUTINE COMPUTES THE MASS CREATION TERM FROM CHEMICAL     *
*  REACTION RATE EQUATIONS PROVIDED BY THE USER.  NOTE THAT THIS     *
*  PROCEDURE IS CURRENTLY SET UP TO HANDLE THE FOLLOWING SET OF      *
*  REACTIONS FOR CHEMICAL OXYGEN-IODINE LASERS, COIL:                *
*  SEE V&K; 210-228.                                                 *
*                                                                    *
*                                                                    *
**********************************************************************
*
*    1.  O2(1D) + O2(1D)    -->  O2(1S) + O2(3S)
*    2.  O2(1S) + H2O       -->  O2(3S) + H2O
```

```
*    3.  I2(X) + O2(1S)     -->  I + I + O2(3S)
*    4.  I2(X) + O2(1D)     -->  I2(STAR) + O2(3S)
*    5.  I2(X) +I(STAR)     -->  I2(STAR) + I
*    6.  I2(STAR) + O2(1D)  -->  I + I + O2(3S)
*    7.  I2(STAR) + H2O     -->  I2(X) +H2O
*    8.  I + O2(1D)         -->  I(STAR) + O2(3S)
*    9.  I(STAR) + O2(3S)   -->  I + O2(1D)
*   10.  I(STAR) + O2(1D)   -->  I + O2(1S)
*   11.  I(STAR) + H2O      -->  I + H2O
*
*
      SUBROUTINE RATE(W,R,T,WD,MW)
      INTEGER L,N,Q,NS
      PARAMETER (NS=10,N=32)
      REAL*8 W(NS,0:N),R(0:N),T(0:N),WD(NS,0:N),MW(NS),F(NS)
     +  ,K(11)
      REAL*8 NAV
      PARAMETER (NAV=6.02252E+23)
*
*  COMPUTE THE RATE COEFFICIENTS.
*
      K(1)=2.7E-17*NAV
      K(2)=5.5E-12*NAV
      K(3)=4.0E-12*NAV
      K(4)=7.0E-15*NAV
      K(5)=3.6E-11*NAV
      K(6)=3.0E-10*NAV
      K(7)=3.0E-10*NAV
      K(8)=7.6E-11*NAV
      K(9)=7.1E-12*NAV
      K(10)=1.1E-13*NAV
      K(11)=2.0E-12*NAV
*
*  START THE LOOP FOR Y.
*
      DO 10 L=0,N
*
*  COMPUTE THE TEMPERATURE DEPENDENT RATE COEFFICIENTS.
*
          K(1)=9.5E-28*T(L)**3.8*EXP(700.0/T(L))*NAV
          K(5)=1.4E-13*EXP(1660/T(L))*NAV
          K(8)=2.33E-8/T(L)*NAV
          K(9)=3.1E-8/T(L)*EXP(-403/T(L))*NAV
          K(10)=4.0E-24*T(L)**3.8*EXP(700.0/T(L))*NAV
*
*  COMPUTE THE MOLE-MASS FRACTIONS FOR EACH SPECIES.
*
          DO 5 Q=1,NS
              F(Q)=W(Q,L)/MW(Q)
    5     CONTINUE
          WD(1,L)=(K(1)*F(2)**2+K(2)*F(3)*F(9)+K(3)*F(4)*F(3)+
     +       K(4)*F(4)*F(2)+K(6)*F(5)*F(2)+K(8)*F(6)*F(2)-
     +       K(9)*F(7)*F(1))*MW(1)*R(L)**2
          WD(2,L)=(-2.0*K(1)*F(2)**2-K(4)*F(4)*F(2)-K(6)*F(5)*F(2)-
```

```
     +       K(8)*F(6)*F(2)+K(9)*F(7)*F(1)-K(10)*F(7)*F(2))
     +       *MW(2)*R(L)**2
             WD(3,L)=(K(1)*F(2)**2-K(2)*F(3)*F(9)-K(3)*F(4)*F(3)+
     +       K(10)*F(7)*F(2))*MW(3)*R(L)**2
             WD(4,L)=(-K(3)*F(4)*F(3)-K(4)*F(4)*F(2)-K(5)*F(4)*F(7)+
     +       K(7)*F(5)*F(9))*MW(4)*R(L)**2
             WD(5,L)=(K(4)*F(4)*F(2)+K(5)*F(4)*F(7)-K(6)*F(5)*F(2)-
     +       K(7)*F(5)*F(9))*MW(5)*R(L)**2
             WD(6,L)=(2.0*K(3)*F(4)*F(3)+K(5)*F(4)*F(7)+
     +       2.0*K(6)*F(5)*F(2)-K(8)*F(6)*F(2)+K(9)*F(7)*F(1)+
     +       K(10)*F(7)*F(2)+K(11)*F(7)*F(9))*MW(6)*R(L)**2
             WD(7,L)=(-K(5)*F(4)*F(7)+K(8)*F(6)*F(2)-K(9)*F(7)*F(1)-
     +       K(10)*F(7)*F(2)-K(11)*F(7)*F(9))*MW(7)*R(L)**2
             WD(8,L)=0.0
             WD(9,L)=0.0
             WD(10,L)=0.0
          10 CONTINUE
             RETURN
             END
```

Bibliography

1. McDermott, W. E., N. R. Pchelkin, D. J. Benard, and R. R. Bousek, "An Electronic Transition Chemical Laser," Applied Physics Letters, 32, 469-470 (1978).

2. Perram, Capt G. P., and G. D. Hager, The Standard Chemical Oxygen-Iodine Laser Kinetics Package, AFWL-TR-88-50, Air Force Weapons Laboratory, Kirtland AFB, NM, October 1988.

3. Arnold, S. J., N. Finlayson, and E. A. Ogryzlo, "Some Novel Energy-Pooling Processes Involving $O_2(^1\Delta_g)$," Journal of Chemistry and Physics, 44, 2529-2530 (1966).

4. Derwent, R. G. and B. A. Thrush, "Measurements on $O_2(^1\Delta_g)$ and $O_2(^1\Sigma_g)^+$ in Discharge Flow Systems," Transactions of the Faraday Society, 67, 2036-2043 (1971).

5. Derwent, R. G.and B. A. Thrush, "Excitation of Iodine by Singlet Molecular Oxygen," Journal of the Chemical Society, Faraday Transactions, 2, 720-728 (1972).

6. Shea, R. F., "Overview of the Singet Oxygen-Iodine Laser System," Unpublished Report, Air Force Weapons Laboratory, Kirtland AFB, New Mexico, 1984.

7. Seliger, H. H.,"Chemiluminescence of H_2O_2 - NaOCl Solutions," Journal of Chemistry and Physics, 40, 3133 (1964).

8. Benard, D. J., W. E. McDermott, N. R. Pchelkin, and R. R. Bouseck, "Efficient Operation of a 100-W Transverse-Flow Oxygen-Iodine Chemical Laser," Applied Physics Letters, 34, 40-41 (1978).

9. Heidner, R. F. III, C. E. Gardner, T. M. El-Sayed, and G. I. Segal, "Dissociation of I_2 in $O_2(^1\Delta)$ - I Atom Transfer Laser," Chemical Physics Letter, 81, 142-146 (July 1, 1981).

10. Avilés, R. G., D. F. Muller, and P. L. Houston, "Quenching of Laser-Excited $O_2(b^1\Sigma_g^+)$ by CO_2, H_2O, and I_2," Applied Physics Letters, 37, 358-360 (August 15, 1980).

11. Heidner, R. F. III, C. E. Gardner, G. I. Segal, And T. M. El-Sayed, "Chain Reaction Mechanism for I_2 Dissociation in the $O_2(^1\Delta)$ - I Atom Laser," The Journal of Physical Chemistry, 87, 2349-2360 (1983).

12. Hall, G. E., W. J. Maninelll, and P. L. Houston, "Electronic-to-Vibrationl Energy Transfer from $I^*(5^2P_{1/2})$ to $I_2(25 < v < 43)$," The Journal of Physical Chemistry, 87, 2153-2161 (1983).

13. Van Benthem, M. H. and S. J. Davis, "Detection of Vibrationally Excited I_2 in the Iodine Dissociation Region of Chemical Oxygen-Iodine Lasers," The Journal of Physical Chemistry, 90, 902-905 (1986).

14. Computaions and Figures prepared by D. N. Plummer, R and D Associates. Kirtland AFB, New Mexico, July, 1987.

15. Jumper, E. J., R. G. Wilkins, and B. L. Preppernau, "Adaptation of a Wall-Catalytic Fluorine Recombination Model to Fluid-Dynamic Computations in an HF Laser Nozzle," Proceedings of the AIAA 18th Fluid Dynamics and Plasmadynamics and Lasers Conference. AIAA-85-1598, (1985).

16. Jumper, E. J., R. G. Wilkins, and B. L. Preppernau, "Wall-Catalytic Fluorine Recombination in an HF Laser Nozzle," AIAA Journal, 26: 57-64 (January 1988).

17. Kays, W. M. and M. E. Crawford. Heat and Mass Transfer (Second Edition). New York: McGraw-Hill Book Company, 1980.

18. Schlicting, H. H. Boundary Layer Theory (Seventh Edition). New York: McGraw-Hill Book Company, 1979.

19. Birkhoff, G. and E. H. Zarantaonello. Jets, Wakes, and Cavities. New York: Academic Press Inc, 1957.

20. Pai, S. I. Fluid Dynamics of Jets. New York: D. Van Nostrand Company, 1954.

21. "JANAF Thermochemical Table," The Dow Chemical Company, Midland, MI, 1963.

22. Crowell, P. G., Personal correspondence. R and D Associates, Albuquerque, New Mexico, 10 November 1988.

23. Herzberg, Gerhard, F.R.S. Molecular Spectra and Molecular Structure. New York: Van Nostrand Reinhold Company, 1950.

24. Bird, R. Byron, W. E. Stewart, and E. N. Lightfoot. Transport Phenomena. New York: John Wiley & Sons, 1960.

25. Svehla, R. A., Estimated Viscosities and Thermal Conductivities of Gases at High Temperature, NASA TR-R-132, (1962).

26. Vincenti, Walter G., and C. H. Kruger Jr. Introduction to Physical Gas Dynamics. Florida: Robert E. Krieger Publishing Company, 1965.

VITA

Captain Jeffrey A. Miller [redacted]

[redacted] 1979 [redacted] attended the Pennsylvania State University from which he received a Bachelor of Science Degree in Aeronautical Engineering. Upon graduation, he received a commission in the USAF through the ROTC program. He then immediately entered the School of Engineering of the Air Force Institute of Technology. In 1985 Captain Miller was assigned to the Air Force Weapons Laboratory, Advanced Radiation Technology Office. He is currently working as a research engineer in the field of chemical lasers, specifically, Chemical Oxygen-Iodine Lasers.

UNCLASSIFIED
SECURITY CLASSIFICATION OF THIS PAGE

ADA206137

REPORT DOCUMENTATION PAGE

Form Approved
OMB No. 0704-0188

1a. REPORT SECURITY CLASSIFICATION UNCLASSIFIED	1b. RESTRICTIVE MARKINGS
2a. SECURITY CLASSIFICATION AUTHORITY	3. DISTRIBUTION/AVAILABILITY OF REPORT Approved for public release; distribution unlimited
2b. DECLASSIFICATION/DOWNGRADING SCHEDULE	
4. PERFORMING ORGANIZATION REPORT NUMBER(S) AFIT/GAE/AA/89M-3	5. MONITORING ORGANIZATION REPORT NUMBER(S)
6a. NAME OF PERFORMING ORGANIZATION School of Engineering 6b. OFFICE SYMBOL (If applicable) AFIT/EN	7a. NAME OF MONITORING ORGANIZATION
6c. ADDRESS (City, State, and ZIP Code) Air Force Institute of Technology Wright-Patterson AFB, OH 45433	7b. ADDRESS (City, State, and ZIP Code)
8a. NAME OF FUNDING/SPONSORING ORGANIZATION Air Force Weapons Laboratory 8b. OFFICE SYMBOL (If applicable) AFWL/ARDI	9. PROCUREMENT INSTRUMENT IDENTIFICATION NUMBER
8c. ADDRESS (City, State, and ZIP Code) AFWL/ARDI Kirtland AFB, NM 87117-6008	10. SOURCE OF FUNDING NUMBERS PROGRAM ELEMENT NO. / PROJECT NO. / TASK NO. / WORK UNIT ACCESSION NO.

11. TITLE (Include Security Classification)
NUMERICAL SIMULATION OF THE DISSOCIATION OF IODINE BY SINGLET DELTA OXYGEN IN A TWO DIMENSIONAL PARALLEL JET

12. PERSONAL AUTHOR(S)
Jeffrey A. Miller, B.S., Captain, USAF

13a. TYPE OF REPORT	13b. TIME COVERED	14. DATE OF REPORT (Year, Month, Day)	15. PAGE COUNT
MS thesis	FROM _____ TO _____	1989 March	120

16. SUPPLEMENTARY NOTATION

17. COSATI CODES			18. SUBJECT TERMS (Continue on reverse if necessary and identify by block number)
FIELD	GROUP	SUB-GROUP	
09	03		Two dimensional jet, Parallel Jet, Thin-shear-layer, Reacting Flow, Iodine Dissociation, Chemical Oxygen-Oxygen-Iodine Laser
07	04		

19. ABSTRACT (Continue on reverse if necessary and identify by block number)

Thesis Chairman: Eric J. Jumper, Lt Col, USAF

20. DISTRIBUTION/AVAILABILITY OF ABSTRACT ☒ UNCLASSIFIED/UNLIMITED ☐ SAME AS RPT. ☐ DTIC USERS	21. ABSTRACT SECURITY CLASSIFICATION UNCLASSIFIED
22a. NAME OF RESPONSIBLE INDIVIDUAL Eric J. Jumper, Lt Col, USAF, Adj. Professor	22b. TELEPHONE (Include Area Code) (505) 844-1808 / 22c. OFFICE SYMBOL AFWL/ARD

DD Form 1473, JUN 86 *Previous editions are obsolete.*

SECURITY CLASSIFICATION OF THIS PAGE
UNCLASSIFIED

The thin-shear-layer equations are solved for a two dimensional parallel jet of molecular iodine in singlet delta oxygen freestream, to investigate the effect of mixing and water vapor on molecular iodine dissociation in Chemical Oxygen-Iodine Lasers (COIL).

Predicting the dissociation of molecular iodine has been identified as the largest source of error in COIL performance modeling. Although some doubt still remains about the current COIL kinetics package, recent experimental and modeling experience have indicated that much of the problem may be due to the coupled iodine mixing and dissociation process. The numerical code was used to study the combined mixing and dissociation problem on a simpler (i.e. simpler than laser nozzles) 2-D, parallel injection nozzle geometry. Comparison of a set of 1-D premixed cases and 2-D jet cases with varying jet velocity ratios (and therefore mixing rates) indicates that, counter to the accepted belief, imperfect mixing which results in initial regions of high iodine concentration leads to faster dissociation rates. High laser gain, however, does require efficient mixing. The results of both premixed and jet-mixed cases with and without water vapor in the oxygen stream demonstrate the strong dependence of the dissociation efficiency (i.e., the penalty paid to dissociate iodine) on both the device geometry and operating conditions which challenges the wisdom of suing empirically determined efficiency factors to predict COIL performance.